Dottorato di Ricerca in Geologia
Dipartimento di Scienze della Terra e del Mare
Settore Scientifico Disciplinare GEO04 – Geografia fisica e Geomorfologia

Tesi in cotutela con
Institute of Geography - Eberhard Karls Universität Tübingen

Optimizing stochastic susceptibility modelling for debris flow landslides: model exportation, statistical techniques comparison and use of remote sensing derived predictors. Applications to the 2009 Messina event.

Luigi Lombardo

Tutors:

Prof. Edoardo Rotigliano

Prof. Volker Hochshild

UNIVERSITÀ DEGLI STUDI DI PALERMO
Dottorato di Ricerca in Scienze della Terra, indirizzo Geologia
Dipartimento di Scienze della Terra e del Mare
Settore Scientifico Disciplinare GEO04 – Geografia fisica e Geomorfologia

Tesi in cotutela con
Institute of Geography - Eberhard Karls Universität Tübingen

Optimizing stochastic susceptibility modelling for debris flow landslides: model exportation, statistical techniques comparison and use of remote sensing derived predictors. Applications to the 2009 Messina event.

IL DOTTORE
Lombardo Luigi

IL COORDINATORE
Prof. Enrico Di Stefano

IL TUTOR
Prof. Edoardo Rotigliano

CO TUTOR
Prof. Volker Hochshild,

CICLO XXV
ANNO CONSEGUIMENTO TITOLO 2015

INDEX

1 INTRODUCTION

1.1 PROBLEM STATEMENT

The International Disaster Database recorded from 1901 to 2014 a comprehensive dataset of disaster occurrences through our planet. The information related to natural disasters is included and can be freely accessed by any operator. Among the main natural disasters (Tab.1.1), mass movements are recorded as a major source of casualties and homeless despite their relative low occurrences. Similarly, Van Asch et al. (1999) and Petley (2012) recognised landslides as one of the main hazards on earth that cause the most casualties and damages.

Disaster type	Occurrence	Deaths	Homeless
Drought	647	$1.2*10^7$	$2.0*10^4$
Flood	4309	$6.9*10^6$	$8.9*10^7$
Earthquake	1260	$2.6*10^6$	$2.2*10^7$
Storm	3696	$1.4*10^6$	$5.2*10^7$
Extreme temperature	504	$1.7*10^5$	$2.6*10^5$
Volcano	231	$9.6*10^4$	$3.7*10^5$
Mass movement	680	$6.5*10^4$	$4.2*10^6$
Wildfire	381	$3.7*10^3$	$2.0*10^5$

Table 1.1– a summary of disaster events in the last century.

In fact, people are not the only vulnerable targets of landslides. In most of the mountainous regions, mass movements can easily lay waste to everything in their path, threatening human properties, infrastructures and natural environments.

The available landslide data at the International Disaster Database, depicts a terrible series of tragedies throughout the whole century, particularly in Americas, Asia, and Europe.

In particular, Europe has certainly taken a great toll in terms of landslide damage history, being the third continent for number of disasters and victims but the first in terms of cost of damage (Fig.1.1).

Within the European Union, Sassa and Canuti (2008) estimated an annual loss of one to 5 billion US dollars considering only the region comprising Italy, Austria, Switzerland and France. Among these nations, Italy has undoubtedly suffered more than other nations being the first country for economic damage, number of disasters and victims (Fig.1.2).

Within the Italian territory, several hydro-geomorphologic calamitous events happened in the last decade, among which, the more severe recent being Sarno 1998, Messina 2009 and Genova 2013.

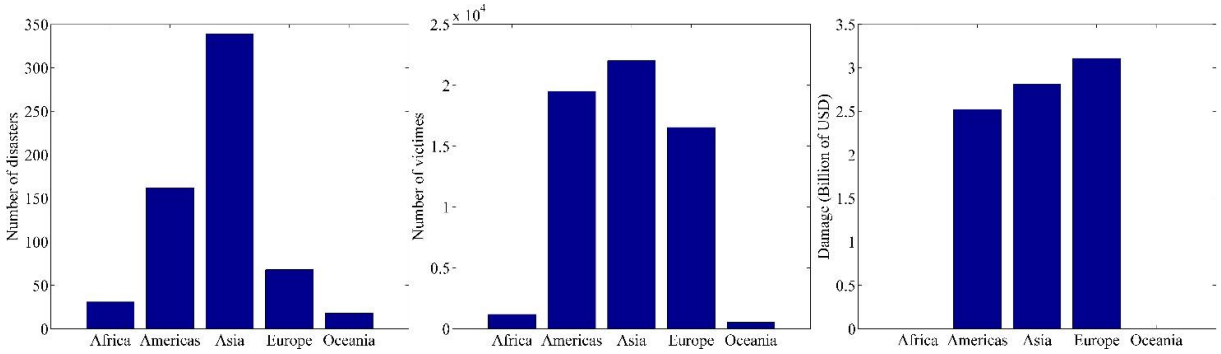

Figure 1.1 - Number of disasters (left), number of victims (centre) and cost of damage (right) globally recorded . Data from EM-DAT - International Disaster database between 1900 and 2013.

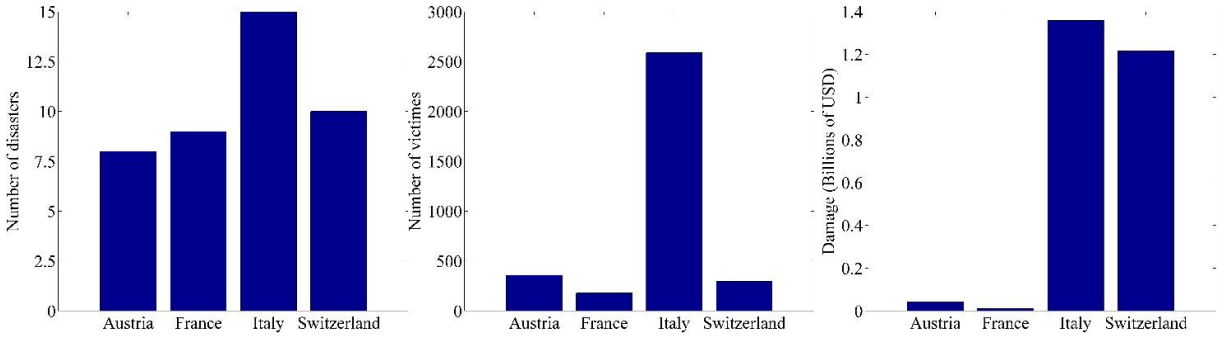

Figure 1.2 - Number of disasters (left), number of victims (centre) and cost of damage (right) recorded in the central alpine region. Data from EM-DAT - International Disaster database between 1900 and 2013.

Several are the landslide typologies, the potential causes, and the triggers, however the failure mechanism is shared between all the different cases. In fact, the main movement occurs when the shear stress exceeds the shear strength of the considered material, making the system unstable.

The slope stability can be compromised by both natural and human-caused changes in the environment.

The primary causes can be summarised into earthquake, heavy rain, rapid snow-melt, slope cut due to erosion, and variation in groundwater levels for the natural cases whilst slopes steepening through construction, quarrying, building of houses, and farming along the foot of mountainous zone correspond to the human component.

The present work exploit the aforementioned disaster occurred in the Italian Province of Messina on the 1st of October 2009 to address methodological problems within the scientific

area of landslide hazard and risk. A Multiple Occurrence of Regional Landslide Event (MORLE), according to Crozier (2005) took place in this occasion, triggering almost simultaneously thousands of shallow landslides in the time lapse of 5-8 hours, causing 36 victims, around 100 injured and half a million of Euros of damage to infrastructures. The main landslide typology pertaining this event was represented by rapid shallow landslides, which can be classified as debris flows or debris slides at the initiation area, evolving to debris flow or debris avalanche in the propagation phase.

In recent years MORLEs have been studied with a constantly increasing interest because of their destructive power. The multiple shallow landslides that trigger on the slopes initially mobilise only a superficial portion of the regolithic mantle moving then down onto the hillslope. The primary danger resides in the ability of the moving mass to deeply erode the detrital mantle and increase its mass during the propagation phase. As a response to this process of jointed erosion and entrainment, the volume of a single landslide can drastically increase before reaching the runout zone. In addition, in the specific case of a MORLE, different landslides from the same slope can converge along the same tracks multiplying the mass of transported materials and the potential force that will be discharged once the moving body will hit a given object.

The specific case of Messina 2009 is to be related to an extreme heavy rain trigger due to an extreme climatic event. In fact, intense rainfall leads to the abrupt increase of pore pressure (Campbell, 1975; Wilson, 1989) in the shallow weathered mantle which has typically a permeable structure.

. The cause-effect relationship between hydrologic status and morphodynamic response of slopes,, are further related to rainfall as a function of the infiltration properties and general soil characteristics as well as pre-event moisture content and rainfall history (Wieczorek, 1996). Since the early 80ies, many studies proved the importance of extreme precipitation in landslide activation mainly in terms of combination between rainfall intensity and duration (Caine, 1980; Cannon and Ellen, 1985; Crozier, 1986; Johnson and Sitar, 1990; Montgomery and Dietrich, 1994; Iverson et al. 1997; Iverson, 2000; Hengxing et al., 2003; Dhakal and Sidle, 2004; Malet et al., 2005). Despite the effort of the international community to derive rainfall thresholds for early-warning systems, due to the spatial variability and related complexity of these phenomena several difficulties still arise when limit precipitation values are to be calculated for specific locations (Althuwaynee et al., 2014; Nikolopoulos et al., 2014).

As a complementary approach to the management of landslide risk for storm-induced multiple landslide occurrence, , the international community focussed for the last decade on recognising the landslide hazard/susceptibility of a given area of interest. This phase becomes crucial in land use planning activities aimed tothe protection of people and infrastructures. Only with an appropriate risk assessment governments, regional institutions, and municipalities can in fact prepare the countermeasures at the different scales.

With respect to the risk topic, Schuster and Highland (2007) summarised four approaches in order to counter the risk from landslides: (i) restricting development in landslide-prone areas; (ii) implementing and enforcing excavation, grading, and construction codes; (iii) protecting existing developments by physical mitigation measures and (iv) developing and installing local monitoring and warning systems.

All the four approaches above start from a basic premise: landslide managers and urban planners know, plan and act in areas where landslide are more likely to occur, in other words, they assume to know what is called landslide susceptibility of the given environment where they are working.

Landslide susceptibility is therefore the keystone of a long chain of procedures that are actively implemented to manage landslide risk at all levels.

Landslide susceptibility has been defined by Brabb (1984) as the likelihood of a landslide occurring in a given area on the basis of local terrain conditions. In particular, the present work fits within the framework of landslide susceptibility studies that since their first appearance in the scientific literature (early 80's) have nowadays recalled more and more efforts from the scientific community to standardise and enhance the methodologies and the approaches at the base of this topic. The specific event of Messina 2009, is an important case study because of the exhibited landslide activations during the disaster. This pattern of multiple simultaneous landslide activations has been recognised worldwide in a large number of cases (Del Prete et al., 1998; Ahrendt and Zuquette, 2003; Baum et al., 2005; Matsushi et al., 2006; Godt et al., 2008) and only recently defined as Multiple Occurrence of Regional Landslide Events.

Several experiments have been performed in the present work In the framework of modeling procedures for the prediction of the landslide scenario of the aforementioned disaster to improve the landslide susceptibility knowledge.

In fact, despite the high international profile of the susceptibility subject and the huge number of published papers on the topic of landslide susceptibility assessment (Parise and Gibson, 2000; Clerici et al., 2002; Lee et al., 2004; Guzzetti et al., 2006; van Westen et al., 2008; Yilmaz, 2010; Conforti et al., 2012), several subtopics still need further consideration. The present thesis represents an attempt to address these subtopics and makes a step further in the current corresponding researches. Some aspects of these studies will be described in details as corresponding to the specific core topics developed during this PhD project, whilst others will be described as collaborative works, which have been carried out in a wider research team involving different institutions and corresponding expertises.

The first interest has been focussed in studying the model spatial transferability, also known as model exportation, for landslide susceptibility purposes (Costanzo et al., 2012; (Lombardo et al., 2014; Petschko et al., 2014;). This concept expresses the possibility of training susceptibility models in a given area and subsequently apply the obtained predictive functions to depict the susceptibility in a different region of interest.

Spatial exportation is a fundamental instrument in case of lack of landslide inventories. In particular, noteworthy is the application in case of landslides driven by extreme climatic events in the Mediterranean sector where inventories are limitedly distributed in time and space.

Another important subject correspond to the methodology itself that one can use to assess the susceptibility of a given area. In fact, susceptibility maps can be obtained through different methods: inventory, heuristic, statistical, and deterministic (e.g., Montgomery and Dietrich, 1994; Soeters and van Westen, 1996; Hoek and Bray, 1997; Petley, 1999; van Westen 2000; Dietrich et al., 2001; Guzzetti, 2005; van Westen et al., 2006; Clerici et al., 2006; Alexander, 2008; Carrara and Pike, 2008; Muntohar and Liao, 2010; Mergili et al., 2012). Each of the above-mentioned procedures has proven to be reliable for the specific purpose, however the statistical approach is the one that in recent years undertook the strongest differentiation due to a constantly increasing interest from the scientific community.

Among the statistical methods classification (e.g., Nefeslioglu et al., 2010; Vorpahl et al., 2012) and regression (e.g., Süzen and Doyuran, 2004; Brenning, 2008) algorithms have been adopted from statistics and data mining applications and effectively tested in the framework of landslide spatial prediction. Due to the number of available methods, we selected two among the currently most used techniques and compared their performances in predicting multiple landslide occurrences so to ascertain advantages and disadvantages.

The last reserach has been made to integrate new sources of predictors linked to the mass movement initiation. Glade and Crozier (2005) recognised the importance of selecting appropriate causal factors, as their choice varies depending on the scale of analysis, the characteristics of the study area, the landslide type, and the failure mechanisms. For the specific case of debris flow landslides, geology and land use layers are almost systematically adopted in landslide susceptibility studies and further coupled with attributes derived from Terrain Analysis in GIS environments (e.g., van Westen, 2008).

Only in recent years the use of remote sense data is steadily increasing in this field proving its effectiveness in several works (e.g., Pachauri and Pant, 1992; Nagarajan et al., 1998; Sarkar and Kanungo, 2004; Hong et al., 2007).

In this research a third learning algorithm is tested by basing the training and validation phase on a joint covariate dataset, made of topographic attributes, vegetation and mineral indexes obtained from satellite data processing. The strength of using a remotely derived set of predictors in the framework of landslide susceptibility resides in the almost un-limited spatial availability of satellite imagery. This widespread coverage can lead to potential applications in areas with poor or no field data or with limited budget for digital elevation models.

Ultimately, the scientific literature is currently lacking of debris flow landslide susceptibility studies through stochastic approaches in the north-eastern side of the Sicilian sector. The present thesis aims also to fill this gap presenting the first experiments on stochastically-based debris flow susceptibility available in Sicily.

2 THEORETICAL BACKGROUND

2.1 LANDSLIDES

Although a large number of definition and classifications has been given in literature for landslides (e.g., Nemčok et al., 1972; Varnes, 1978; Hutchinson, 1988; WP/WLI, 1990; Cruden, 1991; Cruden and Varnes, 1996), a very simple one was proposed by Varnes (1978): a downward and outward movement of a mass of rock, debris, or earth down a slope, under the influence of gravity.

Several causes can lead to a landslide activation as a result of the gravitational force field acting upon a mass along a slope.

Since one of the earliest attempt to describe this phenomenon, several classifications have been proposed within the scientific community each one depending on a specific factor criterion. Materials, geomorphic attributes, geometries, type of movements, climates, water contents, speed of movement, and triggering mechanism represent the criteria that have been used to cluster landslides into groups. Some of these factors have been selected more than others and scientists are still debating for a uniform classification.

The classification of Varnes (1978) is the first that has been widely adopted, however several efforts have been made to update it and modify it to include different aspects of slope failures.

The modified Varnes (1996) classification approved by IAEG Commission UNESCO Working Party on World Landslide Inventory (WP/WLI) of landslides takes into account most of the aspect described above as shown on tables (2.1, 2.2, 2.3, 2.4).

Type of movement	**Type of material**		
	Bedrock	*Engineering soils*	
		Predominantly coarse	*Predominantly fine*
Fall	Rock fall	Debris fall	Earth fall
Topple	Rock topple	Debris topple	Earth topple
Slide	Rock slide	Debris slide	Earth slide
Spread	Rock spread	Debris spread	Earth spread
Flow	Rock flow	Debris flow	Earth flow

Table 2.1 - Landslide Classification as a function of the composing materials.

Activity		
State	*Distribution*	*Style*
Active	Advancing	Complex
Reactivated	Retrogressive	Composite
Suspended	Widening	Multiple
Inactive	Enlarging	Successive
Dormant	Confined	Single
Abandoned	Diminishing	
Stabilized	Moving	
Relict		

Table 2.2 - Landslide Classification as a function of the activity.

Description of first movement			
Rate	Water content	Material	Type
Extremely rapid	Dry	Rock	Fall
Very rapid	Moist	Soil	Topple
Rapid	Wet	Earth	Slide
Moderate	Very wet	Debris	Spread
Slow			Flow
Very slow			
Extremely slow			

Table 2.3 - Landslide Classification as a function of the first movement.

Description of second movement			
Rate	Water content	Material	Type
Extremely rapid	Dry	Rock	Fall
Very rapid	Moist	Soil	Topple
Rapid	Wet	Earth	Slide
Moderate	Very wet	Debris	Spread
Slow			Flow
Very slow			
Extremely slow			

Table 2.4 - Landslide Classification as a function of the second movement.

Some of the aspects used to describe a mass movement are still a source of debate because of a non-uniform agreement among the whole community.

The material criterion for example has been revised through time. In the contribution of Varnes (1978) the definition of the landslide-forming media was incompatible with accepted geotechnical and geological terminology of rocks and soils. For this reason, Cruden and Varnes (1996) specified that the mass waste is not bounded to granular soils but it can include several type of materials. More recently, Hungr et al. (2014) have proposed to update the threefold material classes to a homogeneous multi-disciplinary description inspired to the geotechnical

properties of rocks and soils. The material classification proposed by Hungr et al. (2014) suggested a subdivision into rock, clay, mud, silt, sand, gravel, boulders, debris, peat, and ice. Each of these materials can be described through a specific table including character descriptors, simplified field descriptions, corresponding unified soil classes, and laboratory indices.

Going beyond the typology of a given mass movement, another important information describes those conditions that can contribute to the proneness of a slope to result in a failure, also called preparatory or causative factors. On the other hand the actual phenomenon that gives rise to a landslide suddenly changing the stability state to actively unstable is known as landslide trigger. Causative factors (Glade and Crozier, 2005b) and triggers (Dikau and Schrott, 1999) clearly interplay a fundamental role in generating mass movements however they are distinctly separated in the scientific literature. Preparatory factors constantly act upon a slope slowly affecting the stability in a relatively long time without generating the actual failure. Common examples of these factors list processes such as weathering, altered slope morphology, deforestation, pre-existing shear-surfaces, tectonic uplift and environmental changes. Conversely, triggers are able to modify the stability in a relatively short time disrupting the slope balance and actively initiating the failure process. Typical examples of triggering mechanisms are recognised as prolonged rainfall, rapid snow melting, earthquakes, and human activities.

A specific category of mass movements, known as flow-like landslides, is strongly affected by all this causes, making it the type of mass movement that in recent studies has primarily focussed the attention of the international community (Hungr et al., 2001; Pastor et al., 2009, Travelletti and Malet, 2012). Hungr et al. (2014) summarise flow-like landslides as including:

- Rock/ice avalanches;
- Dry (or non-liquefied) sand/silt/gravel/debris flows;
- Sand/silt/debris flow slide;
- Sensitive clay flow slide;
- Debris flow;
- Mud flow;
- Debris flood;
- Debris avalanche;

- Earth flow;
- Peat flow.

Within this framework, the present thesis concentrates in studying debris flows and debris avalanches in terms of landslide types and behaviours expressed during the disaster of 1 October 2009 (Messina, Italy). The landslide typologies exhibited during the aforementioned disaster are one of the primary causes of concern at a societal scale in all the worldwide mountainous regions because of their difficult predictability and the potential damage hidden in each activation. Even nowadays these classes probably attract most of the attention of the professionals involved in the mass movement science with hundreds of scientific contributions published per year, also from different disciplines and perspectives (e.g. Calvo et al., 2014; Chen et al., 2014; Cheng et al., 2014; Chiou et al., 2014; Eidsvig et al., 2014; Elkadiri et al., 2014; Gartner et al., 2104; Legg et al., 2014; Lombardo et al., 2014; Mast et al., 2014; Ni et al., 2014; Pavlova et al., 2014; Šilhán et al., 2014; Stoffel et al., 2014; Turkington et al., 2014; Yoshida, 2014;).

The most recent review of the landslide classification (Hungr et al., 2014) defines the debris flows as "very rapid to extremely rapid surging flow of saturated debris in a steep channel. Strong entrainment of material and water from the flow path", whilst the debris avalanche type correspond to a "very rapid to extremely rapid shallow flow of partially or fully saturated debris on a steep slope, without confinement in an established channel. Occurs at all scales". The two definitions share the common feature of velocity and in particular the two landslide types are the most rapid within the whole mass movement spectrum. This characteristic is directly linked to the risk that these phenomena pose to everything they intercept in their travel. Their speed and the contextual ability to erode and absorb new material masses can result in extreme forces applied when colliding with any objects. Recent studies from Moriguchi et alii (2009) established on a basis of both empirical and numerical simulations that just 50kg of granular material can generate forces reaching a maximum of 500N against a rigid obstruction positioned at the bottom of the slope. For the specific case of debris flows another element contributes to their dangerousness, in fact these mass movements can channelize along the track, converge, and intersect their path joining the transported masses from multiple failures into a single one. As a consequence, the multiple transported volumes can cumulate together resulting in a unique and extremely powerful landslide.

With regard to the catastrophic event of Messina 2009, it must be noted that on that day, almost all of the recognised phenomena belonged to the debris flow and debris avalanche classes, however the displayed initiation mechanism can be further subdivided. The triggering features were in fact recognised again as debris flow, however debris slide (Hungr et al., 2001; Hungr et al., 2005; Larsen and Wieczorek, 2006) mechanisms were also detected at the landslide crowns.

Debris slides are defined as "Sliding of a mass of granular material on a shallow, planar surface parallel with the ground. Usually, the sliding mass is a veneer of colluvium, weathered soil, or pyroclastic deposits sliding over a stronger substrate. Many debris slides become flow-like after moving a short distance and transform into extremely rapid debris avalanches" (Hungr et al., 2014). The evolution here described is exactly what happened to the approximate total number of debris slide cases in Messina 2009, as recognised from field and remote observations. Further detail will be given in chapter 4.

2.2 LANDSLIDE SUSCEPTIBILITY

Efforts of the scientific community have been concentrated on landslide hazard and risk over the last ten years. During this period, two scales of investigation have been primarily pursued: site-specific analysis and regional assessment (Glade et al. 2012). The two types of investigations have their roots into different branches of the research, the former corresponding to engineering and geotechnics, the latter to geology and geomorphology.

Nowadays the boundary between the two approaches has been strongly smoothed and a broad spectrum of scientists from different fields indistinctly carry out their researches at the two scales.

The site specific analysis involves direct measurements used to reconstruct the landslide geometry and its extension over the space, laboratory tests to derive geo-mechanical and geo-physical parameters and ultimately solve geophysical, geotechnical, hydrological, and hydrogeological deterministic problems.

The advantage of pursuing this approach resides in the ability to quantify the physical properties that play an important role in describing the laws of physics governing the slope stability. Mastering this knowledge allows to calculate and plan appropriate countermeasures to

reduce the landslide risk. However due to the high cost of each test necessary to quantify the physical parameters, reliable site specific analyses are often confined in space, generally at the scale of a single landslide or of a single slope (Leynaud et Sultan, 2010; Jia et al., 2012; Keaton et al., 2013; James and Sitharam, 2014; Kostic et al., 2014; Luna et al., 2014; Raia et al., 2014;).

On the other hand, the regional assessment is performed to take into account properties spatially distributed over large areas, typically ranging from a few hectares to thousands of square kilometres. The core interest of this approach is aimed to indirectly detect those physical-environmental properties which are responsible for landslide activation and exploit the knowledge of their spatial distribution to produce landslide predictions in time and space.

The advantage of this approach is the ability to recognise areas prone to fail on a wide surface expressed at the catchment or regional scale. This information is crucial to plan the territory management and can be jointly integrated with the site specific analysis when, at a broader scale, significant risk has been pointed out and more detailed models are needed. The methods applied to achieve the goal of landslide prediction on a wide scale generally pertain to the field of geo-statistic and can be summarised into heuristic (Ruff and Czurda, 2006; Günther et al., 2013), inventory-based analysis (Casagli et al., 2004) and stochastic (Rossi et al., 2010; Rotigliano et al., 2012).

Within this framework, the landslide susceptibility concept has been developed to address the problem of predicting landslide spatial distributions. Landslide susceptibility is defined as the likelihood of a landslide occurring in an area on the basis of local terrain conditions (Brabb, 1984) and represents the degree to which a terrain can be affected by slope movements. Temporal and magnitude predictions are not included and the concept itself primarily answers to the question “where” a landslide is more likely to occur.

Mihai et al. (2014) and also Mancini et al., (2010) give a clear example of how important susceptibility studies are, demonstrating a real example of potential integration of susceptibility mapping directly into the urban planning strategies. This approach can prove to be extremely useful in providing administrations with a simple tool usable to inform and control the decision making processes for areas under development.

The use of regional stochastically-based approaches for landslide susceptibility has increased proportionally with the Geographic Information Systems (GIS). GIS is a relatively new technology that since its first appearance a few decades ago has drastically revolutionised

the management of all sort of spatial data in all the fields of science, including the landslide susceptibility branch. Susceptibility maps reached a far greater efficiency and accuracy (Saha et al., 2005) than ever before applying GIS. This is predominantly due to possibility of collecting, manipulating and analysing a variety of spatial and non-spatial data related to landslide geometries, extent, and recognition as well as the potential causal factors responsible for the landslide activity in a region (Carrara et al. 1991; Nagarajan et al. 1998; Conoscenti et al., 2008).

Integrating an managing into a unique digital environment a bulk of spatial data connected to the mass movement processes allowed to perform calculations, to build advanced statistics, and to apply several methods that lead to a constant improvement for landslide susceptibility studies.

In terms of methods, as stated above, a wide range of approaches is available to researchers to understand spatial distribution of landslide-prone areas. However, machine learning and stochastic methods have recently gained an equal consent from most of the international community in order to assess the landslide susceptibility of a given area.

The application of stochastic and/or machine learning methods allow to obtain uni-, bi- or multivariate functional relationships that, on the basis of morphodynamic and geomechanical criteria, links the mass movements to their driving forces and stability conditions.

Taking aside the choice among the multitude of available algorithms, in order to assess landslide susceptibilities, differences in these studies arise as a function of three primary components at the base of the validity domain of the susceptibility concept.

1) the selected general assumptions (Varnes and IAEG Commission on Landslides and other Mass-Movements, 1984; Carrara et al., 1991a; Hutchinson and Chandler, 1991; Hutchinson, 1995; Turner and Schuster, 1996; Guzzetti et al., 1999a);

2) mapping units (Carrara et al., 1999; Guzzetti et al., 1999);

3) diagnostic (Rotigliano et al., 2011; Costanzo et al. 2012a) or seed areas (Süzen and Doyuran, 2004).

2.2.1 *General assumptions*

Landslide mapping and susceptibility commonly share a set of four assumptions upon which their theoretical background and scientific validity are based. The following description

has been put together within the scientific milestone of Guzzetti F. (2006) and here synthetically recalled for clarity.

1) "Slope failures leave discernible features that can be recognized, classified and mapped in the field or through remote sensing, chiefly stereoscopic aerial photographs (Rib and Liang, 1978; Varnes, 1978; Hansen, 1984; Hutchinson, 1988; Cruden and Varnes, 1996; Dikau et al., 1996; Griffiths, 1999)".

2) "Landslides are controlled by mechanical laws that can be determined empirically, statistically or in deterministic fashion. Conditions that cause landslides (instability factors), or directly or indirectly linked to slope failures, can be collected and used to build predictive models of landslide occurrence (Crozier, 1986; Hutchinson, 1988;

Dietrich et al., 1995)".

3) "For landslides, the past and present are keys to the future (Varnes and IAEG Commission on Landslides and other Mass-Movements, 1984; Carrara et al., 1991a; Hutchinson, 1995). The principle implies that future slope failures will be more likely to occur under the conditions which led to past and present instability. Hence, the understanding of past failures is essential in the assessment of landslide hazard (Varnes and IAEG Commission on Landslides and other Mass-Movements, 1984; Carrara et al.,1991a, 1995; Hutchinson, 1995; Guzzetti et al.,1999a)".

4) "Landslide occurrence, in space or time, can be inferred from heuristic investigations, computed through the analysis of environmental information or inferred from physical models. Therefore, a territory can be zoned into susceptibility (or hazard) classes ranked according to different probabilities (Carrara et al.,1995; Soeters and van Westen, 1996; Aleotti and Chowdhury, 1999; Guzzetti et al., 1999a)".

2.2.2 *Mapping units*

A mapping unit is a portion of the earth surface that includes a set of properties different from those recognisable across a definable boundary in the adjacent units (Carrara et al., 1995; Hansen, 1984; Luckman et al., 1999; van Westen et al., 1993, 1997). In susceptibility studies, the investigated area must be subdivided into mapping units and the functional areas prior to the modelling phase. The latter, will be used to define the area where the stability prediction will be reproduced and estimated over each constituent mapping unit.

An important observation by Guzzetti et al. (1999) and Guzzetti (2006) refine the definition of mapping unit as a domain that maximises internal homogeneity and between-units heterogeneity.

A large set of mapping unit is proposed in the literature (Carrara et al.1995, 1999; Soeters and van Westen, 1996; Guzzetti et al.1999), each depending on the criteria adopted in partitioning the area:

1) Grid cell.
2) Terrain unit.
3) Unique condition unit.
4) Slope unit.
5) Geo-hydrological unit.
6) Topographic unit.
7) Administrative boundary.

Each of these units is characterised by advantages and disadvantages (van Westen et al., 1993; Carrara et al., 1995; Guzzetti et al., 1999; Van Den Eeckhaut et al., 2005; Guzzetti, 2006; and references therein). However only a limited literature is available on the influence of different partition units for susceptibility mapping purposes (Carrara et al., 1995, 2008; Van Den Eeckhaut et al., 2009).

The most used mapping units in literature essentially pertain to the slope unit, unique condition unit, and grid cell types.

Slope units subdivide the area of interest into hydrological zones limited by divide and drainage lines (Carrara, 1988; Carrara et al., 1991, 1995, 2008; Guzzetti et al., 1999) and can be obtained either manually or automatically through specific programs.

The automatic digitization of slope units is generally preferred because of the low computational time, the objectivity of the procedure and the reproducibility of the experiments. The first attempts in reproducing slope units from high resolution Digital Elevation Models (DEMs) date back to Carrara (1988) and Fairfield and Laymarie (1991) and kept its validity until today (e.g. Rotigliano et al., 2012; Wu et al., 2013)

Unique condition unit (UCU) represent a specific combination of different classes corresponding to a set of factors that are thought to be related to the landslide activation.

The procedure to obtain a UCU involves the primary selection of suitable predictors that are subsequently reclassified into classes and ultimately crossed together to generate a set of unique combinations. The literature is also plenty of studies that demonstrate the advantages of this mapping unit, particularly when used to apply specific statistic techniques (Clerici et al., 2002; Poiraud 2014; Rotigliano et al., 2011).

The two aforementioned units partition the territory into irregular polygons. Conversely, grid cell units subdivide the whole study area into squared cells of a given side length. The applications of this unit are numerous and the principal reason for their success is to be related to the often coincident structure between the grid representing the discretised area and the raster structure of the predictors, making the research outcomes straightforward for the operators (Baeza et al 2009; Federici et al 2007; Lombardo et al 2014).

The grid cell is the mapping unit adopted to carry out all the experiments described in this thesis.

2.2.3 *Diagnostic areas*

Pike (1988) introduced the concept of geomorphic signature to define numerically describable geomorphologic features to be used for geologic hazard. In this statement he included the possibility to tailor the analysis to topographically represent different landslide processes. In other words, depending on the available pre- or –post event data, one can quantify the conditions that lead to a specific mass movement.

In a way not so different from this approach, Süzen et Doyuran (2004) before and Rotigliano et al., (2011) after, put forward the notion of seed and diagnostic areas respectively defining the regions of space that need to be recognised and quantitatively described in order to build reliable landslide susceptibility models.

The former authors proposed the concept of seed-cells as the best-undisturbed morphological conditions before a landslide occurrence to be extracted from the close vicinity of the landslide polygons.

Rotigliano et al., (2011) added a further detail to this definition, identifying as the diagnostic areas the portions of land surface that include conditions for new potential failures as

similar as possible to those where past landslides occurred. Furthermore, in order to recognise these areas similarity statistic and geomorphic criteria must be fulfilled.

The idea of spatially discriminate instability conditions over past occurrences in order to produce reliable predictions for new potential activations is a crucial step in the training phase of a modelling procedure.

Misjudgements of diagnostic areas in the training phase could directly propagate into the validation and final prediction biasing the probabilities of occurrence. Such bias could be difficult to be detected and at the same time could produce a prediction only partially related to the conditions that are strictly connected to the triggering processes.

Diagnostic areas as well as seed cells can assume different shapes, some of those available in literature correspond to the landslide typologies in Dikau et al. (1996) e.g. scarps, areas uphill from crowns and landslide areas for rotational slides; source areas and landslide areas for flows.

The regions of space cited above are generally represented by irregular polygons, however, diagnostic areas can also have regular morphology.

In the present thesis a circular diagnostic area has been adopted for several experiments.

2.2.4 *Presence-absence and presence-only approaches in landslide susceptibility studies.*

When performing any presence-absence predictive algorithm in order to assess the landslide susceptibility of a given area one of the fundamental step is represented by the selection of locations where instability and stability conditions are expressed. These locations enter into the modelling procedure allowing the applied predictive model to discriminate between the two binary cases, namely landslide occurrences (pos) and landslide absences (neg). The international literature still debates whether the actual number of unstable cases should be balanced by a corresponding number of stable ones. For the specific case of Binary Logistic Regression studies part of the community suggests to use an equal number of pixels for landslide and no landslide areas (Suzen and Doyuran, 2004b, Yesilnacar and Topal, 2005; Nefeslioglu et al., 2008a, b). Conversely, there are many scientific contributions with unequal proportions of positives and negatives (Atkinson and Massari, 1998; Guzzetti et al, 1999; Dai and Lee, 2002; Ohlmacher and Davis, 2003; Ayalew and Yamagishi, 2005; Can et al., 2005;

Van Den Eeckhaut et al., 2006; Domínguez-Cuesta, M.J.et al, 2007; Hakan A. Nefeslioglu). The present thesis has been structured using a proportionate number of binary cases. The choice of negatives is a methodological aspect pertaining to presence-absence methods, however a minor category of algorithms base their prediction only upon the presence information such as GARP (Stockwell and Noble, 1992; Stockwell and Peters, 1999) and MAXENT (Phillips et al., 2006; Phillips and Miroslav, 2008; Elith et al., 2010). These algorithms are generally used in ecology rather than earth sciences but recent studies, even in comparative contributions, proved the effectiveness of the presence-only approach for landslide susceptibility assessment. In the present doctoral thesis the maximum entropy approach was selected to model the landslide scenario of Giampilieri 2009.

3 STUDY AREA

3.1 GEOMORPHOLOGICAL SETTING OF THE AREA

The present work has been developed taking as study case the landslide disaster occurred on the first of October 2009 in the area to the south of the Messina municipality (Italy). The catchments that exhibited the widespread failing response on 1st of October 2009 are located on the eastern side of the Peloritan belt (Fig. 3.1). These mountains are aligned NE to SW from Capo Peloro to the Alcantara sector and are incised from NW to SE by several narrow valleys resulting in an up-hill landscape made of steep slopes. Conversely, the downstream landscape is characterised by a continuous succession of approximately flat surfaces with variable extents. Fluvial incision dissects these flat surfaces giving rise to floodplains.

Plio-Quaternary uplifting (Catalano and De Guidi, 2003; Catalano et al., 2003; Di Stefano et al., 2012; Tortorici et al., 1995), due to tensions along the principal fault alignments linked to the Tyrrhenian Basin opening, modified the large scale topography of the area, contributing to the rough aspect of the area.

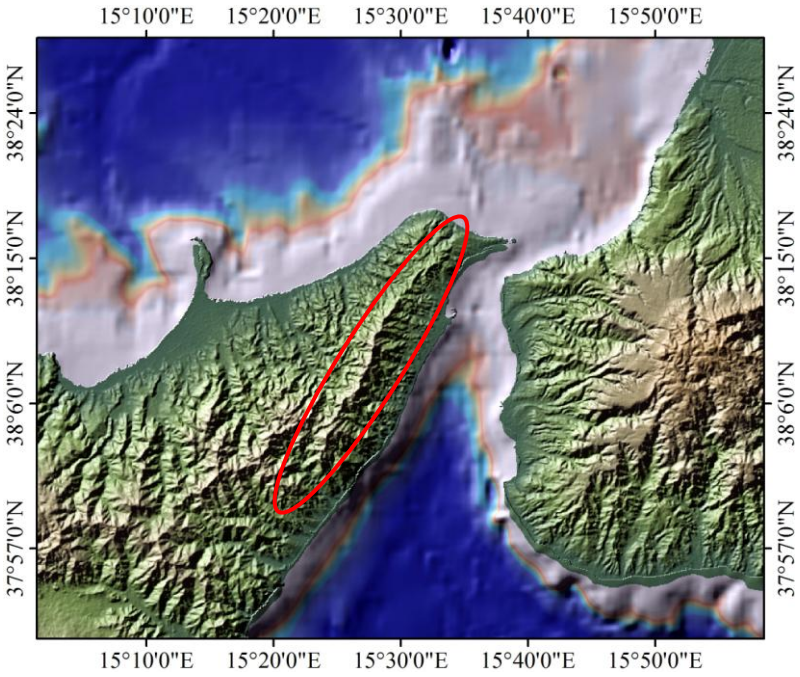

Figure 3.1 - Peloritan Belt.

3.1.1 *Hydrography*

The streams that drain the eastern slopes of the Peloritan ridge, which are locally known as "fiumare" (Casalbore et al 2011; Sorriso-Valvo and Terranova, 2006), are characterised by torrential regimes. The primary streams on the Ionian side of the Peloritani are the Fiumara S. Filippo, Fiumara Larderia, Fiumara Briga, Torrente Fiumedinisi, Torrente Torrente Giampilieri, Pagliara, Torrente Savoca, Fiumara d'Agrò, Torrente Letojanni and Fiume.

The climate in the area is typically Mediterranean, being characterised by rainfall of short durations and high intensities during the wet season (Aronica et al., 2012). The seasonal variability exposes the territory to greater precipitations from October to February, whilst the remaining months are characterised by low values with the minimum rainfall between June and July (Fig. 3.2).

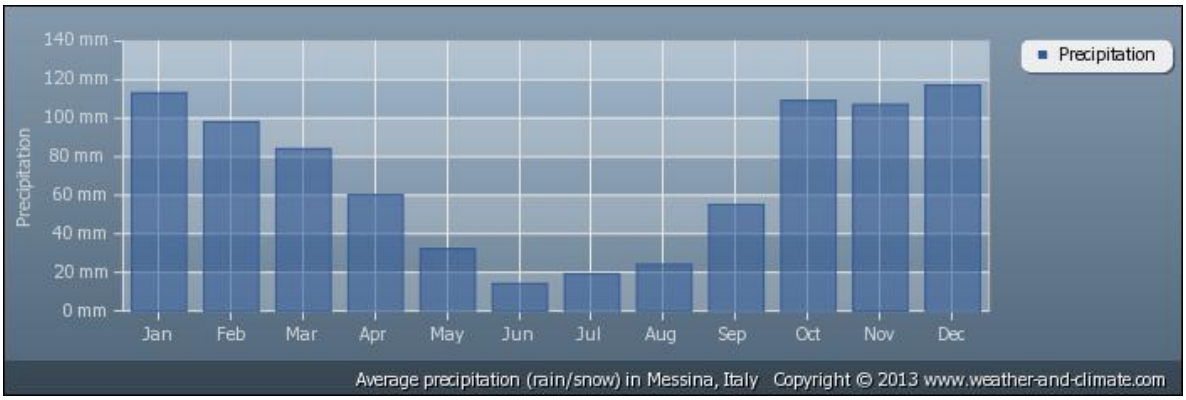

Figure 3.2 - Yearly average precipitation in Messina.

During the wet months the magnitude of the precipitation is bounded to approximately one hundred of mm/month whilst on the other hand poor or absent discharges are recorded during the summer.

The discharge along the channels is fed by water from local springs that in most of the cases are not collected for anthropic purposes.

All the fiumare have a torrential behaviour, however, the benefit from the spring water supplies either directly into the flows or as a form of hypodermic hydrogeological fluxes can quite last the effect of the precipitations.

The hydrographic network in the Ionian side of the Peloritan Mounts shows (Fig. 3.3) those diagnostic features that are typical of recently uplifted areas. The stream incisions are all aligned at approximately 90 degrees with respect to the coastline. The path from the ridge to the outlets is essentially straight with a limited length of around five to ten kilometres, increasing from the north to the south sectors of the ridge.

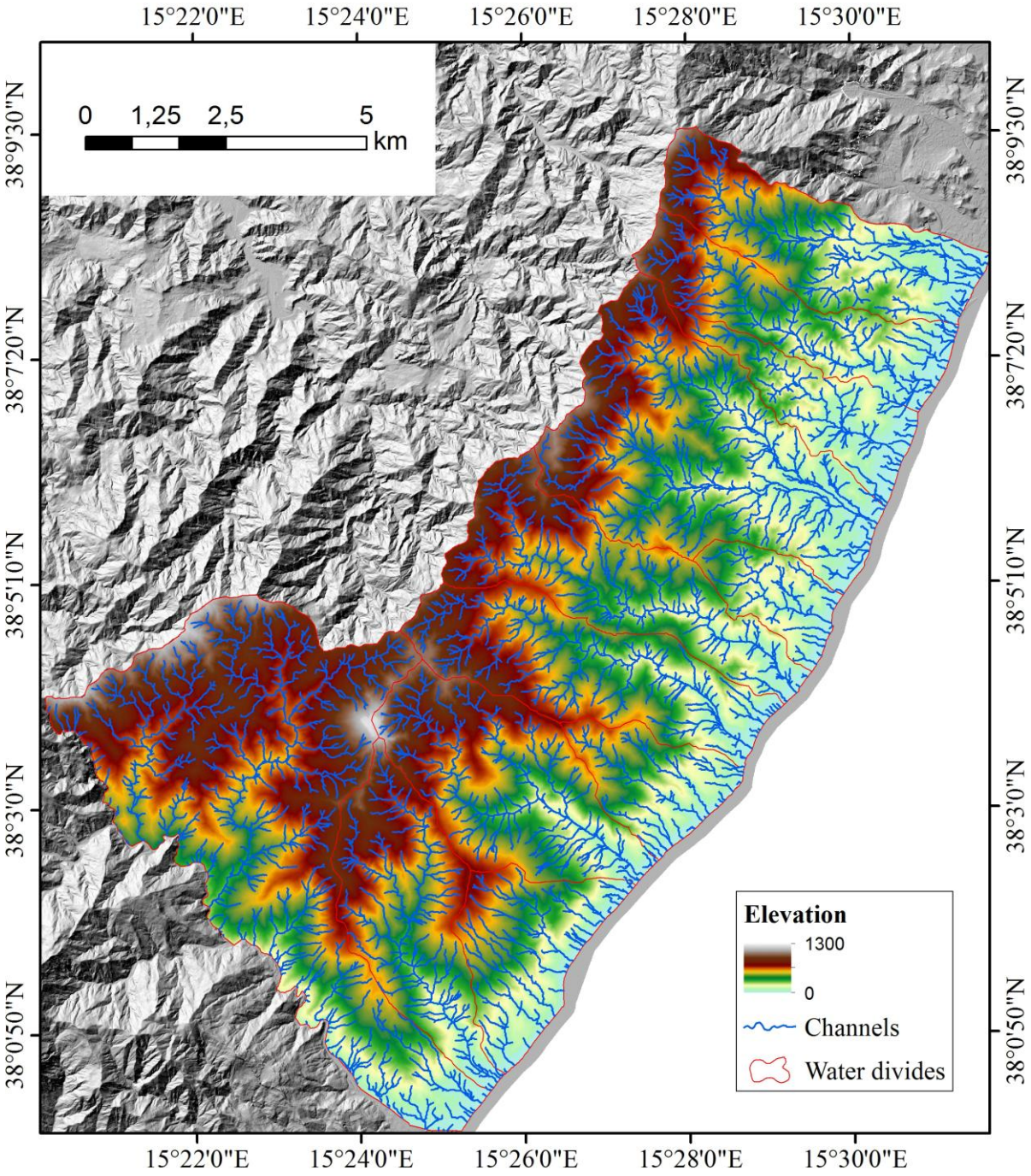

Figure 3.3 - Hydrographic network within the study area.

Common morphologic features are shared among the different fiumare, with highly steep thalwegs, narrow channels enclosed by rocky slopes on the highest portions becoming wider and filled by alluvial sediments on the lowest ones.

Differences between high and low sectors of the basins are also reflected into the sub-catchments morphology, with widths increasing with the height.

Two catchments, among those which were involved on the 1st October disaster, have been selected to run several experiments. These catchments include the hydrographic units of the Briga and the Giampilieri streams, coinciding with the centre of the area that endured the greatest damage. These two steep basins both extend approximately for 10km^2 draining south-eastward to the Ionian Sea, being characterized by a similar morphology marked by asymmetric main valleys (Fig. 3.4). They both have an average width and length of ca 1.6 km and 6.5 km respectively, including areas having altitudes ranging from approximately 1050 m.a.s.l. to sea level.

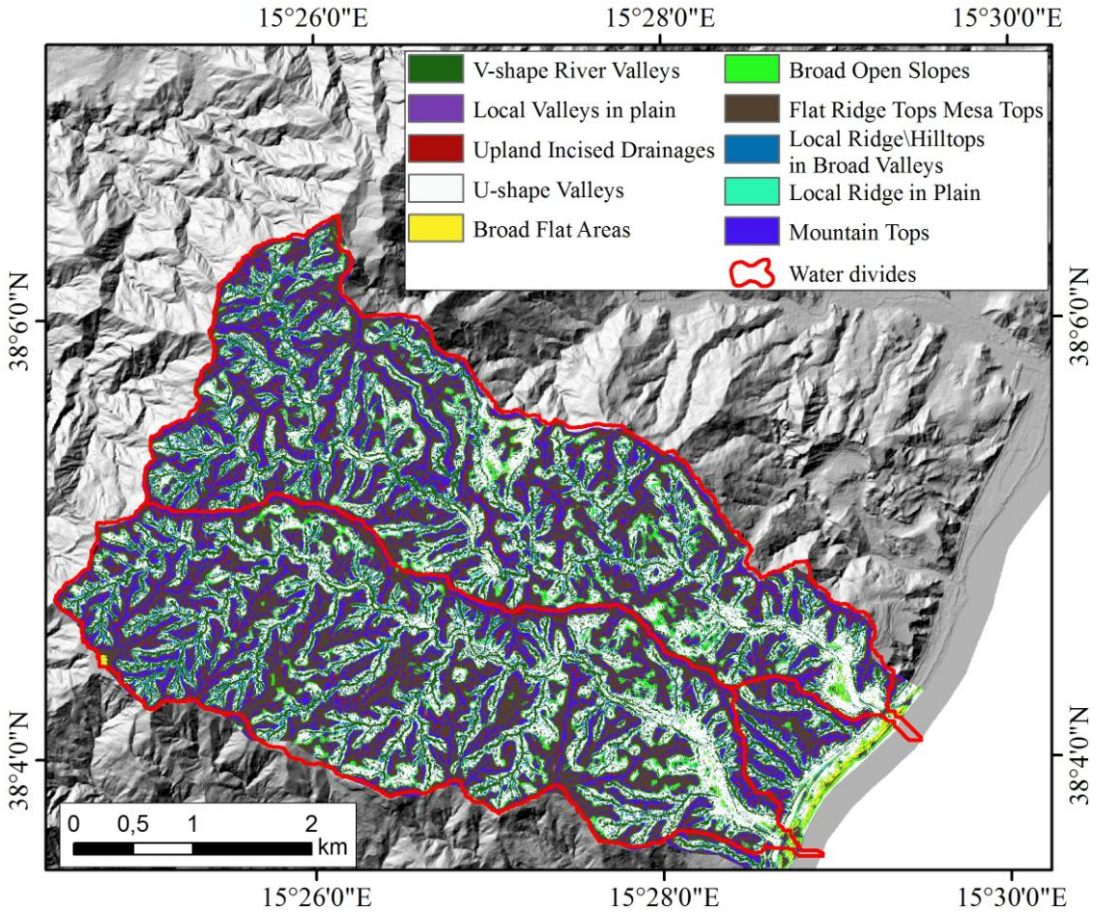

Figure 3.4 - Landform classification of the study area.

3.2 GEOLOGICAL SETTING OF THE AREA

The Peloritani Thrust Belt is located in the southern sector of the Calabrian Arc (Messina et al., 2003) constituting a stack of crystalline basement nappes that subdued a

complex tectono-metamorphic evolution over the geological times. The whole Peloritani Thrust Belt is included between a Hercynian basement and a seal of late-orogenic clastic sediments, corresponding to the Stilo–Capo d'Orlando Formation (Bonardi et al., 2003). The peri-Mediterranean area originated from the late Miocene juxtaposition of two different terranes (Bonardi et al., 1980, 2001) during the Alpine compression. Vitale and Ciarcia (2013) recently calculated the thrust front velocities and subdivided the orogenic evolution in five main kinematic stages each one characterised by different velocities.

Seven Alpine units constitute the Peloritani Thrust Belt in a stack that is geometrically ordered from the bottom to the top otherwise from south to north shows (Messina et al., 2004):

- the Longi-Taormina Unit;
- the Fondachelli Unit;
- the Alì Unit;
- the Mandanici Unit;
- the Piraino Unit;
- the Mela Unit;
- the Aspromonte Unit.

Many tectonic units corresponding to the pre-Alpine basements consist of epimetamorphic rocks, ranging from anchizone (Longi-Taormina Unit) to low-amphibolite facies (Mandanici Unit). Conversely, medium to high grade metamorphic rocks are recognisable only in the Aspromonte and Mela Units (Bonardi et al., 2003).

The landslide phenomena that affected the study area on the 1 October 2009, mostly involved part of the shallow (0.5-2.5m thick) weathered layer of the lithologies pertaining to the aforementioned Mandanici, Aspromonte, and Mela Units (Fig. 3.5). The rocks corresponding to these Units broadly outcrop in the southern portion of the Messina municipality and can be summarised into:

- phyllites of the Mandanici Units;
- paragneiss and micaschists of the Mela Units;
- gneiss and paragneiss metamorphic rocks of the Aspromonte Units.

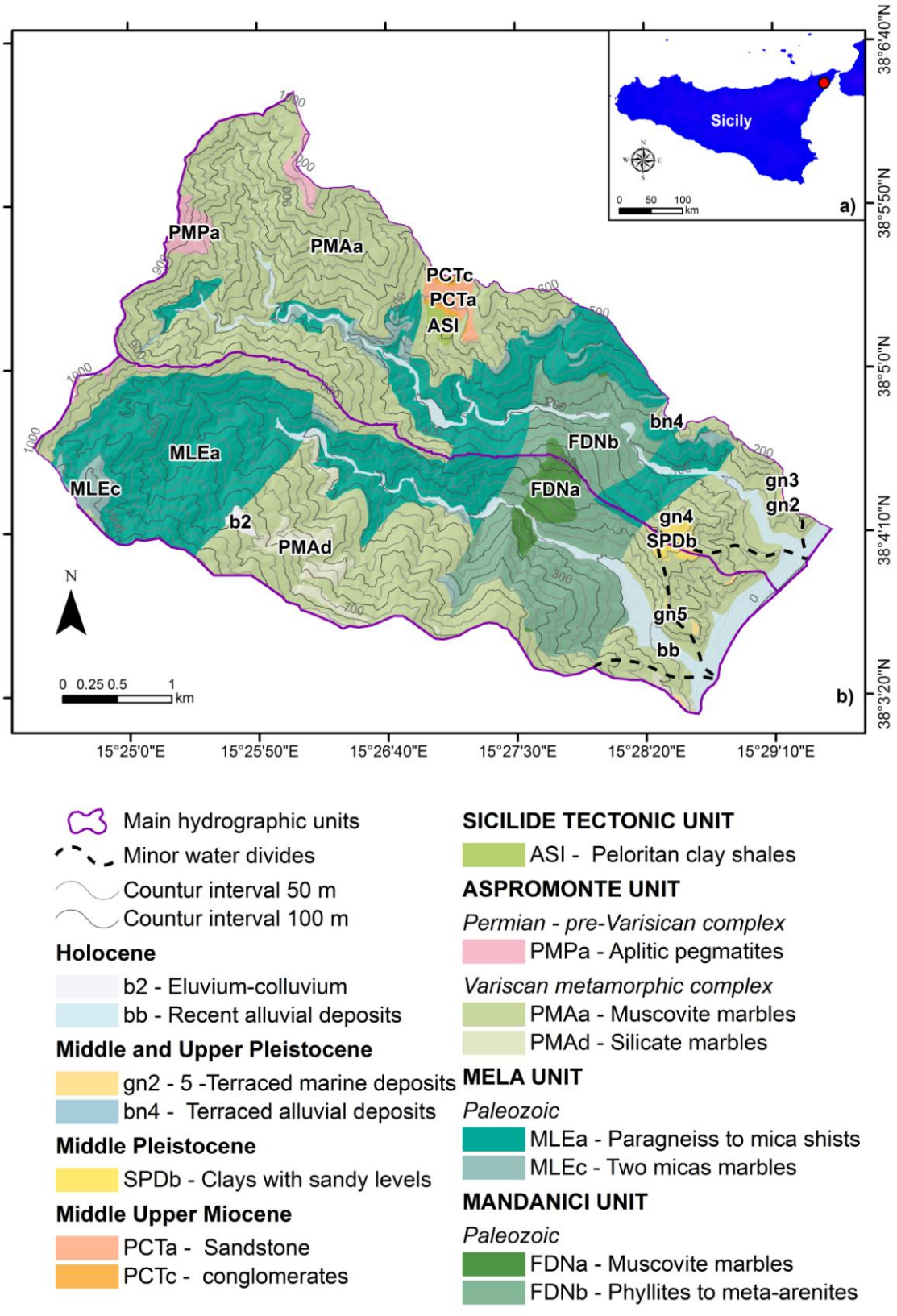

Figure 3.5 - Geological map of the study area.

The Mandanici Unit is known (Messina A., et al., 2004) as a Varisican metamorphic basement made of phyllite, metarenite, quartzite, marble, porphyroid and amphibolite schist, overlying the Paleozoic level of greenschist and amphibolite facies.

The Mela Units are made of Eo-Varisican eclogite facies metamorphites (paragneiss, micaschist, eclogite and marble Palaeozoic) re-equilibrated into Varisican amphibolite facies (kyanite-staurolite-garnet zone) to greenschist facies (albite-andalusite zone).

The Aspromonte Units belong to an old pre-Hercynian basement on which terrigenous sediments were deposited from the Cambro-Ordovician to the Carboniferous (Ferla, 1994). During the Hercynian orogenesis these rocks were reworked, undertook greenschist-facies metamorphism, and exhibited ductile deformations (Platt &/and Compagnoni, 1990).

Structural features in the study area are represented by S–SW-verging Cambrian to Aquitanian thrusts and syn-orogenic low-angle normal faults (Somma R., et al., 2005; Somma R., 2006). The Mandanici Units, in particular, are characterized by Alpine deformation cycles. Giunta and Somma (1996) identified four Alpine ductile deformation phases, showing a very complex structure characterized by two structural sets. The structurally uppermost group was formed by several tectonic slices, while the lowermost one by numerous duplexes.

3.3 THE CATASTROPHIC EVENT OF MESSINA 2009

On the first of October 2009, an Extreme Climatic Event (ECE) struck the Messina area resulting in 250mm of rain in just 8 hours (Fig. 3.6), as recorded at a foothill rain gauge located in the S. Stefano Briga territory.

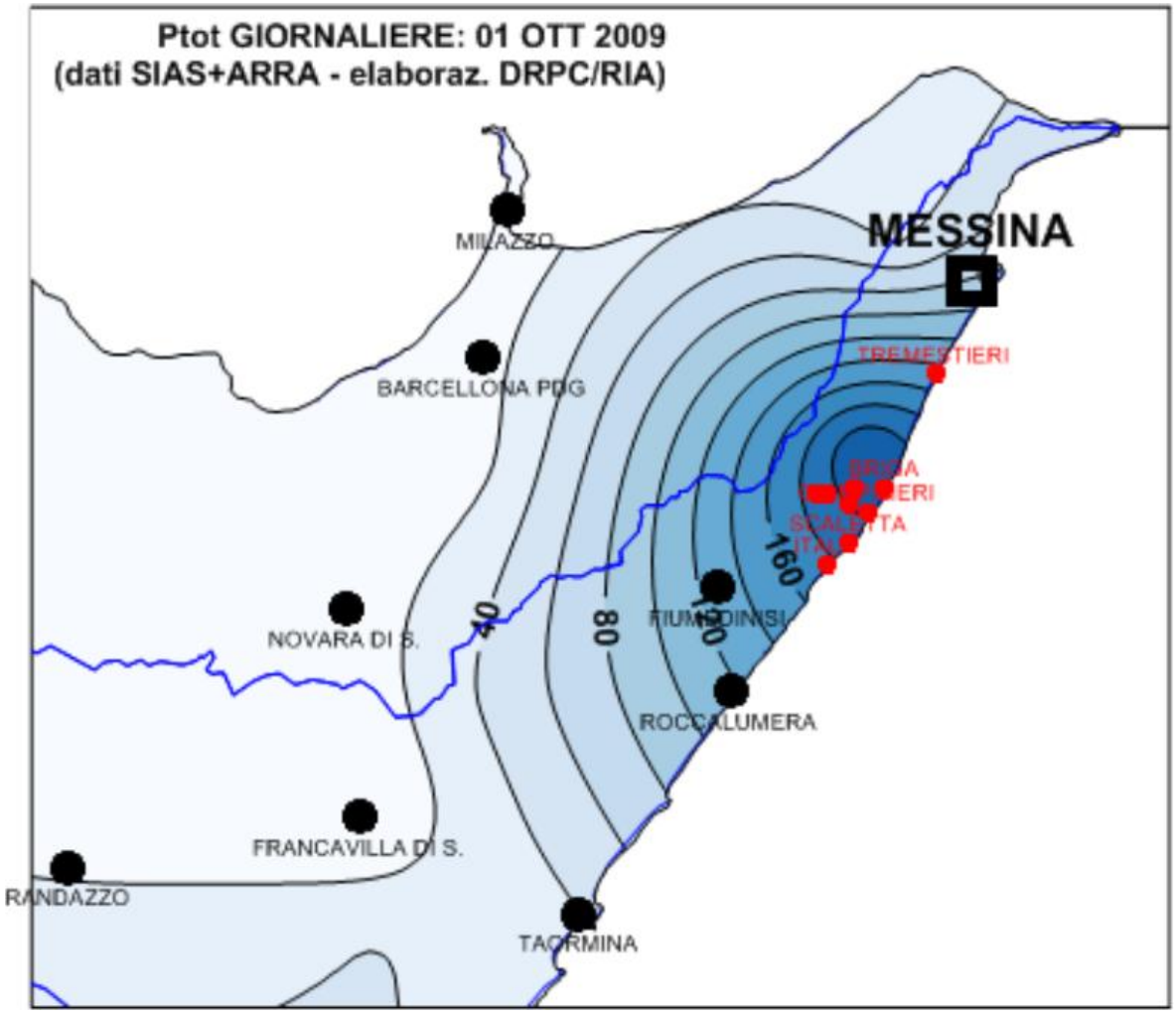

Figure 3.6 - Daily precipitation recorded on the 1st October 2009.

In particular, this amount of rainfall cumulated to that of two previous (Fig. 3.7) events (16/09: 75mm; 23/09: 190mm) for a total amount of more than 500mm in less than two weeks. The discharges antecedent to the disaster already reached values three or four times greater than the average monthly precipitation in the study area (Fig. 3.8) actively contributing to the saturation of the soil cover.

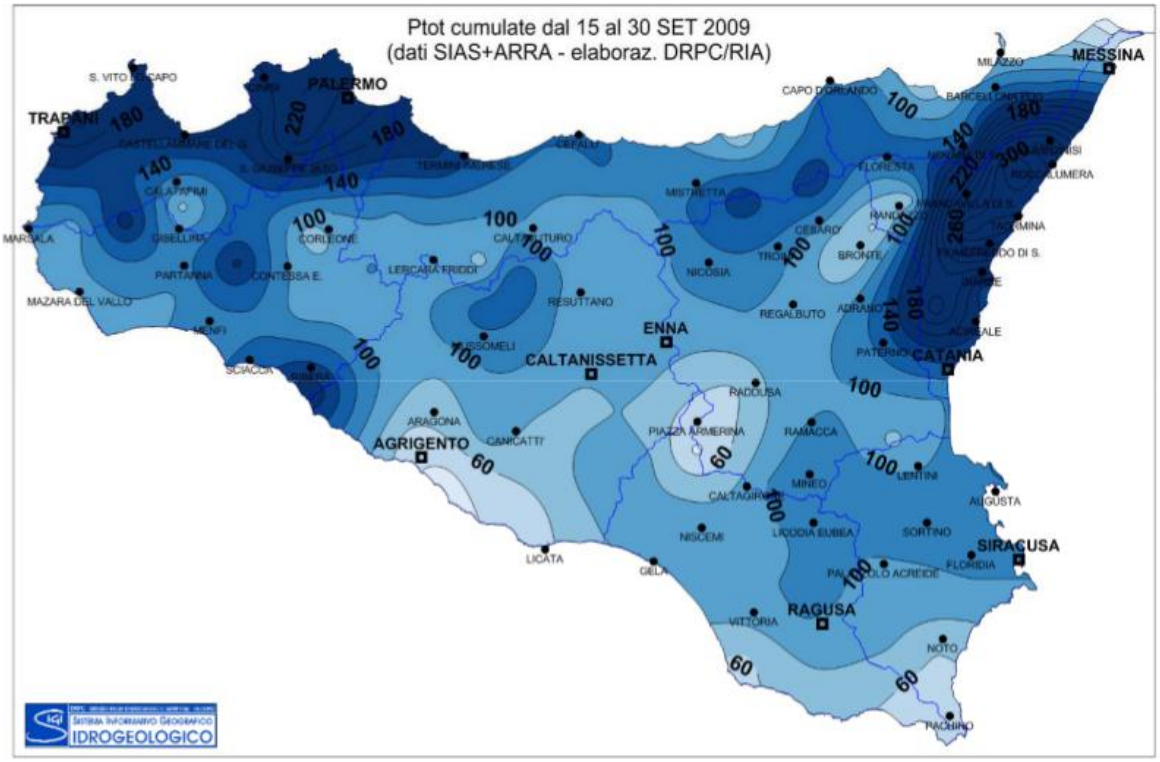

Figure 3.7 - Cumulated rainfall between the 15th and the 30th of September 2009.

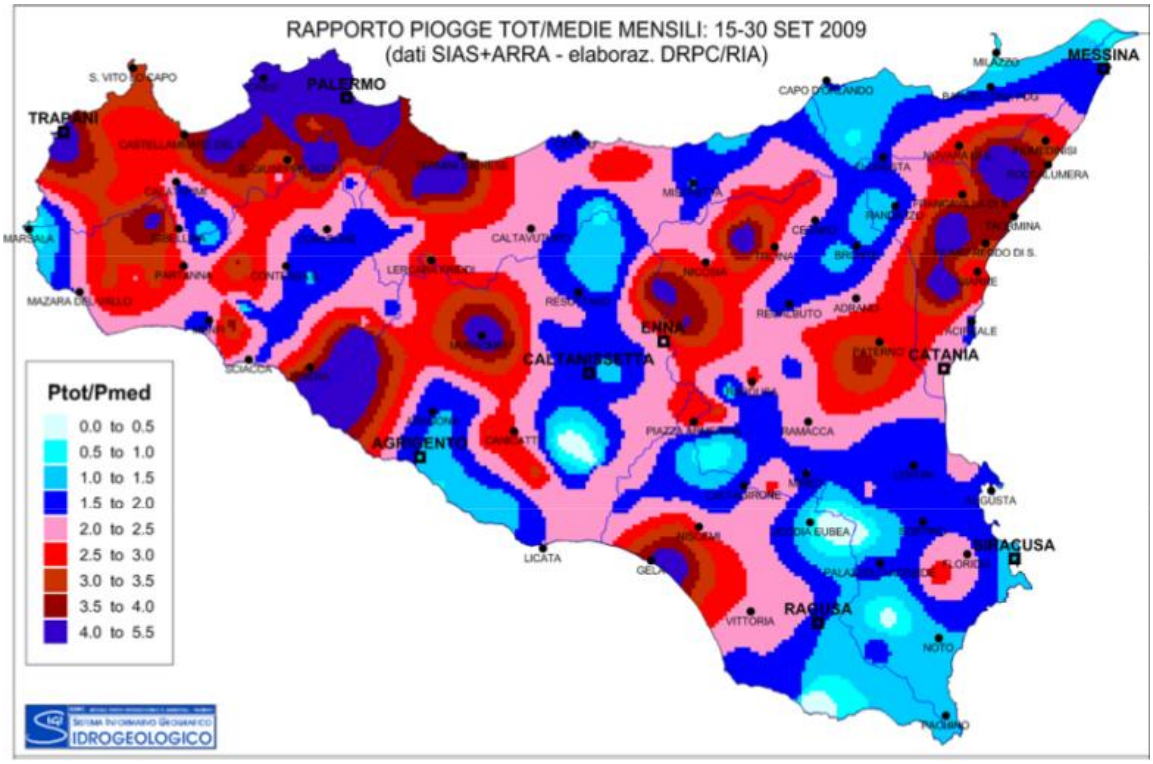

Figure 3.8 - Map showing the ratio between the cumulated rainfall between the 15th and the 30th of September 2009 and the average monthly rainfall.

By comparing the 2009 ECE to the 30-years average monthly rainfall, it is evident its anomaly (Fig. 3.9). The epicentre of the ECE included several villages to the south of the city of Messina, such as Giampilieri, Scaletta Zanclea, Altolia Superiore and Molino and all of them endured severe damages on the day of the disaster. In fact, in the time-lapse of only about five hours thousands of landslides triggered in the whole region exposed to the ECE.

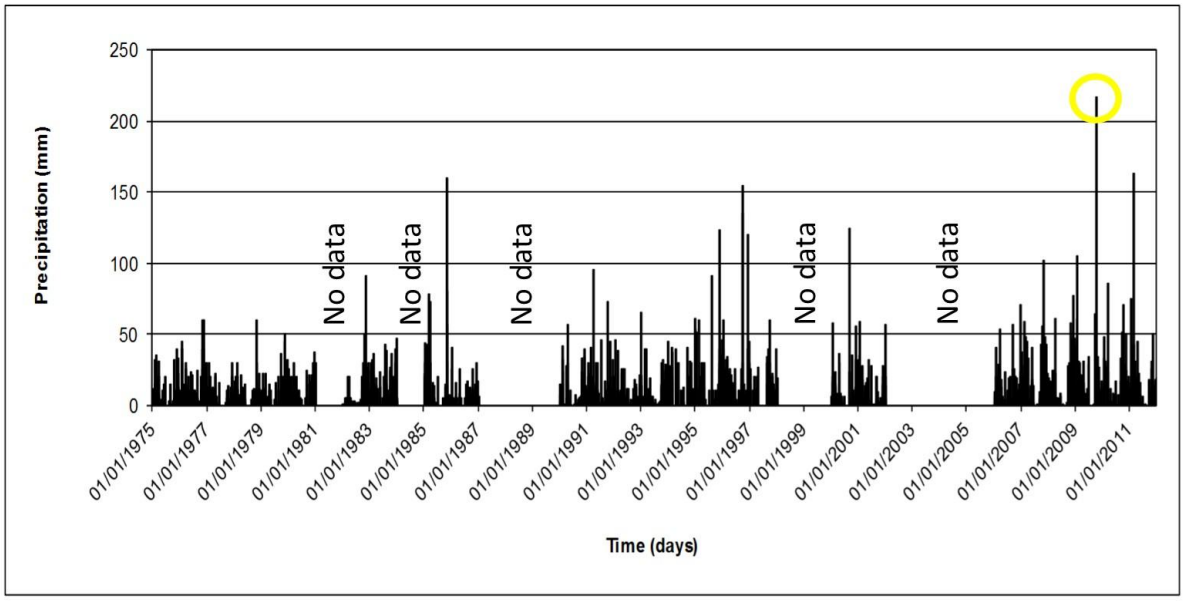

Figure 3.9 - Thirty-year record of daily rainfall for the Briga rain gauge.

The impact of the widespread failures caused thirty-seven (+1 still missing) victims, injured more than one hundred, and more than half million Euro of structural damage.

The magnitude of the disaster and the lack of comparable past events serve as a local example of the potential impact of climate changes in the Mediterranean region (Agnesi et al., 2009; Aronica et al., 2012; De Guidi and Scudero, 2013; Del Ventisette et al., 2012).

Several researches have been published so far in order to fully understand what happened on the day of the tragedy from many different points of view (Ardizzone et al., 2012; Aronica et al., 2012; Casalbore et al., 2011; Lombardo et al., 2014; Penna et al., 2014; Reichenbach et al. 2014).

For example, in their contribution Aronica et alii (2012) investigated the event using observed data from the raingauge network. They were able to assess the magnitude of precipitation focussing their effort in modelling the main trigger of the mass movements that

took place in village of Giampilieri. In this contribution the remarkable intensity of this storm was highlighted, especially as a function of the spatial concentration, with values of rainfall greater than 200 mm in less than 4h and a peak of about 120mm/h in 10’ only for the Giampilieri catchment.

These quantities largely diverge from the local trends and owed their exceptionality due to a auto-regenerating convective cell trapped in the Peloritan relief (Fig. 3.10, Regional Department of Civil Protection for Sicily).

Further details on specific mass movement behaviours, classes and materials involved, please see Chapter 4.

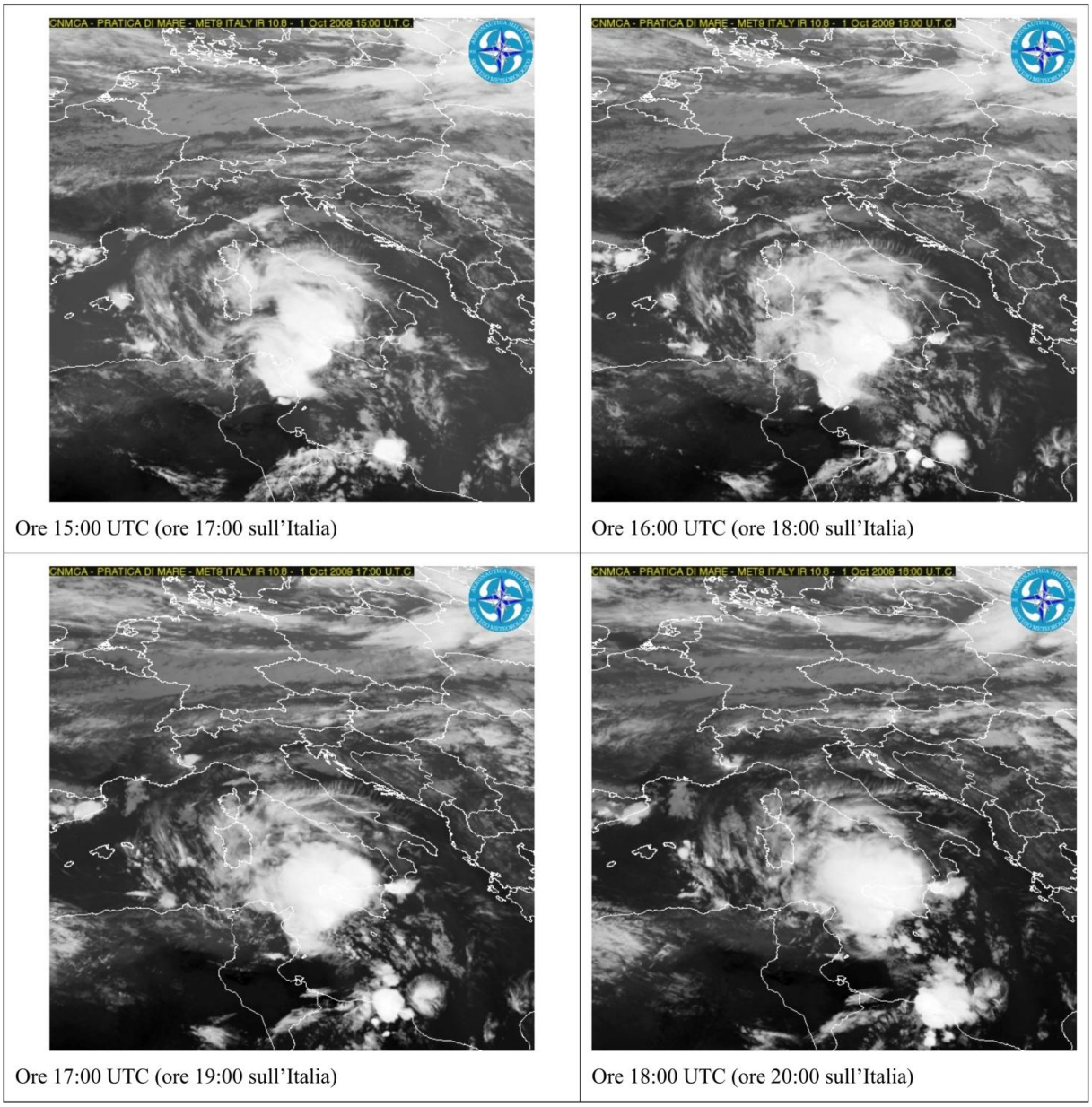

Figure 3.10 - Regional Department of Civil Protection for Sicily, images acquired on the 1st October 2009.

4 DATA

4.1 LANDSLIDE INVENTORY

In order to lay the foundation for this whole research a landslide archive has been built beforehand on the basis of both remote and field surveys.

Field surveys were carried out soon after the event of Messina, between the second and the fifth of October and subsequently in November 2009.During the fieldwork, landslide maps were drawn where geomorphological features were mapped such as crown morphology and topographic position, track incision, runout intersection with the hydrographic network, and size of the transported materials.

Remote landslide recognition was performed on parallel by comparing pre- and post-event images of the area, taken from Google Earth™ and from the catalogue of ARTA (Assessorato Territorio e Ambiente – Regione Sicilia).

The landslide archive of the disaster was built by subtracting –pre 2009 event landslides from the –post, isolating in this way the new activations, which were further refined with the collected field data.

The final archive includes 871 and 1121 debris flows/debris avalanches landslides (Hungr et al., 2001; Hungr et al., 2005) for the Briga and the Giampilieri catchments respectively.

A second landslide archive has also been obtained to cover the whole sector of the Messina municipality that was exposed to the extreme climatic event on the 1 October 2009. The approach also in this case, included the isolation of the 2009 data by subtracting pre- and post- event landslides; however, the second archive was built only through remote sensing recognition due to the total size of the area.

On the basis of the landslide survey, including the whole stricken area, two main movement typologies have been recognised (Fig. 4.1), depending on the reconstructed propagation phase: (i) debris flows, which are characterised by the channelling of the moving mass along the topographic plan concavities downhill to the first- second-order drainage axis, frequently producing a typically funnel-shaped geometry; and (ii) debris slide/avalanches, with a less effective topographic control, which propagate more rectilinearly on slopes producing

triangular or rectangular shapes. Both of the landslide typologies generally activated as pure slides or flows movements modifying their kinematics in the propagation phase, depending on the source volume and the morphologic features of the slopes (steepness, plan curvature and runoff drainage network).

Figure 4.1 - Landslide activations.

Due to the hydro-morphological features of the area, very rarely were the bottoms of the valley open enough to allow the landslides to form a fan in their run out zone, more frequently having conditions for feeding debris flood phenomena in the main stream bed (Fig. 4.2).

Figure 4.2 - Material transported across the slope to intersect the river network.

The main geo-hydrological triggering mechanism was the rapid saturation of the soils which led to the increasing of the pore water pressure and weight creating the condition, for single landslides to activate slope failure mechanism, when the threshold value of the safety factor was overcome (Iverson, 1997). In some cases, the landslide trigger was due to intense water erosion acting at the foot of the slopes or to effective piping at the interface between the weathered layer and the bedrock. Multiple converging debris flows were frequently observed, demonstrating the important role that lateral coupling effects have played in their simultaneous triggering (Fig. 4.3).

Figure 4.3 - Interacting mass movement example.

On the field, it was very evident the very limited depth of the deformed volumes, which in the depletion zone reached just few decimetres. This thickness rose for debris flow types up to few meters within the track, due to the high erosive power of the moving mass. The material involved in the initiating movements mainly derived from the weathered eluvial/colluvial layer of the outcropping lithologies; debris flow phenomena eroded and also transported coarser debris and boulders, during the propagation phase.

Another important role in causing the failures was played by the local lithologies was also well-rendered at the crowns of most landslides. Due to the medium to high metamorphosed rocks characterising the area, schistosity planes with beddings parallel or sub-parallel to the slopes acted as a favourable discontinuity for instability conditions, especially for the debris-slide cases.

In spite of the shallowness and the limited extensions of the landslides, the severe damage scenario which resulted is to be related to the convergence from the source areas downward along limited flow paths or tracks, which frequently cross the urban structures (houses, buildings, roads) of the villages (Fig. 4.4).

Figure 4.4 - Multiple converging landslides intersecting settlements.

A few larger slides and falls were also observed, whose modelling was beyond the scope of this thesis.

Focussing on the primary catchments taken into consideration within the present thesis, statistics have been produced exploiting the detailed fieldwork and the joint remote mapping. In particular, the total area involved in the widespread landsliding process extends for 293,000m^2 (Briga) and 334,000m^2 (Giampilieri), with landslide average surface of 340m^2 and 435m^2 respectively (Fig. 4.5), revealing that the Giampilieri catchment shows a higher landslide density and frequency.

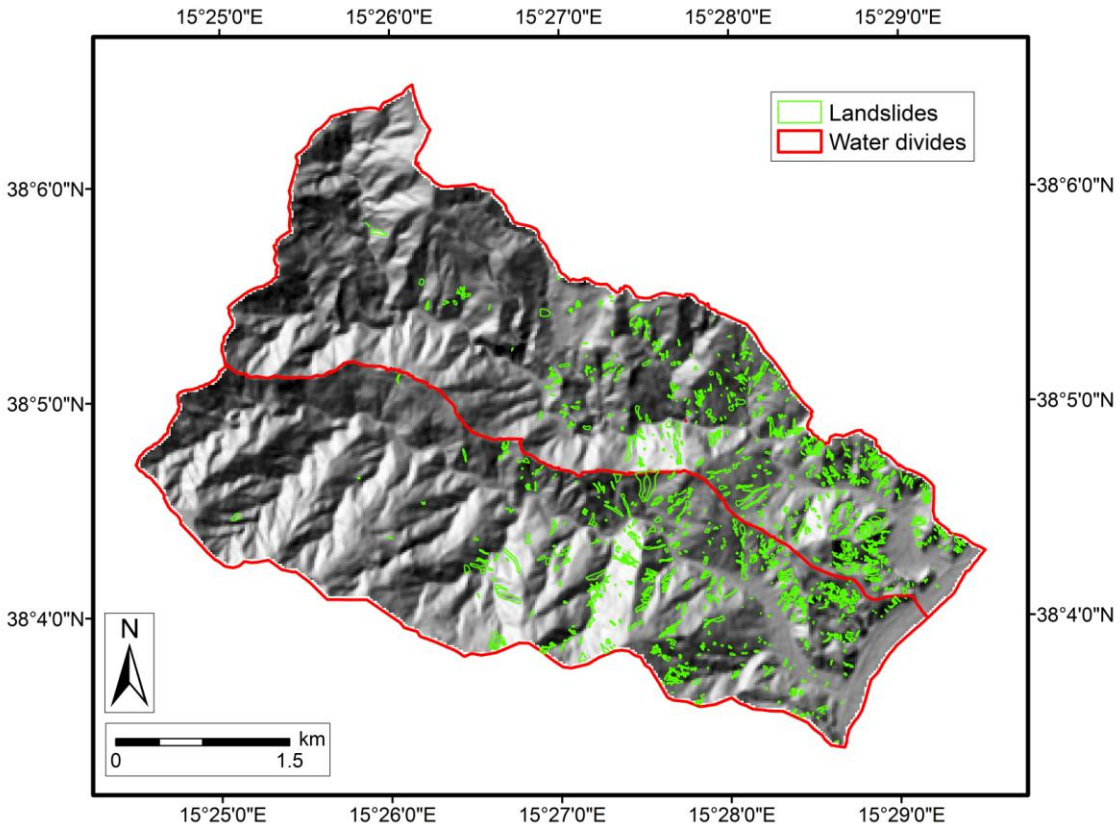

Figure 4.5 - Landslide map of the two study catchments.

It must be noted that landslides are more concentrated in the lower portion of the two catchments, probably due to the main moving direction of the storm (Aronica et al, 2012; Regional Department of Civil Protection of Sicily, 2009) which was advancing from the sea toward the inner sectors. Another explanation could be related to geological control on the landslide distribution which will be discussed in more details in chapter 5.

On the basis of the landslide recognition, some morphometric and kinematic features have been classified: initiation movement typology and slope position, run-out slope position, channelling, maximum depth along the track (Fig. 4.6).

In the Briga catchment, pure debris flows (76.69%), subordinately channelled (48.91%) and reaching the foot of the slopes only in few cases (24.11%), prevail. Differently, landslides in the Giampilieri catchment, mainly consisting of pure debris flows (73.50%), after channelling (74.22%) have reached the slope foothill (68.24%). For both of the catchments, the movements mainly triggered from the intermediate portion of the slopes (Briga: 83.80%; Giampilieri:

79.66%). As regarding to the maximum depth of the incised track, three classes have been distinguished. Data shows a higher erosive power for the flows in Giampilieri (86.08% more than 0.5m deep), with respect to Briga (28.93% less than 0.5m deep).

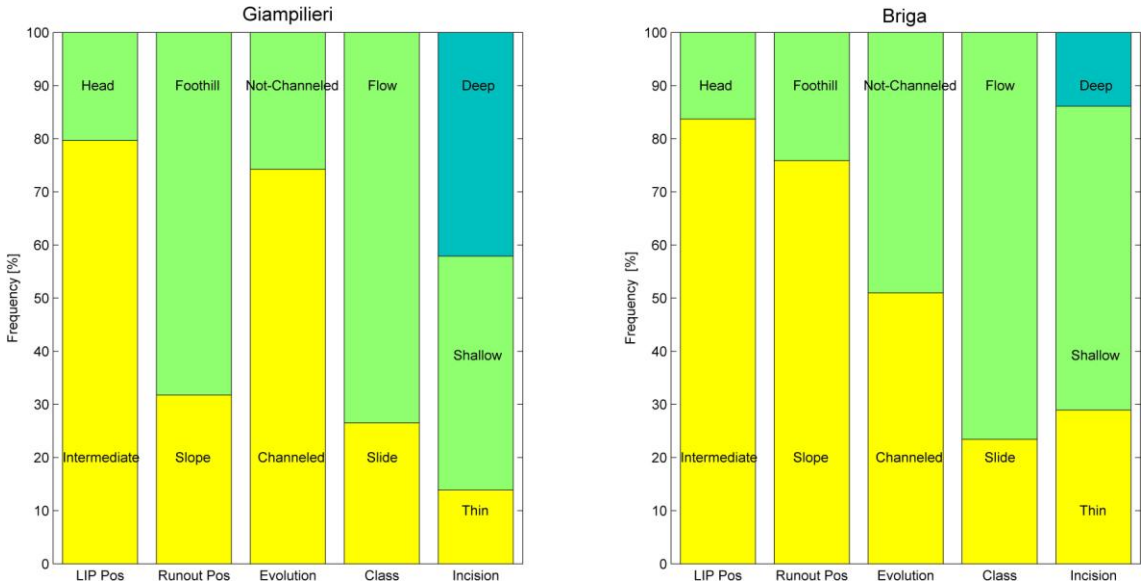

Figure 4.6 - Landslide kinematic attributes.

In this research we used the available archive following two approaches: in most of the experiments the whole landslide inventory has been processed as one, no matter the initiating source phenomenon (pure slide or flow) from which debris flow or avalanche evolutions derived. We assumed in fact that with respect to the selected predictors used for most of the analysis, none if any difference between slides and flows initiation would arise. The predictive models obtained through this approach refer uniquely to the activation phase and the derived maps "simply" try to depict where slides or flows are likely to initiate, possibly giving the trigger downslope to debris flow or debris slide/avalanche phenomena propagations.

The second approach aimed at compensating the lack of the first one. As a result, models have been built to predict the two major landslide classes activated during the 2009 event, namely debris slides and debris flows (Hungr et al. 2014). In order to do so, a new set of predictors has been used for the specific purpose including the mineral composition of the shallow blankets of weathered materials. In this experiment, we assumed that the composition of the superficial mantle could generate a different response in activating different types of mass movements.

4.2 DATA FROM THE LASU PROJECT.

The present thesis fits within a wider research framework between the University of Palermo and the regional institution that manages the environment and territory in Sicily (Italy), ARTA - Assessorato Territorio ed Ambiente - Regione Sicilia. The SUFRA or LASU (LAndslide SUsceptibility) project represents the final outcome of the relationship between these two institutions allowing the academic component to access high quality data in exchange of state-of-the-art scientific applications to assess the landslide susceptibility at different scales within the Sicilian region.

Thanks to the LASU project, several data regarding the area of Messina have been acquired and exploited throughout the present research:

- Orthophotos recorded after the disaster, from 6 to 19 October 2009 (Italian Civil Protection), with a spatial resolution of 0.15m and geo-referenced in UTM33/WGS84.
- Post-event Digital Elevation Model (D.E.M.) acquired simultaneously to the aforementioned orthophotos with a overall coverage of 22km, a horizontal accuracy of 0.4m, and a vertical accuracy of 0.15m.
- Ortofoto 2006/2008 (A.R.T.A.) recorder by the "Assessorato regionale territorio e ambiente" or the regional institution for territory and environmental management, with a spatial resolution of 0.25m.
- CTR 1:10000 (A.R.T.A.) 2006/2008 topographic maps provided by the "Assessorato regionale territorio e ambiente" or the regional institution for territory and environmental management.
- Pre-event Digital Elevation Model (D.E.M.) provided by the "Assessorato regionale territorio e ambiente" or the regional institution for territory and environmental management, with a horizontal resolution of 2m and a vertical resolution of 0.17m.

4.3 DEM DERIVED ATTRIBUTES

The modelling procedures have been supported throughout this research by including independent variable obtained from terrain analysis. The pre-event HRDEM provided by the Sicilian institution for territory and environmental management has been processed to derive

primary and secondary attributes. The landslide susceptibility literature is rich of articles that adopted topographic attributes as causative factors for shallow landslides. In the present research the following list of basic topographic predictors has been used for modelling purposes with a 2m cell spatial resolution:

- HEIGHT: expresses the elevation of each grid cell, this is the original information from the HRDEM.

- SLO: slope steepness, measures the rate of change of elevation in the direction of steepest descent (Wilson and Galland, 2000) thus expressing the slope steepness. Nine different algorithms are available in literature in order to produce slope maps from digital elevation models (Rodríguez and Suárez, 2010). The slope used in the present research had been computed through the Neighbourhood Method (Burrough and Mcdonell,1998). This technique is employed by both Arc/Info GRID (ESRI, 1995) and GRASS (Geographical Resources Analysis Support System) (CERL, 1988) and uses a moving three by three mask over a DEM to predict slope for the centre cell from its eight neighbours (Dunn and Hickey, 1998). The units of the slope steepness can be expressed in two ways, the first one correspond to the angle, either in degrees or radians whilst the second is the percent of slope.

- ASP, slope aspect, is the direction of steepest downwards slope from each cell to its neighbours and can be thought of as the slope direction. The angle is a compass bearing (Wilson and Galland, 1996). Using a grid-based DEM, the common approach is to use a moving 3x3 window to derive finite differential or local surface fit polynomial for the calculation (Skidmore, 1989; Florinsky, 1998a, b). The units of the slope aspect are typically expressed in degrees, with a domain limited between zero and 360.

- TWI, Topographic Wetness Index, is the natural logarithm of the upslope area draining through a certain point per unit contour length divided by the local slope, following the idea of Beven and Kirkby (1979). It expresses the topographic effect on soil moisture. For this reason it has been extensively used to study spatial scale effects on hydrological processes (Beven et al., 1988; Famiglietti and Wood, 1991; Sivapalan and Wood, 1987; Siviapalan et al., 1990) and in case of landslide susceptibility researches it is one of the most common proxy causative factors in the scientific literature (Conforti et al., 2014; Iovine et al., 2014). The units representing the topographic wetness index are dimensionless and the interpretation of this parameter distribution correspond to a general increase of the soil moisture as a function of the increase of the values that the parameter expresses across the area.

- SPI, Stream Power Index, is a proxy variable for the stream power or the energy of the flowing water expended on the bed and banks of a channel. It is calculated as the natural logarithm of the catchment area multiplied by the tangent of the slope gradient (Florinsky I.V., 2012). Due to the direct relationship to the potential for the flowing water to perform geomorphic processes such as erosion, the Stream Power Index is a common proxy predictor in several international contributions (Pradhan and Kim, 2014; Youssef et al., 2014). The units representing the stream power index are dimensionless and the interpretation of this parameter distribution correspond to a general increase of the energy of the water flowing onto the topography as a function of the increase of the values that the parameter expresses across the area.

- FLA, Flow Accumulation, is a typical output of hydrologic modelling procedures in GIS environments and represents the number of upslope cells that flows into each cell of a given raster. Gruber and Peckham (2009) summarize the approach used in this thesis to obtain the Flow Accumulation. The concept at the base of this predictor embodies the amount of rainfall directed to a given cell from the surrounding area assuming that the flowing water does not infiltrate during its descent. Scientific contributions extensively use this variable as a proxy in alternative or addition to the flow direction (Meyer et al., 2014; Wang et al., 2012).

The units that represent the flow accumulation can be expressed as the raw number of upslope cells contributing to the target cell or, by multiplying this value by the square of the cell size. In the second case the units represent a squared length, for this reason this predictors is also known as Upslope Contributing Area (Mondal and Maiti, 2012).

- General Curvature (Fig. 4.7). The pioneer study that gave rise to this extremely useful predictor dates back to Zevenbergen and Thorne (1987). It represents the curvature of a line formed by the intersection of the surface with a plane with a specific orientation passing through this point and for this reason it is calculated as the second derivative of the elevation. The value of the curvature is reciprocal of the radius of the curve. Numerous are the applications integrating this parameter within the modelling phase for landslide susceptibility studies (Sujatha et Rajamanickam, 2011). The units of the curvature are radians per linear unit (the unit of the spatial reference of the raster) but due to the fact that generally small values are obtained from the calculation, the outcome is commonly multiplied by one hundred modifying the above statement to the change of the orientation resulting from travelling one hundred linear units along the respective line.

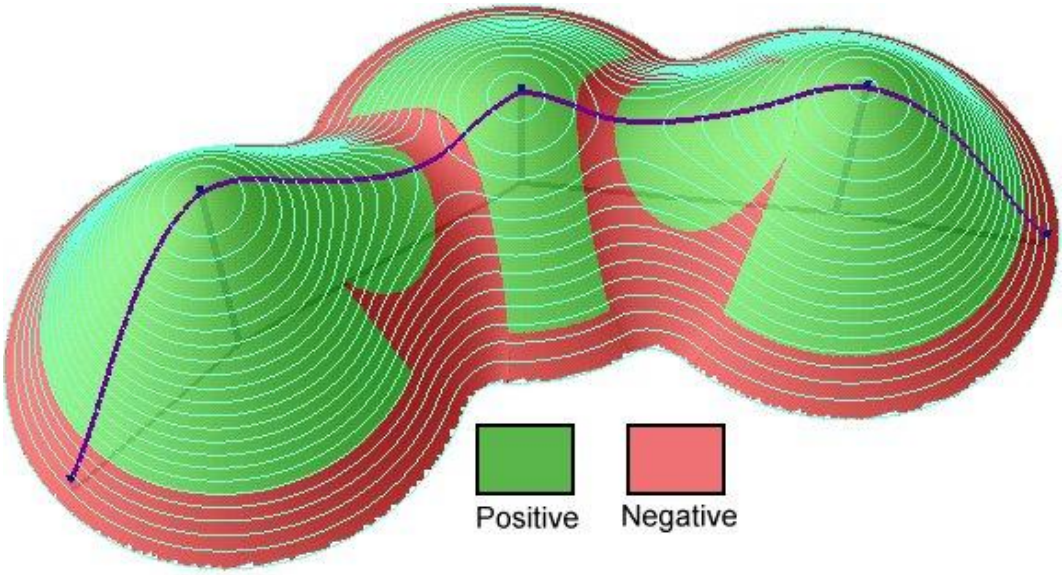

Figure 4.7 - General topographic Curvature

- Profile Curvature (Fig. 4.8), represents the curvature of the surface in the direction of the steepest slope (in the vertical plane of a flow line). This is a powerful causative factor due to the effects on the water flowing velocity draining the given topography. Pixels with convex (negative) profile curvature tend to be subjected to erosion whilst pixels with concave (positive) curvature are characterized by deposition processes. The units of the curvature are radians per linear unit, again, to discriminate between small values these are multiplied by 100.

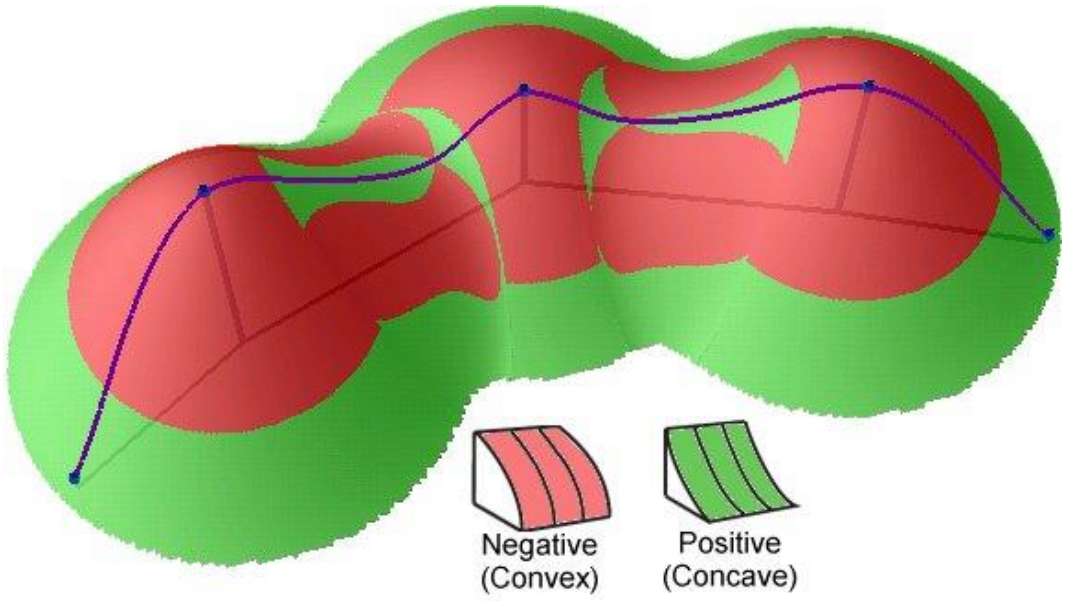

Figure 4.8 - Profile topographic Curvature

- Plan Curvature (Fig. 4.9) is the curvature of the topography intersecting a horizontal plane. In other words it is the curvature of the hypothetical contour line that passes through a specific cell. The plan curvature assumes positive values for cells with concave contours and negative values for cells with convex contours. Ohlmacher (2007) recognised the influence of concave and convex condition in converging and diverging the flows along a given topography, thus influencing mass movement potential activation and/or propagation.

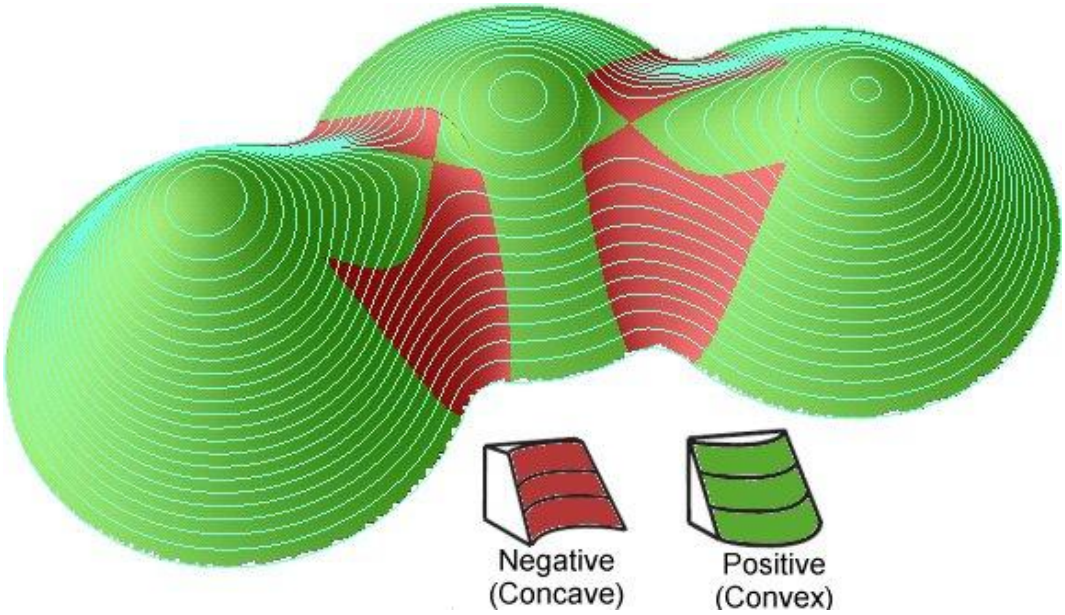

Figure 4.9 - Plan topographic Curvature

- Landform classification is the outcome of an automated procedure that recognise landforms on a gridded elevation distribution. The concept of providing objective and quantitative descriptions of landforms origins with Bates and Jackson (1987) and Denizman (2003) but the decisive advancement corresponds to the work of

Gallant and Wilson (2000) and Tagil and Jenness (2008). The contribution of Gallant and Wilson introduced the so-called topographic position index (TPI) which measures the relative topographic position of the central point as the difference between the elevation at this point and the mean elevation within a predetermined neighbourhood. The approach of Tagil and Jenness is similar to other contemporary studies (Burrough et al., 2000; Deng, 2007; Hengl and Reuter, 2009; Iwahashi and Pike, 2007) and exploits the TPI distributions in a certain area. Comparing the TPI values within two selected radii, generally at shorth and long distance from a given cell, it is possible to automatically recognise several classes of landforms. Among the available algorithms in the present work the landform classifications have been obtained following Tagil and Jenness (2008).

Further analysis has been performed to the aforementioned predictors to generate more complex predictors, the details about this procedure is discussed in chapter 5.

4.4 GEOLOGIC MAP OF THE AREA

The geological map used in the present thesis correspond to the Italian tile number 601. It is known as the tile of Messina-Reggio Calabria and it is part of the Italian geologic mapping with a scale of 1:50.000. The CARG project funded the whole work. The tile 601 is located to the North-Easternmost sector of Sicily and includes both sides of the Messina strait, Messina itself and part of the Calabrian sector. The quality of the geological information is high due to the integration of previous mapping between 1980's and 2000's (Lentini, 2000) with further detail added with new fieldwork performed at 1:10.000 scale for the Sicilian side.

The characterisation of the stratigraphy has been performed adopting a multi-disciplinary approach in order to obtain exhaustive data to describe the variety of lithologies across the area.

- Sedimentary rocks have been analysed through micropaleontological dating using 150 samples from stratigraphic sections broadly distributed;
- Petrographic analysis of sedimentary rocks relied on the already available vast literature;
- Petrographic analysis of the metamorphic rocks was performed at micro- and meso- scale through 250 rock samples and 100 thin sections.

4.5 LAND USE MAP OF THE AREA

The European Union funded in 1985 the Corine (Coordination of Information on the Environment) programme and subsequently the European Environment Agency took over the Corine databases and several of its programmes.

The Corine Land Cover (CLC) inventory is a project with the primary objective of mapping and monitoring the characteristics of land cover and consequently the land use at the European scale.

The relationship between land cover and land use reside in a causative-effect connection with the first one being the physical expression of the material at the surface of the earth whilst the second represents the socio-economic function that the society bestows upon the same earth surface.

The Corine Land Cover (CLC) inventory has been constantly updated since its beginning resulting in different outputs in 2000 and 2006 and the latest, in 2012, is currently

under production. CLC adopts a Minimum Mapping Unit (MMU) of 25 hectares for areal phenomena and a minimum width of 100 metres for linear phenomena.

CLC is produced by interpretation of high resolution satellite imagery. The application of remotely sensed data changed in time accordingly with the evolution of the Corine programme:

- CLC1990 relied on Landsat-5 MSS/TM;
- CLC2000 relied on Landsat-7 ETM;
- CLC2006 used SPOT-4/5 and IRS P6 LISS III;
- CLC2012 used IRS P6 LISS III and RapidEye.

The CLC2006 product is freely accessible for all users and represents the information used in the present thesis. The application of land use as causative factor has been chosen to take into account the anthropologic effect to landslide initiation during the disaster of Messina 2009.

4.6 REMOTE SENSING DATA

In order to integrate the available set of predictors derived from geomorphometric procedures on DEMs, indexes from satellite imagery have been obtained by processing ASTER scenes acquired before the event of Messina 2009.

On December 18, 1999 the NASA launched the Earth Observing System's flagship satellite "Terra". This satellite records data regarding the Earth’s bio-geochemical and energy systems using five state-of-the-art sensors that observe the atmosphere, land surface, oceans, snow and ice, and energy budget. Each of sensor has unique features or in other words, collects the data investigating particular spectra, this setting enable scientists to meet a wide range of science objectives. The five Terra onboard sensors are:

- ASTER, or Advanced Spaceborne Thermal Emission and Reflection Radiometer;
- CERES, or Clouds and Earth's Radiant Energy System;
- MISR, or Multi-angle Imaging Spectroradiometer;
- MODIS, or Moderate-resolution Imaging Spectroradiometer;
- MOPITT, or Measurements of Pollution in the Troposphere.

The co-existence of five sensors (Fig. 4.10) and their connection to a platform allow to collect complementary observations of Earth's surface and atmosphere. These varying perspectives of the same event can yield unique insights into the processes that connect Earth's systems.

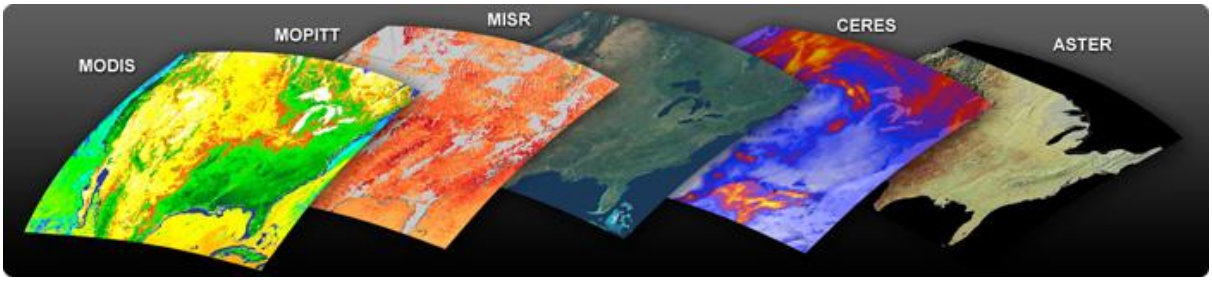

Figure 4.10 - Different spectral resolution among the five sensors.

The ASTER is the only high-spatial resolution sensor onboard. It can investigate the electromagnetic spectrum by sampling 14 wavelengths centred to the Visible/Near Infrared to the Short-Wave Infrared and to the Thermal Infrared. The spatial resolution varies accordingly to the aforementioned signals decreasing from 15m to 30m and to 90m cell side pixel.

The ASTER scene used in this thesis (FIG XXX) was acquired on the 10/07/2009, exactly at 09:53'10'' GMT, and represents the best option available in terms of cloud cover among the close pre-event acquisitions with this sensor.

The scene (Fig. 4.11) cover most of the North-Eastern Sicilian sector, from the Etna Mount to the south to Messina to the North.

As all the other Aster images, the scene is expressed through 14 different bands:

- VNIR_BAND1, wavelength between 0.52 µm and 0.60 µm corresponding to Visible green/yellow;
- VNIR_BAND2, wavelength between 0.63 µm and 0.69 µm corresponding to visible red;
- VNIR_BAND3, wavelength between 0.76 µm and 0.86 µm corresponding to near infrared;
- SWIR_BAND4, wavelength between 1.600 µm and 1.700 µm;
- SWIR_BAND5, wavelength between 2.145 µm and 2.185 µm;
- SWIR_BAND6, wavelength between 2.185 µm and 2.225 µm;
- SWIR_BAND7, wavelength between 2.235 µm and 2.285 µm;

- SWIR_BAND8, wavelength between 2.295 µm and 2.365 µm;
- SWIR_BAND9, wavelength between 2.360 µm and 2.430 µm;

The signal recorded within the interval between BAND4 and BAND9 correspond to Short-wave infrared.

- TIR_BAND10, wavelength between 8.125 µm and 8.475 µm;
- TIR_BAND11, wavelength between 8.475 µm and 8.825 µm;
- TIR_BAND12, wavelength between 8.925 µm and 9.275 µm;
- TIR_BAND13, wavelength between 10.250 µm and 10.950 µm;
- TIR_BAND14, wavelength between 10.950 µm and 11.650 µm;

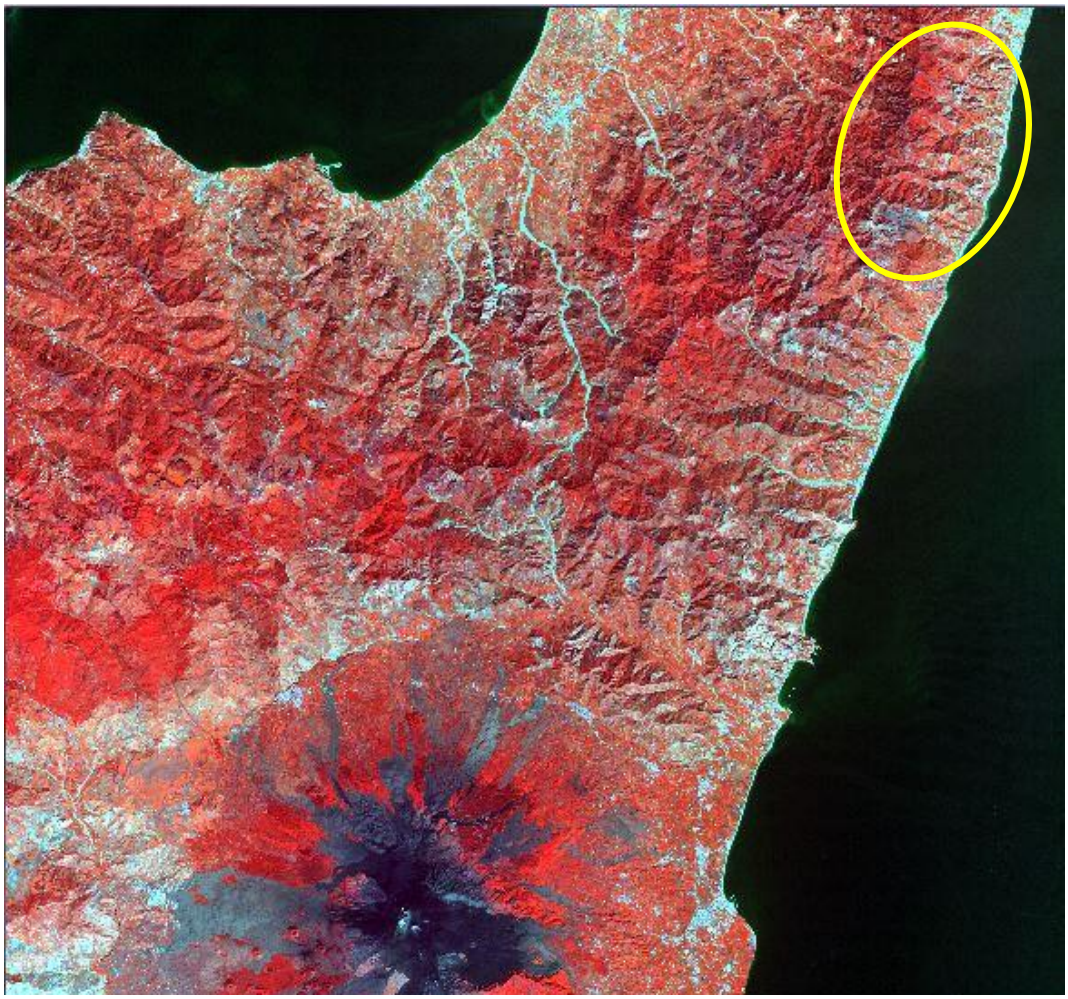

Figure 4.11 - This scene has been built by combining the first three bands (VISIBLE) among the 14 available. The area included within the yellow polygon corresponds to the sector exposed to the disaster 2009.

Further detail regarding the processing of the ASTER scene and the calculation of vegetation and mineral indexes will be discussed in chapter 5.

5 APPLICATIONS

The present chapters includes all the experiment that have been developed during the three-year doctoral experience. Particular emphasis will be given to the three primary tests carried out with a major impact from the PhD student whilst a limited description will be given for tests in which the student contributed as part of a wider research team.

5.1 A TEST OF TRANSFERABILITY FOR LANDSLIDES SUSCEPTIBILITY MODELS UNDER EXTREME CLIMATIC EVENTS: APPLICATION TO THE MESSINA 2009 DISASTER.

Lombardo, L., Cama, M., Maerker, M., Rotigliano, E., 2014. Natural Hazards Volume 74, Issue 3 , pp 1951-1989.

5.1.1 *Research objectives*

A number of recent studies have explored the relationship between the frequency of landslide occurrence and climate change (Borgatti and Soldati 2010; Crozier 2005, 2010; Gulla` et al. 2012; Jakob and Lambert 2009); the basic premise being that severe morphodynamic responses are typically caused by high frequency climatic inputs such as intense meteorologic events. The simultaneous manifestation of thousands of debris flows and debris avalanches that occurred in a few hours on 1 October 2009 in the Messina area (Ionian side of the Peloritani belt, southern Italy), in which thirty-seven people died, more than one hundred people were injured and more than 0.5 M € damage to structures caused, serves as a local example of the potential impact of climate change in the Mediterranean region (Agnesi et al. 2009; Aronica et al. 2012; De Guidi and Scudero 2013; Del Ventisette et al. 2012). In fact, this disaster was triggered by an extreme climatic event (a storm rainfall) far greater than any recorded in the previous 30-year period.

Many research efforts have been dedicated to the prediction of landslide occurrence since the late 1970's (e.g. Carrara et al. 1977) so that good performing and geomorphologically reliable quantitative models can be nowadays obtained through the use of GIS-supported stochastic methods (Brenning 2005; Carrara et al. 1999; Glade et al. 2002; Guzzetti et al. 1999), which furnish quantitative, objective and rigorous modelling and validation procedures (Carrara

and Pike 2008; Costanzo et al. 2013; Fabbri and Chung 2008; Frattini et al. 2010; Guzzetti et al. 2006; Rossi et al. 2010). However, when applied to predict the landslide scenarios potentially triggered by extreme climatic events (ECEs), the use of such methods is subject to a severe limitation. In fact, ECEs in the Mediterranean region are typically very local and rare phenomena and, as such, storm-triggered landslide inventories are made of randomly scattered (both in time and space) cases: few randomly distributed areas have been stricken in the past, each of which being characterized by large time recurrences. Therefore, for a given study area, two conditions are frequently verified, both resulting in the lack of the landslide inventory, which is required to train a stochastic predictive model: no ECE occurred in the past or, inside a past-stricken area, due to large time recurrence, the almost complete erasing of the past landslides (which are typically of surficial type) by water erosion.

In order to deal with this limitation, in this study, a model building strategy based on an exportation procedure (Costanzo et al. 2012) is tested: a susceptibility model, which is prepared in a source area exploiting the landslide scenario produced by an extreme event, is used to predict landslides in a neighbouring target area. In the present case, the target area is a neighbouring catchment that was struck by the same event, so to allow us a verification of the method and the results.

The adopted strategy is quite similar to one of those which are used to validate predictive models (spatial partition, Chung and Fabbri 2003), but it here assumes a very different perspective and application procedure in approaching the prediction of ECE-driven landslides. We actually performed a verification of the spatial transferability of a susceptibility model (Petschko et al. 2014). A non-Mediterranean example of research facing the same subject, which is the focus we dealt with, was proposed by von Ruette et al. (2011). Differences in the research strategy and results will be discussed in the following.

Two catchments located inside the core area of the Messina 2009 ECE are exploited for testing our approach: susceptibility models prepared (trained) in the Briga catchment are tested in predicting the landslides distribution in the Giampilieri catchment.
In order to estimate the landslide susceptibility, we applied the binary logistic regression (BLR) statistic technique (Bai et al. 2010; Can et al. 2005; Conforti et al. 2012; Costanzo et al. 2013; Goetz et al. 2011; Luca` et al. 2011; Nandi and Shakoor 2008; Nefeslioglu et al. 2008; Ohlmacher and Davis 2003; Su¨zen and Doyuran 2004; Van Den Eeckhaut et al.

2006, 2009, 2010; von Ruette et al. 2011; Yalcin et al. 2011), which provides the regression coefficients for a set of explanatory variables to compute a logit (log odds) function of a binary dependent, expressing stable/unstable conditions. The explanatory variables can be either dichotomous, polychotomous or continuous. Among the fan of the statistical techniques that are exploited in predicting landslides (see Carrara et al. 1999; Guzzetti et al. 1999), BLR has proved to be one of the most suitable and performing methods for assessing landslide susceptibility on a basin scale also in comparative studies (Akgün and Türk 2011; Guzzetti et al. 2005; Rossi et al. 2010; Vorpahl et al. 2012). Level 4 validation procedures (Guzzetti et al. 2006) are then applied to verify the quality of the predictive models and of the whole research as well.

5.1.2 *Materials and methods*

Binary logistic regression (BLR) allows us to estimate the odds of unstable conditions for a mapping unit (e.g. cell, topographic or slope units), on the basis of a set of predictors, which describe its physical-environmental conditions (Hosmer and Lemeshow, 2000). In BLR, predictors can correspond either to numerical or categorical variables. *Specifically,* BLR aims at modelling a linear relationship between the logit (or log odds) of the outcome (stable/unstable) and a set of *p* independent variables or covariates:

$$g(\boldsymbol{x}) = ln\left[\frac{\pi(\boldsymbol{x})}{1-\pi(\boldsymbol{x})}\right] = \alpha + \beta_1 x_1 + \beta_2 x_2 + \cdots + \beta_p x_p,$$

where $\pi(\boldsymbol{x})$ is the conditional mean of the outcome given the multivariate site properties $\boldsymbol{x}$, α is the constant term, the x's are the input predictor variables and the β's are their coefficients, which are regressed by using maximum likelihood estimation through an iterative process. The iterative procedure aims at making the model converge to the best solution. Odds ratios (ORs) are obtained by exponentiating the β's of the independent variables. The ORs are measures of association between the independent variables and the outcome of the dependent and directly express how much more likely (or unlikely) it is for the outcome to be positive (unstable cell) for unit changing of the considered independent. Negatively correlated variables will produce negative β's and OR limited between 0 and 1, whilst positively correlated variables will result in positive β's and OR greater than 1.

As the fit of the model is based on maximizing the value of the likelihood, comparing the likelihood itself allows us to estimate the goodness of different nested regression models. In particular, by multiplying the log-likelihood ratio by -2, the negative log-likelihood (-2LL) statistic is obtained. This has an approximate chi-square (χ^2) distribution, so that the significance of a difference between the fitting of two nested models can be estimated in terms of probability of occurrence by chance.

The -2LL statistic can also be exploited to estimate the goodness of fit, by comparing the fitting of the model only having the constant term (all the β_p are set to 0) with that which includes the considered predictors with their estimated non-null coefficients. At the same time, testing the significance of the -2LL statistic allows us to compare models obtained by considering nested sets of predictors so that, for example, the significance of the changing in the model fitting produced by including a single landslide factor can be quantitatively assessed (Hosmer and Lemeshow, 2000). Forward stepwise selection procedures for BLR method exploits this tool so that the best performing and most parsimonious set of variables can be achieved. This is done by choosing a restricted group of predictors, consisting of only those that significantly increase the performance of the multivariate model, from the larger set of potential predictors. At any step, the most important variable is the one that produces the greatest increase in the log-likelihood relative of the model which does not contain it.

In this research, in order to perform the forward stepwise logistic regression an open source software was used (TANAGRA: Rakotomalala 2005).

Following the above described scheme, applying BLR in the case of a landslide susceptibility assessment GIS procedure requires: 1) the preparation of the grid layers of those geo-environmental attributes that we expect, on the basis of a geomorphological landslide model, to act as controlling factors; 2) the partitioning of the investigated area into mapping units; 3) the assignment of the status (stable/unstable) to the mapping units, depending on their positions (inside/outside) relative to the so-called diagnostic areas (Rotigliano et al., 2011); 4) by combining the grids of the predisposing factors with the grid of the status, the extraction of a main data matrix, in which a row corresponds to an individual case (a single mapping unit) whilst columnar data show the values of the *p* explanatory variables and the response binary status; 5) finally, by applying geostatistical GIS tools, the random extraction from the main data matrix of one or more balanced data-subsets, including an equal number of positive (unstable)

and negative (stable) cells, as required for BLR (Atkinson and Massari, 1998; Bai et al., 2010; Frattini et al., 2010; Nefeslioglu et al., 2008; Süzen and Doyuran, 2004; Van Den Eeckhaut et al., 2009).

5.1.3 *Predisposing factors*

The set of potential controlling factors selected to predict unstable cells was defined on the basis of (i) the recognized landside typologies and (ii) the availability and resolution of the source data. In particular, outcropping lithology, soil use and topographic features were considered.

By processing geological (Lentini et al., 2000) and the Corine 2006 land use maps, outcropping lithologies and soil use grid layers have been derived, defining the predictor nominal variables GEO_CARG and USE. This type of data has been detailed on the basis of field checks and orthophotos analysis. The GEO_CARG variable simply expresses the site outcropping lithology, here considered as a proxy for the type of regolithic cover and, as a consequence, its mechanical properties. At the same time, possible anthropogenic effects on the site stability conditions are linked to the variable USE.

Regarding the topographic factors, by applying 3-D, spatial and hydrologic GIS tools, we calculated primary and secondary attributes from a 2m cell DEM (vertical resolution = 0.17m) released by ARTA from a LIDAR coverage dated at 2007 (pre-event), obtaining: slope aspect and steepness (ASP, SLO); general, profile and plan topographic curvatures (CUR, PRC and PLC); topographic wetness index (TWI); stream power index (SPI). All these factors were averaged for each cell on a 5m neighbourhood radius.

A further processing was also performed for TWI and SPI. In fact, as the drainage network is characterized by the highest values of contributing area, TWI and SPI typically have their highest values along the high and low order drainage axis, respectively. This produces a saturation of the scale of these variables, responsible for a lower discrimination between the cells onto the slopes (which are the ones from which landslides triggered). TWISLO and SPISLO variables were computed by dividing TWI and SPI values, respectively, for their standard deviation evaluated for a neighbourhood of one cell; the latter in fact ranges from minimum, along the streams, to maximum, away from streams on slopes, where both TWI and

SPI values are lower but more constant. Landform classification was applied using two different couples of analysis radii (20/100m and 50/250m), to derive the LAND1 and LAND2 nominal variables, respectively.

In a predictive model, topographic attributes and the derived variables allow us to, directly or indirectly, consider the role of morphological and hydrological conditioning on the slope failure dynamic. Variation in the aspect and steepness of the slopes can be correlated to attitude changings of the substratum layer. At the same time, the steepness of the slope is obviously of basic importance in determining the static condition of each cell, as it indirectly controls the shear strength acting onto the potential shallow failure surfaces. Topographic curvatures control divergence and convergence, both of surface runoff and shallow gravitative stresses (Ohlmacher, 2007). Wetness and stream power topographic indexes are widely used in landslide susceptibility modelling to express the potential water infiltration volumes and erosion power on slopes, respectively (Wilson and Gallant, 2000). Finally, landform classification describes the geomorphological setting of each mapped unit, by considering its local position with respect to a more general morphological context, with the research radii used to obtain the two predicting variables set according to the mean length of the slopes (LAND1) and the stream valleys (LAND2) in the area.

Table 5.1.1 shows a summary of the 69 independent variables which have been chosen as potential predictors.

It is worth to highlight that all the predictors have been derived from source layers which were acquired before the 1st October 2009 event. This means that values of all the geoenvironmental variables are not affected by the landslides we want to predict.

Independent variables									
Categorical variables: binary response [0,1]						**a**	*Continous variables*		**b**
name:code	*classes*	*variable*	*name:code*	*classes*	*variable*		*description*	*variable*	*units*
	Eluvial – colluvial horizon	GEO_CARG_b2		V-shape river valleys	VSRV		Elevation	HEIGHT	m
	Recent alluvial deposits	GEO_CARG_bb		Local valley in plains	LVP		Local steepness	SLO	degrees
	Terraced alluvial deposits	GEO_CARG_bn4		Upland incised drainages	UID		Neighborhood SLO	SLONH	degrees
	Terraced marine deposits	GEO_CARG_gn2-5		U-shape valleys	USV		Topographic Wetness Index	TWI	none
	Clays with sandy levels	GEO_CARG_SPDb		Broad flat areas	BFA		Neighborhood TWI	TWINH	none
	Arkosic clay marls	GEO_CARG_PCTa	2 LANDFORM	Broad open slopes	BOS		Slope-TWI	TWISLO	none
	Conglomerates	GEO_CARG_PCTc	CLASSIFICATION:	Flat ridge tops mesa tops	FRTMT		Strem Power Index	SPI	none
OUCROPPING	Argille scagliose	GEO_CARG_ASI	LAND1, LAND2	Local ridge/hilltops within broad valleys	LRHBV		Neighborhood SPI	SPINH	none
LITHOLOGY:	Aplitic-pegmatites	GEO_CARG_PMPa					Slope-SPI	SPISLO	none
GEO_CARG	Paragneiss to mica-schists with gneiss and amphibolite intrusions	GEO_CARG_PMAa		Local ridge in plains	LRP		Flow Accumulation	FLA	m^2
				Mountain tops	MT		Neighborhood FLA	FLANH	m^2
	Silicate marbles	GEO_CARG_PMAd		Continous urban fabric	USE_1.1.1		Local Profile concave curvature	PRC2_CONC	rad / 100m
	Paragneiss to mica-schists	GEO_CARG_MLEa		Non-irrigated arable land	USE_2.2.1		Local Profile convex curvature	PRC2_CONV	rad / 100m
	Double micas marbles	GEO_CARG_MLEc		Olive groves	USE_2.2.3		Local Plan concave curvature	PLC2_CONC	rad / 100m
	Muscovite marbles	GEO_CARG_FDNa		Mixed groves	USE_2.2.6		Local Plan convex curvature	PLC2_CONV	rad / 100m
	Phyllites to meta-arenites	GEO_CARG_FDNb		Coniferous	USE_3.1.2		Local General concave curvature	CUR2_CONC	rad / 100m
	North	ASP_N	LAND USE	Partially wooded land or degradated forest	USE_3.1.4		Local General convex curvature	CUR2_CONV	rad / 100m
	North-East	ASP_NE	CORINE 2006:				Neighborhood Profile concave curvature	PRC5_CONC	rad / 100m
SLOPE	East	ASP_E	USE	Shrubland	USE_3.2.1		Neighborhood Profile convex curvature	PRC5_CONV	rad / 100m
ASPECT:	South-East	ASP_SE		Grassland	USE_3.2.2		Neighborhood Plan concave curvature	PLC5_CONC	rad / 100m
ASP	South	ASP_S		Sparsely vegetated areas	USE_3.2.3		Neighborhood Plan convex curvature	PLC5_CONV	rad / 100m
	South-West	ASP_SW		Erosion scars,badlands, rock outcrops	USE_3.3.1		Neighborhood General concave curvature	CUR5_CONC	rad / 100m
	West	ASP_W					Neighborhood General convex curvature	CUR5_CONV	rad / 100m
	North-West	ASP_NW							

Table 5.1.1 - List of the adopted predictors.

5.1.4 *Mapping units and diagnostic areas*

In susceptibility modelling studies, the investigated area has to be partitioned into mapping units, the functional areas for which the modelling procedure is then able to predict the stability conditions. A large set of mapping unit is proposed in literature (Carrara et al., 1995; Guzzetti et al., 1999), each depending on the criteria adopted in partitioning the area. In this study, we hypothesized the initiation of a debris slide or debris flow in a site as to be linked to the conditions in a small neighbouring area, rather than to the general conditions of the whole slope (which, for example, would be the case of rotational slides). For this reason, the mapping unit adopted was the same 2m side cell of the DEM, from which the grid layers of several of the tested predictors were derived. Similar considerations drove the selection of the diagnostic areas (Rotigliano et al., 2011), where, on a post-events scenario, conditions similar to those responsible for the observed landslides, can be identified. The status of the cells inside these diagnostic areas is in fact set as unstable based on the hypothesis that future landslides will activate given the same conditions that triggered past failures.

In light of the considered landslide typologies, which are heavily controlled by the initiation movements and whose failures involve a very shallow volume, we adopted the

following procedure to select the very neighbourhood of the crown areas: 1) for each landslide, a polygon, including the source area, the run-out and the accumulation zone, were mapped; 2) a Landslide Identification Point (LIP) was then extracted as the highest point along the landslide polygon boundaries (Fig. 5.1.1); 3) finally, we used circular diagnostic areas centred at each LIP spanning a 2.82m radius (corresponding to the diagonal of a 2m cell). By performing this procedure, 5646 and 7307 unstable cells were set for the Briga and Giampilieri catchments, respectively.

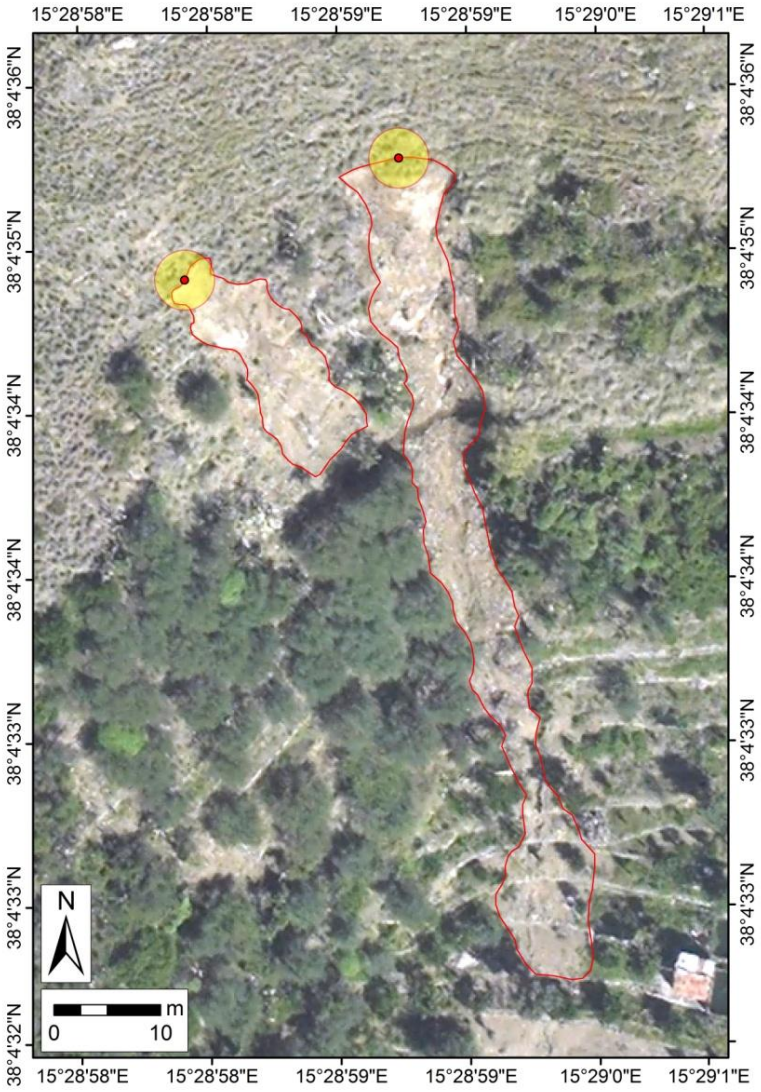

Figure 5.1.1 - Example of LIP positioning in landslide polygons.

5.1.5 *Model building and validation strategy*

The model building strategy that was adopted in assessing the landslide susceptibility in the Briga and Giampilieri catchments is dependent on: the main goal of the research (i.e. testing a method to reproduce ECE-driven landslide scenarios in a catchment, without knowing its past landslide distribution); the requirement for using the forward selection binary logistic regression method; on the application of complete validation procedures (Carrara et al., 2003; Guzzetti et al., 2006; Frattini et al., 2010; Rossi et al., 2010) were adopted for testing goodness of fit, prediction skill, robustness and reliability and quantitatively support the following analysis and discussions.

The prediction skill of a susceptibility model can be estimated if a training and a test subset are available. For each considered dataset, this was accomplished by randomly extracting a balanced (yes/no) 25% subset from the whole dataset and storing it as a testing subset, and applying the forward logistic regression procedure onto the remaining 75% of the data, which represented the training subset. We will hereafter refer to this kind of models as random partition (RP) based models (Chung and Fabbri, 2003). The obtained logit function allowed us to compute the odds for each cell of the model and to verify the skill in predicting the status of the unknown cases (the cells in the test subset). At the same time, the goodness of fit was evaluated by computing the ability of the model to fit the known cases (i.e. the status of the cells in the training subset). The Receiver Operating Curves (ROC) were exploited to quantitatively assess the prediction skill and the goodness of fit, by plotting true positive versus false positive outcomes, for monotonically decreasing probability thresholds, and computing the Area Under Curve (AUC) index. At the same time, contingency tables allowed us to compute the general error rate of the models, by comparing the predicted and observed status of all the cells.

The robustness of the model has to describe its sensitivity with respect to changes in the input parameters, whilst the reliability should also account for more general and/or basic variations, such us the spatial locations of the cells included in the subset. Instead of estimating the robustness and reliability by exploiting a pure boot-strapping technique to generate *n*-fold suites of datasets from a single positive/negative dataset, a model building procedure was implemented for each catchment, so as to obtain suites of different datasets made of randomly assembled cells (Costanzo et al., 2013). In fact, as the first step in applying BLR is to prepare

balanced datasets made of an equal number of positive and negative cases, checking for the spatial representativeness of the selected negatives, should be mandatory. Unstable cells are typically much less than stable ones, so that the widely adopted procedure, consisting in randomly extracting a single balanced (yes/no) subset to obtain the dataset to be regressed, should be verified. Actually, the total extension of the training area is much lower than the whole catchment, even in the case of very high number of landslides such the considered areas show. For example, in the Briga catchment, 11292 cells would be enough to prepare a BLR-model, but it would result in having included just around the 0.5% of the whole catchment in the modelling! The obtained models could suffer from low geomorphologic representativeness and, as a consequence, of very poor reliability.

To cope with the above described limit, we built eight different datasets for each catchment, obtained by merging the same positives with eight different randomly extracted negative subsets, having null mutual intersection. By applying spatial analysis tools, we firstly discretised the two watersheds, creating a 10m squared grid. After erasing the 10m cells which intersected LIPs, the eight subsets of negative cells were obtained by randomly extracting among the centroids of the remaining (Fig. 5.1.2).

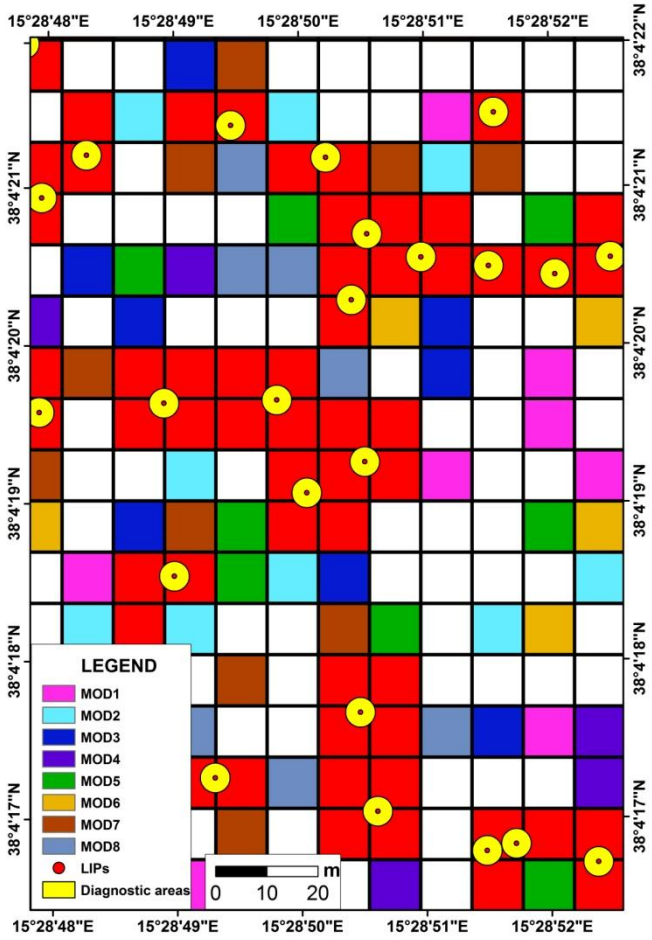

Figure 5.1.2 - Detail of the 10-m2 GRID adopted in the model building procedure to generate the eight subsets of negatives: in red, unstable cells intersecting the diagnostic areas around the LIPs; the other eight colours identify the different randomly selected stable subsets.

Even if, for eight replicates, the cumulated amount of sampled area only accounts for the 2.34% and 2.86%, for Briga and Giampilieri catchments, respectively (Tab. 5.1.2), very highly stable responses for the different models would attest for the robustness of the regressed models with respect to the different locations of the negatives.

		RANDOM PARTITION MODELS			
		TRAINING		TEST	
Id	**MODEL**	***POSITIVE***	***NEGATIVE***	***POSITIVE***	***NEGATIVE***
1	*BRG_RPM01*	75%_BRG	75%_BRG	25%_BRG	75%_BRG
2	*BRG_RPM02*	75%_BRG	75%_BRG	25%_BRG	75%_BRG
3	*BRG_RPM03*	75%_BRG	75%_BRG	25%_BRG	75%_BRG
4	*BRG_RPM04*	75%_BRG	75%_BRG	25%_BRG	75%_BRG
5	*BRG_RPM05*	75%_BRG	75%_BRG	25%_BRG	75%_BRG
6	*BRG_RPM06*	75%_BRG	75%_BRG	25%_BRG	75%_BRG
7	*BRG_RPM07*	75%_BRG	75%_BRG	25%_BRG	75%_BRG
8	*BRG_RPM08*	75%_BRG	75%_BRG	25%_BRG	75%_BRG
9	*GMP_RPM01*	75%_GMP	75%_GMP	25%_GMP	75%_GMP
10	*GMP_RPM02*	75%_GMP	75%_GMP	25%_GMP	75%_GMP
11	*GMP_RPM03*	75%_GMP	75%_GMP	25%_GMP	75%_GMP
12	*GMP_RPM04*	75%_GMP	75%_GMP	25%_GMP	75%_GMP
13	*GMP_RPM05*	75%_GMP	75%_GMP	25%_GMP	75%_GMP
14	*GMP_RPM06*	75%_GMP	75%_GMP	25%_GMP	75%_GMP
15	*GMP_RPM07*	75%_GMP	75%_GMP	25%_GMP	75%_GMP
16	*GMP_RPM08*	75%_GMP	75%_GMP	25%_GMP	75%_GMP

Table 5.1.2 - Description of the RP-models built datasets.

In this way, by comparing the predictive performances of the eight different models of each of the two suites, it was also possible to evaluate their reliability and check if the analysed datasets were representative of the general geomorphologic conditions of the two catchments: the positives were constant among the replicates, whilst the only change in the model building procedure was represented by the negatives.

Finally, in order to verify the possibility of exporting susceptibility models trained in the source catchment to predict the unstable cells of the target catchment, models trained in the Briga catchments were tested in predicting the Giampilieri landslides. To achieve this task, together with the RP-models, trained and validated by using the random partitioning of the landslides within the same two catchments, spatial partition (SP) based models, trained in the Briga source area and validated in the Giampilieri target area, were prepared: exploiting the two suites of eight datasets which were prepared to build the RP-models, it was possible to train eight different models in the Briga catchments (source area), by using the whole 100% of the datasets. These new models were then validated with respect to the 100% of positives and

negatives cells of the eight different datasets in the Giampilieri catchment, obtaining sixty-four SP-models (Tab. 5.1.3).

	SPATIAL PARTITION MODELS			
	TRAINING		TEST	
MODEL	***POSITIVE***	***NEGATIVE***	***POSITIVE***	***NEGATIVE***
GMP_SPM01	100%BRG	100%BRG_RPM01	100%GMP	100%GMP_RPM01
GMP_SPM02	100%BRG	100%BRG_RPM01	100%GMP	100%GMP_RPM02
GMP_SPM03	100%BRG	100%BRG_RPM01	100%GMP	100%GMP_RPM03
GMP_SPM04	100%BRG	100%BRG_RPM01	100%GMP	100%GMP_RPM04
GMP_SPM05	100%BRG	100%BRG_RPM01	100%GMP	100%GMP_RPM05
GMP_SPM06	100%BRG	100%BRG_RPM01	100%GMP	100%GMP_RPM06
GMP_SPM07	100%BRG	100%BRG_RPM01	100%GMP	100%GMP_RPM07
GMP_SPM08	100%BRG	100%BRG_RPM01	100%GMP	100%GMP_RPM08
GMP_SPM09	100%BRG	100%BRG_RPM02	100%GMP	100%GMP_RPM01
GMP_SPM10	100%BRG	100%BRG_RPM02	100%GMP	100%GMP_RPM02
.....				
.....				
GMP_SPM57	100%BRG	100%BRG_RPM08	100%GMP	100%GMP_RPM01
GMP_SPM58	100%BRG	100%BRG_RPM08	100%GMP	100%GMP_RPM02
GMP_SPM59	100%BRG	100%BRG_RPM08	100%GMP	100%GMP_RPM03
GMP_SPM60	100%BRG	100%BRG_RPM08	100%GMP	100%GMP_RPM04
GMP_SPM61	100%BRG	100%BRG_RPM08	100%GMP	100%GMP_RPM05
GMP_SPM62	100%BRG	100%BRG_RPM08	100%GMP	100%GMP_RPM06
GMP_SPM63	100%BRG	100%BRG_RPM08	100%GMP	100%GMP_RPM07
GMP_SPM64	100%BRG	100%BRG_RPM08	100%GMP	100%GMP_RPM08

Table 5.1.3 - Description of the SP-model built datasets.

Figure 5.1.3 allows, taking into consideration some general geomorphological attributes, to verify the large similarity between the two catchments in terms of factor spatial distribution.

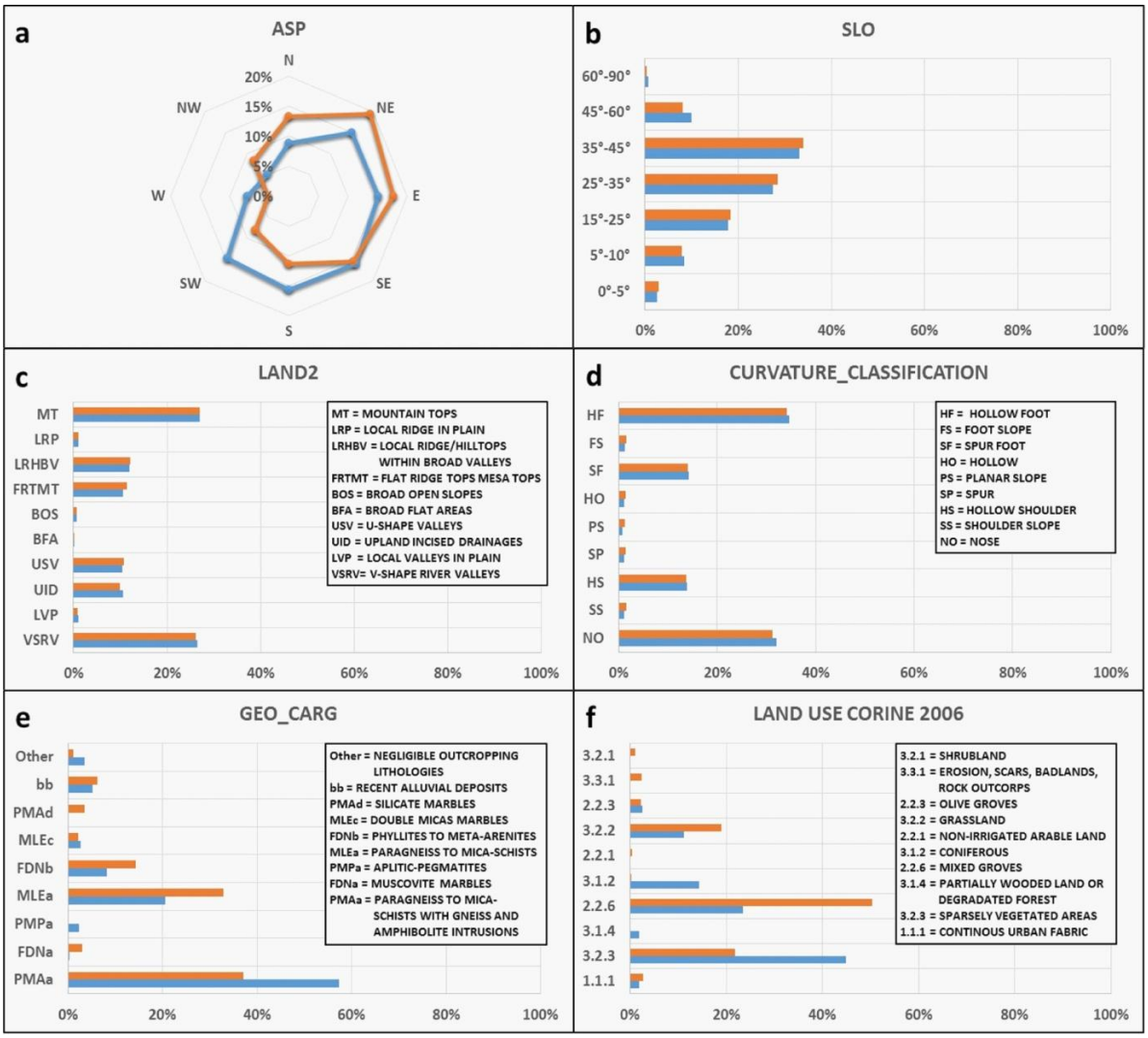

Figure 5.1.3 - Frequency distribution in percentage of some geomorphological attributes for Briga (in orange) and Giampilieri (in blue) catchments: a aspect; b slope; c landform classification; d curvature classification; e outcropping lithology; and f land use.

As we applied BLR according to a stepwise forward selection technique, the coherence between the selected predictors and their ranking (Costanzo et al. 2013), together with the performance indexes and tests, were also considered as basic criteria to estimate both the reliability and the adequacy of the final results. At the same time, as each suite produced more estimates of the probabilities of each mapping unit (8, for RP-models, and 64, for SP-models), the dispersion of each susceptibility estimate, measured by a 2 standard deviations interval, was also computed and plotted in the model error map (Guzzetti et al., 2006). Moreover, to explore the relationship between estimate and precision, mean probabilities against their variations, were also plotted and the best fit curve calculated, using a quadratic regression. The criterion

that was adopted in verifying the quality of the exported SP-models relies on the comparison between their predictive performance with respect to the correspondent Giampilieri RP-models.

5.1.6 *Results for the RP-models*

Both the Briga and Giampilieri suites of models generally show excellent fittings (Tabs. 5.1.4 and 5.1.5), resulting in low and stable mean error rates ($\mu = 0.221$, $\sigma = 0.006$ and $\mu = 0.219$, $\sigma = 0.003$, respectively) and largely acceptable pseudo-R^2 statistics. AUC values, both for training and test-ROC curves, attest for excellent (Hosmer and Lemeshow, 2000) and stable accuracy for the two suites of models, with Briga having a mean AUC of 0.850 ($\sigma = 0.007$) and Giampilieri of 0.844 ($\sigma = 0.003$). At the same time, just higher values for the training-AUCs ($\mu = 0.856$, $\sigma = 0.004$, for Briga, $\mu = 0.848$, $\sigma = 0.003$, for Giampilieri) allow us to consider as negligible any evidence of overfitting. The performance of the worst models of the two suites still proves to be high, with AUC values of 0.839 (GMP_RPM05).

	BRIGA RP, PREDICTION SKILL									
	BRG_RPM01	BRG_RPM02	BRG_RPM03	BRG_RPM04	BRG_RPM05	BRG_RPM06	BRG_RPM07	BRG_RPM08	MEAN	ST.DEV.
Err.rate	0.2301	0.2177	0.2188	0.2167	0.2209	0.2286	0.2143	0.2192	0.221	0.006
AUC(training)	0.8488	0.8593	0.8566	0.86	0.8556	0.8497	0.8588	0.8588	0.856	0.004
AUC(test)	0.8561	0.85	0.8599	0.8474	0.846	0.8451	0.8533	0.839	0.850	0.007
-2LL int.	11740.527	11740.527	11740.527	11740.527	11740.527	11740.527	11740.527	11740.527	11740.527	0
-2LL mod.	7869.261	7510.015	7587.882	7554.683	7638.614	7745.152	7539.017	7532.117	7622.093	125.232
chi sq.	3871.266	4230.512	4152.645	4185.844	4101.913	3995.375	4201.51	4208.41	4118.434	125.232
d.f.	21	26	26	25	27	26	26	22	24.875	2.167
p	0	0	0	0	0	0	0	0	0	0
McFadden's R^2	0.3297	0.3518	0.3537	0.3565	0.3494	0.3403	0.3579	0.3585	0.350	0.010
Cox and Snell's R^2	0.3669	0.386	0.3876	0.39	0.3839	0.3761	0.3911	0.3916	0.384	0.009
Nagelkerke's R^2	0.4892	0.5146	0.5168	0.52	0.5119	0.5015	0.5215	0.5221	0.512	0.011

Table 5.1.4 - Predictive performances of the RP-models for the Briga suite.

	GIAMPILIERI RP, PREDICTION SKILL									
	GMP_RPM01	GMP_RPM02	GMP_RPM03	GMP_RPM04	GMP_RPM05	GMP_RPM06	GMP_RPM07	GMP_RPM08	MEAN	ST.DEV.
Err.rate	0.2195	0.2185	0.2225	0.2193	0.218	0.2247	0.2143	0.2176	0.219	0.003
AUC(training)	0.8458	0.8497	0.8447	0.8503	0.8485	0.8451	0.8445	0.8544	0.848	0.003
AUC(test)	0.8481	0.8469	0.8419	0.843	0.8386	0.8471	0.8427	0.8426	0.844	0.003
-2LL int.	15177.138	15186.85	15193.786	15193.786	15193.786	15193.786	15192.4	15193.786	15190.665	5.967
-2LL mod.	10316.526	10223.747	10387.596	10205.577	10263.96	10341.552	10380.939	10080.622	10275.065	103.789
chi sq.	4860.612	4963.103	4806.19	4988.209	4929.826	4852.234	4811.461	5113.164	4915.600	104.620
d.f.	22	25	23	23	23	24	21	22	23	1
p	0	0	0	0	0	0	0	0	0	0
McFadden's R^2	0.3203	0.3268	0.3163	0.3283	0.3245	0.3194	0.3167	0.3365	0.324	0.007
Cox and Snell's R^2	0.3585	0.3643	0.355	0.3656	0.3622	0.3577	0.3553	0.3728	0.361	0.006
Nagelkerke's R^2	0.478	0.4857	0.4733	0.4875	0.483	0.477	0.4738	0.4971	0.482	0.008

Table 5.1.5 - Predictive performances of the RP-models for the Giampilieri suite.

Table 5.1.6 shows the general confusion matrices for the eight models of the two suites, whilst Figure 5.1.4 shows the training and test-ROC curves which were obtained for the two catchments. Both ways of looking at the model performance attest for the high precision and accuracy of the model.

							RECALL		1-PRECISION		
TP	FN	FP	TN	YES	NO	TOT	YES	NO	YES	NO	SUITE
3571	1285	664	2949	4235	4234	8469	0.84	0.70	0.26	0.18	**BRG_RPM01**
3611	1220	624	3014	4235	4234	8469	0.85	0.71	0.25	0.17	**BRG_RPM02**
3609	1227	626	3007	4235	4234	8469	0.85	0.71	0.25	0.17	**BRG_RPM03**
3590	1190	645	3044	4235	4234	8469	0.85	0.72	0.25	0.17	**BRG_RPM04**
3586	1222	649	3012	4235	4234	8469	0.85	0.71	0.25	0.18	**BRG_RPM05**
3588	1289	647	2945	4235	4234	8469	0.85	0.70	0.26	0.18	**BRG_RPM06**
3637	1217	598	3017	4235	4234	8469	0.86	0.71	0.25	0.17	**BRG_RPM07**
3587	1284	648	2950	4235	4234	8469	0.85	0.70	0.26	0.18	**BRG_RPM08**
3597.4	1241.8	637.6	2992.3	4235.0	4234.0	8469.0	0.85	0.71	0.26	0.18	MEAN
20.6	38.3	20.6	38.3	0.0	0.0	0.0	0.00	0.01	0.01	0.01	ST.DEV
4554	1476	933	3997	5487	5473	10960	0.83	0.73	0.24	0.19	**GMP_RPM01**
4546	1459	937	4018	5483	5477	10960	0.83	0.73	0.24	0.19	**GMP_RPM02**
4525	1484	955	3996	5480	5480	10960	0.83	0.73	0.25	0.19	**GMP_RPM03**
4543	1466	937	4014	5480	5480	10960	0.83	0.73	0.24	0.19	**GMP_RPM04**
4558	1467	922	4013	5480	5480	10960	0.83	0.73	0.24	0.19	**GMP_RPM05**
4534	1517	946	3963	5480	5480	10960	0.83	0.72	0.25	0.19	**GMP_RPM06**
4480	1520	1001	3959	5481	5479	10960	0.82	0.72	0.25	0.20	**GMP_RPM07**
4553	1458	927	4022	5480	5480	10960	0.83	0.73	0.24	0.19	**GMP_RPM08**
4536.6	1480.9	944.8	3997.8	5481.4	5478.6	10960.0	0.83	0.73	0.25	0.19	MEAN
25.4	24.7	25.0	24.5	2.5	2.5	0.0	0.00	0.00	0.00	0.00	ST.DEV

Table 5.1.6 - General confusion matrices for the eight models of the Briga and the Giampilieri suites.

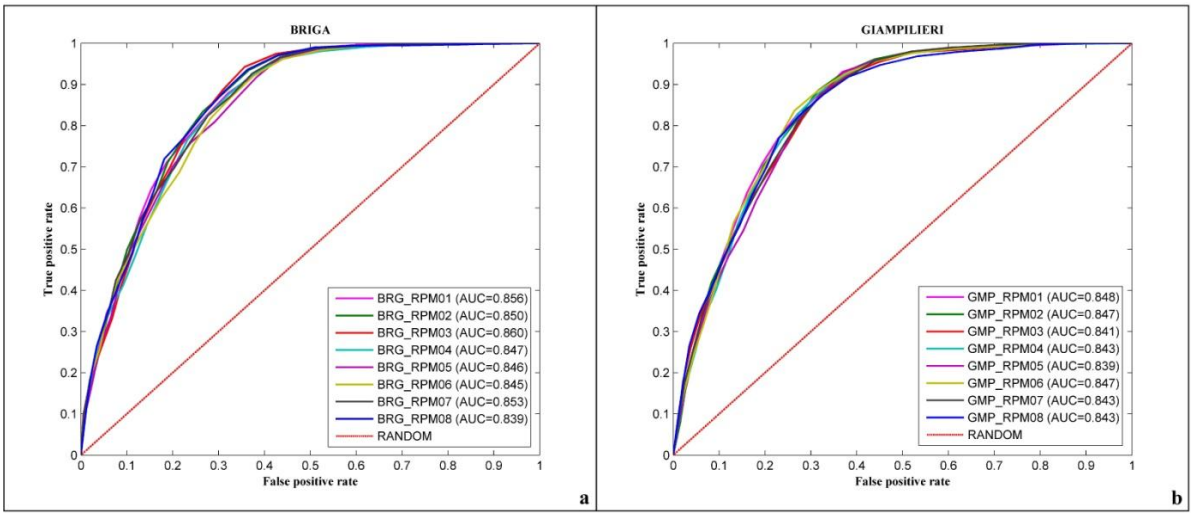

Figure 5.1.4 - Test ROC curves obtained for the Briga (a) and Giampilieri (b) RP-models.

Tables 5.1.7 and 5.1.8 show, for the Briga and Giampilieri catchments respectively, the list of included predictors, with the corresponding frequencies of selection and, for each of the eight models, their ranking (i.e. the step at which the predictor is included within the logit function) and regressed the β coefficient.

For the eight models of the Briga suite (Tab. 5.1.7), an average of 25 variables were found to be significant, at least in one extraction, among the 69 potential predictors when using a stepwise selection. The most important predictors selected for all eight models were the variables: HEIGHT, GEO_CARG_bb, SLONH, USE_3.2.2, whose order of selection was constant in the suite along with the corresponding signs of the regressed coefficients. The variables which were selected between eight and four times showed quite constant ranks and signs, with the exception of USE_2.2.3. ASP had a particular behaviour: for some of the classes, the stepwise selection algorithm alternatively extracted a class or its' opposite, obviously inverting the sign, so that actually eight times this couples controlled the final model. It is the case of ASP_S, which was extracted five times with positive signs; in the other three models of the suite, ASP_N took its place, but with negative coefficients. The same behaviour was shown by the couples ASP_SW/ASP_NE and ASP_W/ASP_E. In the few cases in which both the classes of the three couples of ASP were selected, a lowering of the coefficients of the most important was noted.

BRIGA SUITE: SELECTED PREDICTORS																				
Variables	BRG_RPM01		BRG_RPM02		BRG_RPM03		BRG_RPM04		BRG_RPM05		BRG_RPM06		BRG_RPM07		BRG_RPM08		MEAN		ST. DEV.	
	Rank	β	Rank	β	Rank	β	Rank	β	Rank	β	Rank	β	Rank	β	Rank	β	Rank	β	Rank	β
HEIGHT	1	-0.0067	1	-0.0071	1	-0.0071	1	-0.007	1	-0.007	1	-0.007	1	-0.0072	1	-0.0065	1	-0.0069	0	0.0002
GEO_CARG_bb	2	-3.2019	2	-3.2794	2	-3.1229	2	-3.7481	2	-3.3403	2	-3.4837	2	-3.1694	2	-3.1025	2	-3.306	0	0.2182
SLONH	3	0.0423	3	0.0446	3	0.0676	3	0.0733	3	0.0779	3	0.0386	3	0.0742	3	0.0673	3	0.06072	0	0.0161
USE_3.2.2	4	0.8899	4	2.3184	4	2.1631	4	1.0057	4	0.7609	4	1.3441	4	2.3895	4	0.7624	4	1.4542	0	0.7186
USE_3.1.2	8	-2.1575	6	-0.8719	5	-0.7947	9	-2.1205	5	-2.214	7	-1.7329	9	-0.4172	5	-2.7919	6.75	-1.6375	1.7525	0.842
GEO_CARG_SPDb	7	1.159	12	1.1478	8	1.1913	8	1.5056	11	1.2079	8	1.2372	7	1.3598	8	1.1894	8.625	1.2497	1.8468	0.1225
LAND1_VSRV	13	-0.5029	7	-0.5104	11	-0.5378	14	-0.4665	9	-0.4766	11	-0.4659	12	-0.4673	10	-0.5491	10.875	-0.497	2.2321	0.0333
LAND2_MT	9	0.6095	11	0.3167	13	0.5089	10	0.219	14	0.4943	15	0.2209	19	0.4508	14	0.4138	13.125	0.4042	3.1819	0.1409
SPISLO	12	0.4049	17	0.3536	12	0.4396	13	0.4725	13	0.5621	12	0.4592	22	0.2529	13	0.4264	14.25	0.4214	3.5355	0.0905
LAND1_USV	15	-0.5251	16	-0.501	15	-0.4629	15	-0.6075	10	-0.5312	18	-0.4002	14	-0.4184	15	-0.5134	14.75	-0.4949	2.2519	0.0666
LAND1_LRHBV	18	-0.2991	20	-0.4571	17	-0.3821	16	-0.5697	18	-0.3707	17	-0.444	13	-0.498	16	-0.4827	16.875	-0.4379	2.031	0.0847
GEO_CARG_PCTc	16	-2.8105	22	-3.1161	16	-2.7505	23	-2.0003	22	-2.1503	21	-2.5716	27	-1.7625	18	-14.0664	20.625	-3.9035	3.7772	4.1314
ASP_SE	11	0.5687	14	-0.392	10	0.4151	17	-0.425	24	-0.255	14	0.4735	10	0.6712	11	0.5831	13.875	0.2049	4.764	0.4741
ASP_S	6	0.9391	/	/	6	0.8791	/	/	/	/	6	0.8192	5	1.0459	6	1.0213	6.6666	0.9409	2.1602	0.095
ASP_SW	5	1.08	/	/	7	0.8885	/	/	/	/	5	1.0253	6	1.049	7	0.9758	6	1.0037	1	0.0748
ASP_W	14	0.5893	/	/	9	0.6479	/	/	/	/	13	0.6052	11	0.7481	12	0.7531	11.8	0.6687	1.9235	0.0777
ASP_N	/	/	5	-1.4195	21	-0.3588	6	-1.2543	6	-1.1323	22	-0.365	/	/	/	/	12	-0.9059	8.6891	0.507
USE_2.2.6	/	/	13	1.5228	18	1.5713	22	0.259	/	/	19	0.6573	15	1.6765	/	/	17.4	1.1373	3.5071	0.6382
USE_2.2.3	19	-0.422	25	0.9276	20	1.1003	/	/	19	-0.4405	/	/	18	1.1811	/	/	20.2	0.4693	2.7749	0.8272
SLO	/	/	/	/	25	-0.0211	24	-0.023	16	-0.041	/	/	16	-0.0257	22	-0.0196	20.6	-0.026	4.3359	0.0086
LAND2_VSRV	/	/	18	-0.6541	/	/	18	-0.7346	17	-0.5106	16	-0.5452	/	/	20	-0.2515	17.8	-0.5392	1.4832	0.1837
CUR5_CONC	/	/	8	0.0281	/	/	20	0.0211	21	0.0192	24	0.0162	/	/	/	/	18.25	0.0211	7.0415	0.005
LAND2_USV	/	/	19	-0.454	/	/	19	-0.5156	26	-0.2238	9	-0.4976	/	/	/	/	18.25	-0.4227	6.994	0.1351
USE_3.2.3	/	/	21	1.3072	19	1.3895	/	/	/	/	23	0.4413	17	1.4986	/	/	20	1.1591	2.5819	0.4849
GEO_CARG_PCTa	/	/	/	/	23	0.6916	25	0.6789	23	0.6683		/	23	0.7445	/	/	23.5	0.6958	1	0.0338
GEO_CARG_ASI	21	-12.9321	/	/	26	-12.9744	/	/	27	-13.4157	25	-13.6481	/	/	/	/	24.75	-13.2425	2.6299	0.3477
ASP_NE	/	/	9	-0.8364	/	/	5	-1.1055	8	-0.8342	/	/	/	/	/	/	7.3333	-0.9253	2.0816	0.156
ASP_E	/	/	10	-0.743	/	/	7	-0.82	7	-0.7914	/	/	/	/	/	/	8	-0.7848	1.732	0.0389
PRC5_CONC	10	-0.0454	/	/	14	-0.03622	11	-0.0338	12	-0.0415	/	/	8	-0.0561	9	-0.0466	10.6666	-0.0432	2.1602	0.008
ASP_NW	/	/	15	-0.667	/	/	12	-0.9395	15	-0.8784	/	/	/	/	/	/	14	-0.8283	1.732	0.1429
LAND2_LRP	17	0.7502	26	0.6016	24	0.5808	/	/	20	0.6443	/	/	20	0.8625	17	0.8617	20.6666	0.7168	3.6697	0.1267
LAND2_FRTMT	/	/	23	-0.2929	/	/	21	-0.3549	/	/	20	-0.2813	/	/	/	/	21.3333	-0.3097	1.5275	0.0395
LAND2_UID	20	0.3873	/	/	22	0.4853	/	/	/	/	/	/	24	0.5082	/	/	22	0.4602	2	0.0642
CUR5_CONV	/	/	24	-0.0172	/	/	/	/	/	/	10	-0.0247	/	/	/	/	17	-0.0209	9.8994	0.0053
PLC5_CONV	/	/	/	/	/	/	/	/	/	/	/	/	/	/	21	-0.0261	21	-0.0261	/	/
TWI	/	/	/	/	/	/	/	/	25	-0.1511	/	/	/	/	/	/	25	-0.1511	/	/
GEO_CARG_FDNb	/	/	/	/	/	/	/	/	/	/	26	-0.2179	/	/	/	/	26	-0.2179	/	/
LAND2_BOS	/	/	/	/	/	/	/	/	/	/	/	/	21	0.4898	19	0.3722	20	0.431	1.4142	0.0831
LAND2_LVP	/	/	/	/	/	/	/	/	/	/	/	/	25	0.7962	/	/	25	0.7962	/	/

Table 5.1.7 - Predictors selected by the forward BLR for the Briga RP suite.

GIAMPILIERI SUITE: SELECTED PREDICTORS																				
Variables	GMP_RPM01		GMP_RPM02		GMP_RPM03		GMP_RPM04		GMP_RPM05		GMP_RPM06		GMP_RPM07		GMP_RPM08		MEAN		ST. DEV.	
	Rank	β	Rank	β	Rank	β	Rank	β	Rank	β	Rank	β	Rank	β	Rank	β	Rank	β	Rank	β
HEIGHT	1	-0.0051	1	-0.0052	1	-0.0049	1	-0.0054	1	-0.0054	1	-0.005	1	-0.0051	1	-0.0052	1	-0.0052	0	0.0002
SLONH	2	0.0979	2	0.0929	2	0.0675	2	0.0901	2	0.0869	2	0.1014	2	0.0911	2	0.1005	2	0.091	0	0.0108
USE_3.2.2	3	0.9758	3	0.9296	3	0.852	3	0.9034	3	0.9692	3	0.8763	3	0.9541	3	0.9501	3	0.9263	0	0.045
GEO_CARG_bb	4	-2.0878	4	-2.0489	4	-2.0933	4	-2.1926	4	-2.0201	4	-2.2493	4	-2.1139	4	-2.3447	4	-2.1438	0	0.11
GEO_CARG_MLEa	5	-1.1136	5	-1.0189	5	-1.0524	5	-1.243	5	-1.0786	5	-1.0821	5	-1.1163	5	-1.245	5	-1.1187	0	0.0834
ASP_N	6	-1.3241	6	-1.2529	6	-1.2145	6	-0.784	6	-1.2974	6	-0.8762	6	-1.211	6	-0.8051	6	-1.0957	0	0.2314
ASP_NE	7	-0.7728	7	-0.7049	7	-0.8208	7	-0.4059	7	-0.8624	7	-0.3572	7	-0.6685	7	-0.5031	7	-0.637	0	0.1921
LAND2_MT	10	0.3732	10	0.6032	10	0.5781	15	0.4294	15	0.4185	13	0.4033	9	0.5392	16	0.341	12.25	0.4607	2.8158	0.0988
GEO_CARG_SPDb	11	-2.103	12	-2.1723	16	-1.8279	11	-2.0388	9	-2.2135	18	-1.3696	14	-1.6256	15	-2.1081	13.25	-1.9324	3.0119	0.2999
LAND2_VSRV	16	-0.326	16	-0.3541	17	-0.3667	13	-0.4322	19	-0.342	21	-0.2952	10	-0.4369	19	-0.2772	16.375	-0.3538	3.5431	0.0579
LAND1_VSRV	8	-0.2856	8	-0.2607	8	-0.2827	8	-0.1435	8	-0.3562	8	-0.4374	/	/	11	-0.2872	8.4286	-0.2933	1.1339	0.0898
USE_2.2.3	14	-0.5356	13	-0.4729	/	/	9	-0.6918	13	-0.6299	10	-0.6618	15	-0.4682	12	-0.7807	12.2857	-0.6058	2.1381	0.1178
SLO	15	-0.0238	18	-0.0263	/	/	12	-0.0316	17	-0.0216	11	-0.0378	16	-0.0247	13	-0.0358	14.5714	-0.0288	2.6367	0.0063
SPINH	/	/	15	0.227	22	0.1277	18	0.2252	20	0.2423	20	0.2007	20	0.1868	20	0.2448	19.2857	0.2078	2.2147	0.0411
PRC5_CONV	16	0.0269	9	0.0391	/	/	/	/	18	0.0297	14	0.0359	11	0.0397	14	0.0373	13.6667	0.0348	3.266	0.0053
LAND1_UID	19	0.2286	22	0.2626	19	0.3113	14	0.3567	22	0.2336	/	/	17	0.2357	/	/	18.8333	0.2714	3.0605	0.0519
CUR5_CONV	9	-0.0244	11	-0.0202	/	/	/	/	11	-0.0154	9	-0.0202	/	/	18	-0.0135	11.6	-0.0187	3.7148	0.0043
ASP_E	12	-0.3576	17	-0.4004	11	-0.4985	/	/	10	-0.4712	/	/	12	-0.4551	/	/	12.4	-0.4366	2.7019	0.0568
ASP_NW	17	-0.291	19	-0.435	13	-0.4715	/	/	14	-0.4849	/	/	13	-0.446	/	/	15.2	-0.4257	2.6833	0.0779
LAND2_BOS	21	-0.2901	20	-0.3391	/	/	16	-0.3609	12	-0.4818	22	-0.3441	/	/	/	/	18.2	-0.3632	4.1473	0.0713
FLANH	/	/	14	-0.0003	/	/	22	-0.0002	23	-0.0001	/	/	19	-0.0003	22	-0.0002	20	-0.0002	3.6742	0.0001
LAND2_LRHBV	/	/	23	0.3327	21	0.3715	19	0.4793	21	0.4183	19	0.3944	/	/	/	/	20.6	0.3992	1.6733	0.0548
ASP_SE	/	/	21	-0.2233	14	-0.2868	/	/	16	-0.2821	/	/	21	-0.2276	/	/	18	-0.255	3.559	0.0342
ASP_S	/	/	/	/	/	/	21	0.3074	/	/	12	0.4789	/	/	8	0.6493	13.6667	0.4785	6.6583	0.171
ASP_W	/	/	/	/	/	/	17	0.5397	/	/	16	0.4763	/	/	10	0.6859	14.3333	0.5673	3.7859	0.1075
ASP_SW	/	/	/	/	/	/	20	0.3368	/	/	15	0.3801	/	/	9	0.5536	14.6667	0.4235	5.5076	0.1147
LAND1_BOS	/	/	24	0.7374	15	1.1082	/	/	/	/			18	0.9027	/	/	19	0.9161	4.5826	0.1858
GEO_CARG_FDNb	/	/	25	0.1702	20	0.2037	/	/	/	/	24	0.1712	/	/	/	/	23	0.1817	2.6458	0.0191
CUR5_CONC	/	/	/	/	9	0.0264	10	0.0235	/	/	/	/	/	/	/	/	9.5	0.025	0.7071	0.0021
PLC5_CONV	/	/	/	/	12	-0.0292	/	/	/	/	/	/	8	-0.0417	/	/	10	-0.0355	2.8284	0.0088
LAND1_LVP	13	-1.0359	/	/	23	-0.708	/	/	/	/	17	-1.0308	/	/	/	/	17.6667	-0.9249	5.0332	0.1879
TWISLO	/	/	/	/	/	/	23	0.5378	/	/	23	0.5778	/	/	/	/	23	0.5578	0	0.0283
LAND1_USV	/	/	/	/	/	/	/	/	/	/	/	/	/	/	17	-0.2841	17	-0.2841	/	/
FLA	20	-0.0001	/	/	/	/	/	/	/	/	/	/	/	/	/	/	20	-0.0001	/	/
SPISLO	/	/	/	/	/	/	/	/	/	/	/	/	/	/	21	-0.1865	21	-0.1865	/	/

Table 5.1.8 - Predictors selected by the forward BLR for the Giampilieri RP suite.

Regarding the suite of models analysed for Giampilieri, 23 variables were selected on average as significant through the forward stepwise selection (Tab. 5.1.8). Among the group of ten variables which were systematically extracted, the first seven variables were selected in the same order of importance for all the eight models: HEIGHT, SLONH, USE_3.2.2, GEO_CARG_bb, GEO_CARG_MLEa, ASP_N, ASP_NE. Similarly to the Briga suite, ASP and CUR5 produced a coupling effect in the suite, with ASP_E and CUR5_CONV, having negative coefficients, being replaced for three models by positive ASP_N and CUR5_CONC. Generally, the variables selected at least four times showed quite constant ranks within the suite and a frequency of selection which is inversely correlated to their relevance in the model. The

whole suite of models showed a high stability in the regressed coefficients and no sign inversion for each predictor.

By exponentiating the logit functions produced by each model of the two suites the probabilities of landslide occurrence for each cell were derived, whose values are limited between 0 and 1. The eight averaged susceptibilities obtained from each of the two RP-suites were used to build the landslide susceptibility maps showed in Figures 5.1.5a and 5.1.6a, for Briga and Giampilieri respectively, in which the mean value is plotted. According to Guzzetti et alii (2006) and Rossi et alii (2010), in order to estimate and depict the precision of the method, the dispersion of each susceptibility estimate, measured by a 2 standard deviations interval, was also computed and plotted in a model error map (Figs. 5.1.5b and 5.1.6b).

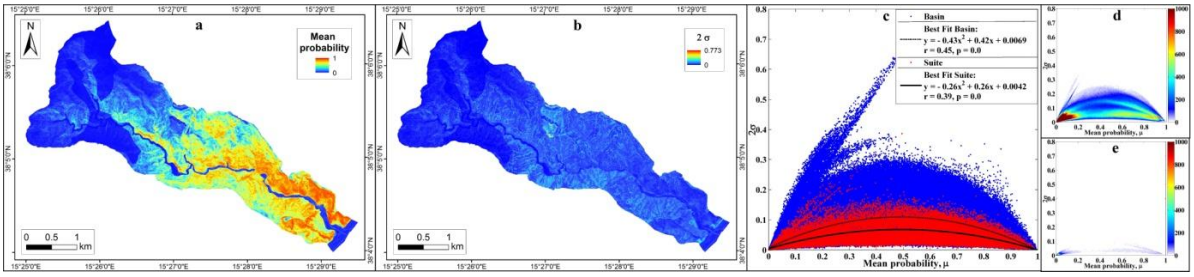

Figure 5.1.5 - Analysis of the precision of the Briga RP-models: a, averaged susceptibility (μ); b, 2σ map; and c, μ versus 2σ plot.

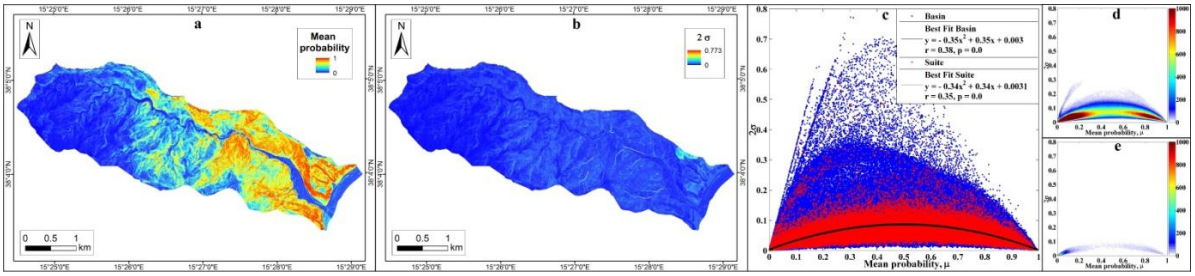

Figure 5.1.6 - Analysis of the precision of the Giampilieri RP-models: a, averaged susceptibility (μ); b, 2σ map; and c, μ versus 2σ plot.

At a low scale analysis, the susceptibility maps of both the two catchments show a zonation effect, being characterized by a very susceptible lower south-eastern sector, an intermediate susceptibility middle sector and an almost unsusceptible uphill north-western zone. In particular, the highly susceptible zone in the Briga catchment is marked by higher values in

the left flank, whilst a more symmetrical susceptibility distribution characterizes the lower south-eastern sector of the Giampilieri catchment.

The error maps attest for the very high precision of the modelling procedure, with the exception of two small poorly susceptible enclaves (in the middle sector of the left flank, the one of Briga, in the lower sector of the left flank, the one of Giampilieri) which are produced by the outcropping of very poorly diffused lithologies.

To explore the relationship between estimate and precision, mean probabilities against their variations, were plotted (Figs. 5.1.5c, 5.1.6c); we then calculated the best fit for the data of two datasets using a quadratic regression. In order to depict the real frequency distribution of the cells in the error plots, the latter have been resampled using a 0.005 mesh so that a more representative view was obtained for the whole catchment (Figs. 5.1.5d, 5.1.6d) and the suites (Figs. 5.1.5e, 5.1.6e). This analysis was performed both on all the cells of the catchments (basin) and only considering the cells which were included into the model datasets (suites). The regression demonstrates a very efficient performance on both types of analysis for the two catchments, highlighting a very limited loss in precision toward the centre of the distribution, which is the critical window of the probability scale: for the largest part of the mapped areas, almost 95% (2σ) of the eight different predictions are dispersed inside an interval of less than 0.1 at the mean sides. The comparison between the regression curves obtained for the whole basins and the suites highlights how the more dispersed distribution of the cells in the μ-2σ plot for Briga, results in a detectable shift between the two curves, in spite of the almost perfect coincidence for Giampilieri.

Both error plots are affected by diagonal effects on the left side, which were verified as due to the poorly low susceptible lithologic enclaves. This effect is larger for the Briga catchment, where the extension of the enclave is larger.

5.1.7 *Results for the SP-models*

Before exporting the SP-models from Briga new modelling procedures were performed by considering the full eight Briga datasets (100% of positives and negatives). This produced the SP-models whose characteristics (extracted predictors, ranking and coefficients) are almost

identical to the ones obtained for the Briga RP-models (Table 5.1.7), as it was expected in light of the high robustness of the model. Table 5.1.9 shows the results for the sixty-four validation procedures obtained by exporting the eight Briga-fully trained models to fit the eight Giampilieri-full test datasets (100% of positives and negatives).

		BRIGA									
		RPM01	RPM02	RPM03	RPM04	RPM05	RPM06	RPM07	RPM08	MEAN	ST. DEV.
GIAMPILIERI	RPM01	0.8185	0.8189	0.8187	0.8185	0.8217	0.8185	0.8172	0.8171	0.819	0.001
	RPM02	0.8235	0.824	0.8242	0.8231	0.8265	0.8235	0.8221	0.8226	0.824	0.001
	RPM03	0.8203	0.8203	0.8200	0.8207	0.8232	0.8203	0.8186	0.8191	0.820	0.001
	RPM04	0.8208	0.8215	0.8209	0.8207	0.8234	0.8208	0.8203	0.82	0.821	0.001
	RPM05	0.8205	0.8202	0.8207	0.8202	0.8229	0.8205	0.8167	0.8188	0.820	0.002
	RPM06	0.8188	0.8739	0.8193	0.8191	0.8222	0.8188	0.8178	0.8188	0.826	0.019
	RPM07	0.8179	0.8736	0.8178	0.8184	0.8220	0.8179	0.8165	0.817	0.825	0.020
	RPM08	0.8248	0.8738	0.8249	0.8241	0.8279	0.8248	0.8228	0.8237	0.831	0.017
	MEAN	0.821	0.841	0.821	0.821	0.824	0.821	0.819	0.820	0.827	
	ST. DEV.	0.002	0.027	0.003	0.002	0.002	0.002	0.002	0.002		

Table 5.9 - Predictive performances of the Briga vs. Giampilieri SP suites.

The sixty-four test-AUC values are all above the 0.8 excellence threshold (Hosmer and Lemeshow, 2000) attesting for a highly stable prediction skill in the exportation phase, with the exception of three of the BRG_M02 trained models. These clearly deviated from this trend, producing AUCs surprisingly higher than the source training when combined with GMP_M06-08. Among the remaining sixty-one combinations, the worst validation was obtained by BRG_M07 Vs GMP_M07 (AUC = 0.8165), while the best validation (BRG_M05 Vs GMP_M02) resulted in an AUC of 0.8265.

By averaging the sixty-four probability values which were produced by the SP-models, a mean susceptibility map was derived (Fig. 5.1.7).

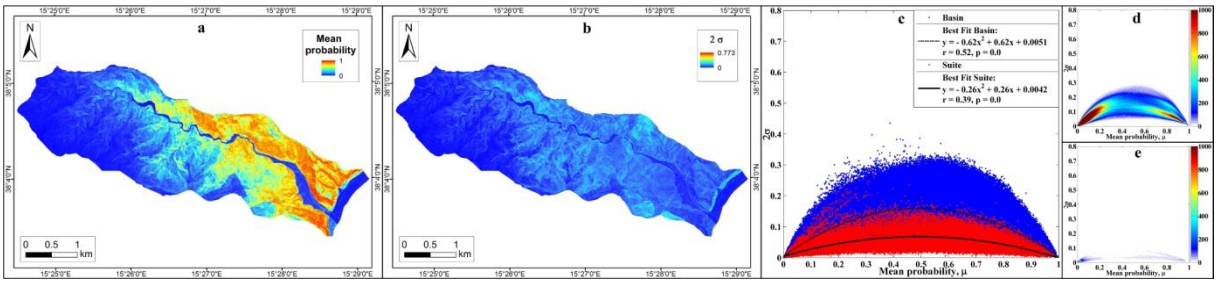

Figure 5.6 - Analysis of the precision of the Briga versus Giampilieri SP-models: a, averaged susceptibility (μ); b, 2σ map; and c, μ versus 2σ plot.

The comparison with the relative RP-map (Fig. 5.1.6) clearly shows a large agreement between the susceptibility zoning in the Giampilieri catchment, with the SP-models resulting in quite larger susceptible areas, whose internal distribution is more spatially autocorrelated and less clustered. The low susceptible enclave in the lower left sector of the catchment is no longer present, because the training in the SP-model was more effective with respect to the lithology in the enclave, which more largely outcrops in the Briga catchment; the error plots (Fig. 5.6c) are now free of diagonal effects thanks also to the absence of the Briga enclave lithology in the training dataset. As regards to the predictive performance, the test-AUC for the SP-model was on average 0.827, just 2% less than the one for the Giampilieri RP-model (0.844).

5.1.8 *Discussion and conclusions*

Debris flows *l.s.* are among the more hazardous phenomena in nature, which typically take the form of widespread multiple events triggered by intense driving inputs such as storms or earthquakes. In this research we test a strategy for preparing susceptibility maps that are focused on the initiation phase. Therefore we processed the whole landslide inventory as one, no matter the initiating source phenomenon (pure slide or flow) from which debris flow or avalanche evolutions derived. We considered in fact that with respect to the selected predictors, none if any difference between slides and flows would arise. The predictive models that are here discussed so refer uniquely to the activation phase and the derived maps "simply" try to depict where slides or flows are likely to initiate, possibly giving the trigger downslope to debris flow or debris avalanche phenomena propagations. Modelling the propagation and run-out phases, which would require multidisciplinary approaches and more data, was out of the focus of this research.

The use of binary logistic regression (BLR) and a set of geo-environmental factors to prepare a cell based predictive model proved to be effective in assessing debris flow/debris avalanche initiation susceptibility in two catchments of south-eastern Sicily, both of which were hit by an extreme climatic event (ECE) in October 2009. In particular, a test was carried out in order to explore the possibility of using an exportation procedure to assess the landslides susceptibility.

Two 8-fold suites of random partition (RP) based models were prepared for the Briga and the Giampilieri catchments. Eight different balanced datasets of positives and negatives were used, each including the same set of positives and one among eight different randomly selected sets of negatives. A stepwise forward selection method was followed in applying BLR, so that the reliability of the regressed models was tested by taking into consideration the general performance of the models (model fitting and prediction skill) as well as their robustness in terms of selected variables (ranking and coefficients). Excellent model fitting and prediction skill values were obtained for both suites of RP-models, with very high AUC values (0.850, for Briga; 0.844, for Giampilieri) and an overall high stability (standard deviations of 0.07 and 0.03, for the AUC of Briga and Giampilieri, respectively).

Adopting a stepwise selection procedure allowed us to evaluate the stability of the core structure of the regressed models (predictors, ranks and coefficients), giving us a further criterion in evaluating the model accuracy. In particular, the ranks were not considered in the only recent papers in which the robustness of the models was estimated by multi-fold techniques (Carrara et al., 2008; Frattini et al., 2010; Guzzetti et al., 2006; Rossi et al., 2010; von Ruette et al., 2011). For both suites, the eight replicates produced very similar ranks and coefficients for the most frequently selected variables, whilst instability in the coefficients or ranks was observed only for those secondary variables selected less than four times; the latter were typically extracted with low rank by the stepwise selection procedure.

The results of the validation procedures demonstrated that in the study area susceptibility conditions are primarily controlled by altitude, steepness, aspect, outcropping lithology and soil use; secondary factors were topographic curvatures and morphological setting. The role of altitude could be linked to the multivariate setting of the study areas along with the fact that the landslides were almost exclusively triggered in the lower-middle and coastal sector of both catchments. This seems to be linked to the combination of geologic and geographic factors. Looking at the susceptibility maps that were obtained, it seems that an increasing susceptibility trend can be defined, depending on the metamorphic grade of the outcropping lithology, when passing from the Aspromonte Unit high grade (gneiss, paragneiss and mica schists), to the Mela Unit intermediate grade (paragneiss and mica schists) up to the Mandanici Unit (phyllites) metamorphic rocks. This could be due to the parallel increasing in the grade of weathering processed, both in terms of thickness of the mantle and mineralogic, hydrologic and mechanic properties of the derived soils. At the same time, as the storm moved

north-westward from the sea up to the inner sectors, we expect that the largest part of rainfall was discharged on the lower areas.

We exported the model trained as RP-model in Briga to predict the landslide distribution in the Giampilieri catchment, obtaining a very high performance on a 64-fold suite of models (AUC = 0.822), demonstrating that the same controlling factors, in the same order of ranking and with the same coefficients allow us to predict the landslides in Giampilieri, by knowing only the landslide inventory in Briga. In light of the similarity between the predictive performances produced by the Giampilieri RP-models and the exported SP-model, we can conclude that the susceptibility conditions for the Giampilieri catchments could have been assessed with the same performance without knowledge of its landslide distribution. This means that, provided a geomorphological homogeneity is verified, reliable prediction images of landslides can be produced by preparing susceptibility models outside the study area, through what we have called an 'exportation procedure'. This method is very similar to the validation procedures based on spatial partition (Chung and Fabbri, 2003), where to model the susceptibility of a catchment, a spatial splitting in two homogeneous sub-areas is applied to obtain one training and on test sub-area. Otherwise, also differently from von Ruette et alii (2011), in this application to verify the effectiveness of the exporting procedure, we compare the performances of the "typical" random partition based model for the target area to that of the spatial partition model obtained from the source area, verifying that a negligible (3%) decreasing in the test-ROC AUC for the latter. Moreover, the quality of the validations is systematically excellent (AUC > 0.8) for all the suites of models we prepared.

The perspective is to check the possibility to export the prediction far from the training source catchment. We start here from comparing two adjacent catchments but it must be noticed that, depending on the local character of the ECE, catchments at a distance of 2-3 kilometres, draining trough the same eastern Ionian slopes of the Peloritani chain, experienced few or any landslides following the event of the 1st of October 2009, so that a severe underestimation of their susceptibility conditions would arise if using local random partition based models. At the same time, for the same reasons, using temporal partition based model (i.e. in the same area, preparing a model by training and testing it, exploiting multi-temporal shifted landslide inventories) could result as impossible or misleading when trying to predict ECE-driven landslide events in the Mediterranean area. Differently from the tropical cyclones, ECE in the southern Mediterranean region are caused by very slow moving thunderstorm cells, which are

produced by self-generating meso-scale convective super-cells, in the autumn season, which develops during the easterlies breakdown stage, when still the seawater of southern Mediterranean is warm (see Tartaglione et al., 2006). Rainfall storms are rare and local events, so that for the majority of areas the required landslide inventories are as a matter of facts non-existent! Some exception is made by the recently stricken areas, which would allow us to properly train stochastic predictive models, provided a landslide recognition is carried out soon after the event. In fact, as the typical morphodynamic response consist of shallow landslides, differently from arid areas, it takes very few time for the "normal" hillslope processes and vegetation to erase or blind all the landforms we have to look for. In this sense, together with immediate field surveys on the post-event scenario, which are mandatory to enter in the morphodynamic and physical details of the phenomena, the optimization of remote sensing techniques for expert semi-automatic landslide recognition is a strategic topic (Mondini et al., 2011).

The above considerations are somewhat confirmed by the limits in the results obtained by von Ruette et alii (2011), which performed exportation procedures to predict landslide scenarios driven by the same rainfall between dissimilar catchments and by different rainfall events between similar catchments. Particularly, what they found to be an overestimation of the susceptibility is here assumed as the rule when training a model with a more severe landslide scenario and exporting it onto less or non-stricken catchments. Comparing landslide inventories produced by different rainfall events is in fact misleading, as it assumes a linearity between climatic input and morphodynamic response. Nevertheless, assessing ECE-driven shallow landslide susceptibility should be based on the most severe expected landslide scenarios for training the model with caution. Moreover, under this kind of triggers, geomorphologic dissimilarities tend to poorly control the slope failure phenomena, which result as driven by few basic features (the weathered mantle: thickness, hydrological and geotechnical properties; the slope morphometry: steepness, plan and profile curvature).

Exporting susceptibility models could represent a very effective strategy in coping with landslide susceptibility assessment with respect to time/money costs savings; at the same time, such models provide what appears to be the only viable approach to prepare stochastic prediction models for ECE-driven landslide scenarios. These predictive models are actually getting more and more compelling: in the whole north-eastern Sicilian sector where the 1st

October 2009 storm moved, which extends for some tens of square kilometres, more than five thousands of landslides triggered in few hours.

5.2 LOGISTIC REGRESSION VERSUS DECISION TREES IN ASSESSING LANDSLIDE SUSCEPTIBILITY FOR MULTIPLE-OCCURRING LANDSLIDE EVENTS: APPLICATION TO THE 2009 STORM EVENT IN MESSINA (SICILY, SOUTHERN ITALY).

Lombardo, L., Cama, Conoscenti, C., M., Maerker, M., Rotigliano, E., Natural Hazards, submitted.

5.2.1 *Research objectives*

Since the earliest landslide susceptibility studies the scientific community have been testing several approaches, which are commonly categorised as analytic, heuristic, deterministic and stochastic (Guzzetti et al., 1999; Brenning, 2005). With regards to the stochastic approaches, several statistic and/or data mining techniques have been applied, each having advantages and disadvantages (Akgun 2012; Den Eeckhaut et al., 2010; Felicísimo et al. 2012; Guzzetti et al. 2005; Rossi et al. 2010; Nefeslioglu et al. 2008; Süzen and Doyuran 2004; Vorpahl et al. 2012; Yalcin et al. 2011; Yesilnacar et al. 2005), among which two techniques have recently been gaining popularity: logistic regression and decision trees methods. Both the methods exploit a set of independent variables, which play the role of predictors, to produce an estimate of the status of each of the mapping units in which the study area is partitioned. The main difference between the two methods lies in the way in which the hyperspace of the predictors is explored and modelled: logistic regression techniques look for linear or multi-linear functions, optimizing the parameters of the multivariate function that links the outcome (stable/unstable condition) to the predictors. Conversely, decision trees techniques aims to identify group membership to one of the two categories (stable/unstable) without looking for linear or simple general laws, instead sequentially partitioning in random trees and nodes the predictors' hyperspace. Logistic regression algorithms are constrained to minimize gradients in the response curves of each single predictor (normally just one coefficient), whilst decision trees based algorithms allow for large and/or frequent discontinuities.

Within the two families of statistic methods, many machine-learning sub-categories can be found, but they all share the same core structure of two key steps, the first one being a calibration step, where they learn how to distinguish between stable and unstable conditions through a set of geological-geomorphological features and a training inventory of landslides. The second step consists of a prediction process, where the estimated stable/unstable probabilities are tested in matching the status of an unknown test landslide inventory. The performance in goodness of the fit, for calibration, and prediction skill, for prediction, can be evaluated through the use of ROC (Receiver Operating Characteristic) plots and confusion matrices, while the evaluation of the reliability of the models requires the implementation of multi-folds based modelling iterative procedure (cross-validation and/or boot strapping methods). This allows the accuracy and the precision of each estimate (selected predictors and coefficients, in the model; predicted status and associated probability of each mapping units, in the map) to be measured (Costanzo et al. 2014; Fabbri and Chung 2008; Frattini et al. 2010; Guzzetti et al. 2006; Irigaray et al. 2007; Lombardo et al. 2014; Petschko et al. 2014; Rossi et al. 2010).

In this paper, we compare two current widely used regression and decision trees classification methods, Binary Logistic Regression (Hosmer and Lemeshow 2000) and Stochastic Gradient Treeboost (Friedman, 1999), using as a case study the Mediterranean multiple-occurrence regional landslide event (MORLE; Crozier 2005) that took place on 1st October 2009 in the Messina area (southern Italy). This disaster was triggered by a storm, which caused the almost simultaneous activation of thousands of landslides, causing massive losses in terms of both infrastructure and human lives. The storm was roughly centred in the area of the two catchments of the Briga and Giampilieri streams (Messina, Italy).

The Messina 2009 event has recently been used in several studies with different topics and approaches (Ardizzone et al. 2012; Aronica et al. 2012; De Guidi and Scudero 2013; Del Ventisette et al. 2012; Gullà et al. 2012; Lombardo et al. 2014; Mondini et al. 2011).

We selected this case study to build and compare predictive models based on logistic regression and a decision trees classification algorithm, Binary Logistic Regression and Stochastic Gradient Treeboost (hereafter BLR and SGT, respectively).

Utilizing the same set of predictors and the 2009-event landslide archive, BLR- and SGT-based susceptibility models were obtained for the two catchments separately, adopting a random partition (*RP*) technique for validation. Additionally, the models trained in one of the

two catchments (Briga) were tested in predicting the landslide distribution in the other (Giampilieri), adopting a spatial partition (*SP*) validation procedure. All the validation procedures were based on multi-folds tests so as to evaluate and compare the reliability of the fitting, the prediction skill, the coherence in the predictor selection, and the precision of the susceptibility estimates.

5.2.2 *Materials and methods*

In this contribution, we analysed the performances of two methods used for predictive modelling aiming to compare the two final susceptibilities. The first method was the Binary Logistic Regression (BLR). The purpose of this statistical technique is to find the best fitting and most parsimonious reasonable model to describe linear relationships between the logit (or log odds) of the outcome (dependent) and a set of *p* independent explanatory variables (Hosmer and Lemeshow 2000):

$$logit(Y) = ln\left[\frac{\pi}{1-\pi}\right] = \alpha + \beta_1 X_1 + \beta_2 X_2 + \cdots + \beta_p X_p,$$

where the logit is the natural logarithm of the odds of Y; the odds are ratios of probabilities (π) of Y occurring (the cell is unstable) to probabilities $(1 - \pi)$ of Y not occurring (the cell is stable); α is the Y intercept; the X's are the input predictor variables and the β's are the regression coefficients. Taking the antilog on both sides of the previous equation, an equation to predict the probability of the occurrence of the outcome π is derived:

$$\pi(Y|\mathbf{X}) = \frac{e^{\alpha+\beta_1 X_1+\beta_2 X_2+\cdots+\beta_p X_p}}{1+e^{\alpha+\beta_1 X_1+\beta_2 X_2+\cdots+\beta_p X_p}}.$$

By comparing the two equations, it is evident how the logit transformation works in linearizing the regression function whose parameters we have to estimate.

BLR can handle any type of predictors (nominal, ordinal, interval and ratio scale), without requiring any specific properties for their distributions; the dependent must be defined on a binary level (stable/unstable). The fitting of the logistic regression model, which is performed by adopting maximum likelihood estimators, enables us to estimate the coefficients βp. In this way, it is possible to predict the outcome from the input predictors and their coefficients.

As the fitting of the model is based on maximizing the value of a likelihood function, comparing the likelihood itself allows us to estimate the goodness of different regression models. In particular, by multiplying by −2 the log-likelihood ratio, the negative log-likelihood (−2LL) statistic is obtained, which has an approximate *chi square* (χ^2) distribution, so that the significance of a difference between the fitting of different models can be estimated in terms of probability of occurrence by chance. Based on this approach, we performed logistic regression following a stepwise basis, which allowed us to select, among a large set of variables, a restricted group made up of only those that significantly increase the performance of the multivariate model. Starting from a "constant only" model, at any step, the most important variable is the one that produces the greatest change in the log-likelihood relative of the model that does not contain it.

In this research, to perform the forward stepwise logistic regression, an open source software for data mining was used (TANAGRA: Rakotomalala, 2005).

The second method we applied was the Stochastic Gradient Treeboost (Friedman 1999, 2001), also called boosted regression trees (Elith et al., 2008), which combines classification and regression trees (CART) with the stochastic gradient boosting algorithm.

The stochastic gradient boosting is a meta-algorithm that builds a model by iteratively and randomly adding to its base form a weak learner whose parameters are set to let it lie approximately on the negative gradient direction of a given loss function, with the purpose of minimizing it step by step. The variable components of this meta-algorithm are the weak learner and the loss function, which in this case are respectively a CART and the Huber-M loss function.

CART analysis recursively partitions observations in matched data set, consisting of a categorical (for classification trees) or continuous (for regression trees) dependent (response) variable and one or more independent (explanatory) variables, into progressively smaller groups (De'ath and Fabricius 2000, Prasad et al. 2006). Each partition is a binary split based on a set of decision rules that identify homogeneous groups of the response variable as a function of a set of explanatory variables. To limit overfitting, algorithms used in CART usually simplify or "prune" the saturated tree, which includes all possible splits of the data, to an optimal tree that contains only the sufficient number of splits to describe the data.

The Huber-M loss function is an improvement over the Square Loss function that is less prone to be influenced by noise, especially in case of heavy-tailed distribution; it treats big deviations linearly and little deviations as an ordinary Square Loss function.

For the application of the SGT, we used the Salford Systems implementation in TreeNet®, training all models with a fixed tree complexity of six nodes and a bag fraction of 0.75. We also adapted the learning rate of each boosted regression tree to achieve a final number for the whole suites of 2000 trees per model, so to reduce prediction uncertainty. The best model was selected among the two thousand through an error function criterion, which was applied for the training data over successive trees and to an independently sampled testing dataset at each stage of the modelling procedure. TreeNet® implements this function in order to reduce the overfitting problem. It is possible in fact to identify automatically the tree where the model begins to overfit the data in correspondence to performance deterioration of the independently sampled test data.

5.2.3 *Datasets*

In order to statistically analyse the spatial relations between the predictors (landslide controlling factors) and the outcome (landslide/not landslide status) in the study area, we needed to partition it into mapping units. Each unit was assigned the values of the *p* predictors and the binary status or outcome. This was easily performed using GIS technology to process the source data and derive the informative raster layers. The intersection of the raster layers enables us to "synchronize" the geographic and the parameters spaces. In particular, the study area was partitioned into 2.5×10^6 (Briga) and 2.6×10^6 (Giampilieri) 2m square cells, each of which was assigned a status and a position in the multivariate domain of the parameters.

The independent variable dataset used in the modelling, consisted of 18 geo-environmental attributes: i) elevation, HEIGHT; ii) local Steepness, SLO; iii) 5m neighbourhood SLO, SLONH; iv) local Topographic Wetness Index, TWI; v) 5m neighbourhood TWI, TWINH; vi) Slope-TWI, TWISLO (TWI divided by its standard deviation); vii) local Stream Power Index, SPI; viii) 5m neighbourhood SPI, SPINH; ix) Slope-SPI, SPISLO (SPI divided by its standard deviation); x) local Flow Accumulation, FLA; xi) 5m

neighbourhood FLA, FLANH; xii) 5m neighbourhood Profile curvature, PRC5 (concave and convex); xiii 5m neighbourhood Plan curvature, PLC5 (concave and convex); xiv) 5m neighbourhood General curvature, CUR5 (concave and convex); xv) outcropping lithology, GEO_CARG (15 classes); xvi) land use, USE (10 classes); xvii) slope aspect, ASP (8 classes); xviii) two different landform classification, LAND1 and LAND2 (10 classes). LAND1 and LAND2 have been computed by setting two different couples of search radii (20/100m and 50/250m respectively).

The topographic variables were derived from a digital elevation model (DEM) with 2m cell size and 0.17m vertical resolution, released by ARTA from a LIDAR coverage dated at 2007 (pre-event). Outcropping lithology and land use were obtained from available geologic (Lentini et al., 2000) and land use (Corine Landcover 2006) maps.

Table 5.1.1 lists the whole set of predictors and the codes we adopted in the following for clarity.

To complete the preparation of the final dataset for the statistical modelling, we needed a layer expressing the status (the outcome) of the dependent, for each of the 2m cells. This is generally done by assigning stable or unstable conditions as derivable from the landslide spatial distribution. However, predictive models are designed to predict future phenomena rather than recognize objects. For this reason, the stable/unstable status of each cell must be evaluated in terms of its predisposing conditions for a future failure. Instead of simply assigning unstable conditions to those cells falling inside past landslides and stable conditions to the outer ones, for susceptibility modelling it is crucial to predict those cells which reasonably express the triggering conditions. These cells, on the basis of a geomorphological model, fall within a so-called (Costanzo et al. 2012a; Rotigliano et al., 2011; Van den Eeckhaut et al., 2009) diagnostic area or seed area (Süzen and Doyuran, 2004). A simple automatically generated diagnostic area was used to obtain an objective (operator-independent) and time saving solution, at the same time respecting a geomorphological criterion in case of shallow landslides. By using GIS tools for DEM processing, LIPs (Landslide Identification Points) were initially derived for each landslide by extracting the highest point along the boundary of each polygon. Subsequently a 2.82m radius (corresponding to the diagonal of a 2m cell) was spanned from each LIP, and all the intersected cells were set as unstable. This resulted in 5646 and 7307 unstable cells for the Briga and the Giampilieri catchments, respectively.

5.2.4 *Model building and validation strategy*

Regression techniques generally require balanced datasets as inputs, in which the number of positive (unstable) cases are the same as negatives (stable). The machine learning process in fact is better supported when the data expressing stability and instability are balanced (Costanzo et al. 2014; Lombardo et al. 2014; Nefeslioglu et al., 2008; Suzen and Doyuran, 2004; Yesilnacar and Topal, 2005). In order to create such balanced datasets we had to define a procedure to select from the negative cases (which were around half-million times more numerous than positives) subsets made of an equal number of the corresponding positives.

We initially generated a synthetic coarser (10m) grid coincident with the two catchments. After having erased the 10m cells that intersected LIPs, eight subsets of negative cells were identified by randomly extracting among the centroids of the remaining. The positives cells where then merged and combined with each of the chosen subset of negative (stable) cases obtaining two suites of eight different datasets, one for the Briga catchment and the other for the Giampilieri catchment. In fact, in order to perform a complete validation of the susceptibility models, suites of *n* (eight, in this case) models were prepared. N replicates enable an estimation of the robustness of the methods, in terms of selected factors, regressed coefficients, and accuracy and precision of the estimates. Each dataset was initially submitted to a validation procedure based on a split-sample (hold-out) method, consisting of the random splitting of the whole balanced dataset, with the selection of a 75% training subset and a 25% test subset. The error distribution of the performance metrics and estimated model was also estimated utilizing the suites of eight datasets.

Each of the eight single datasets for the Briga catchment was modelled with the following parameters: the whole dataset (11292 cases) used for the modelling was randomly separated into a training (8469 counts) and a test (2823 counts) fraction. Similarly, each of the eight single datasets for the Giampilieri catchment had an entire dataset (14614 cases), which was also randomly separated into training (10960 counts) and test (3654 counts). Due to the similarity with random partition based validation procedures described by Chung and Fabbri (2003), the two suites of eight models were referred to as *RP*-models (BRG-*RP* and GMP-*RP*, for the Briga and the Giampilieri catchment respectively).

Analogously to spatial partition based validation procedures (Chung and Fabbri, 2003), we built a third suite (*SP*-models), made of 64 single datasets, generated from the combination

of the eight BRG-*RP* and the eight GMP-*RP*, which we named BRGtoGMP-*SP* models (Costanzo et al. 2012b; Lombardo et al. 2014; Von Ruette et al. 2011). These datasets were exploited to test the capacity of assessing the landslide susceptibility in the Giampilieri catchment by training the models within the Briga catchment. Each of the 64 datasets was modelled using the whole dataset (25906 cases), split into BRG-*RP* 11292 cases for training component and GMP-*RP* 14614 for testing.

The comparison between the two methods was based on the analysis of the reliability of the predictive *RP*- and *SP*-models they produced. The reliability of the models was tested in terms of goodness of fit, prediction skill, precision, and robustness (Costanzo et al. 2014; Frattini et al. 2010; Guzzetti et al. 2006; Irigaray et al. 2007; Petschko et al. 2014; Rossi et al. 2010).).

With regard to the adopted validation procedures and the metrics we selected to compare the two methods, we built ROC (Receiver Operation Characteristic) plots and computed the AUC (Area Under Curve) for each model to estimate the overall prediction skill, whilst on a 0.5 threshold value for probabilities, we calculated True Positives (TP) and True Negatives (TN) to evaluate the error rate of each model.

Exploiting the *n* (8, for *RP*-models, 64, for *SP*-models) replicates, we prepared error density plots and error maps together with the susceptibility maps (expressing the mean probability on the suite). Error density plots show the relations between position and dispersion of the probabilities, while error maps highlight the spatial distribution of the precision (the width of a 2σ interval).

At the same time, the robustness of the models was evaluated by comparing the inner structure of the different models inside each *RP*- and *SP*-suite (Costanzo et al., 2014; Frattini et al. 2010; Lombardo et al. 2014). Selected factors and ranking, for BLR, predictor importance and response curves, for SGT, were the elements evaluated and compared.

Further plots and maps were prepared for comparison purposes and are presented in the discussion section.

5.2.5 *Results for the RP-models*

The two suites of eight datasets have been analysed for the two catchments with both BLR and SGT and the results have been compared in order to ascertain the differences in performances.

The ROC-plots of the *RP*-models obtained for two catchments (Fig. 5.2.1) highlighted that SGT produced a more enhanced prediction skill, reaching an outstanding performance (Hosmer and Lemeshow 2000), with AUCs of 0.94 and error rates above 0.1.

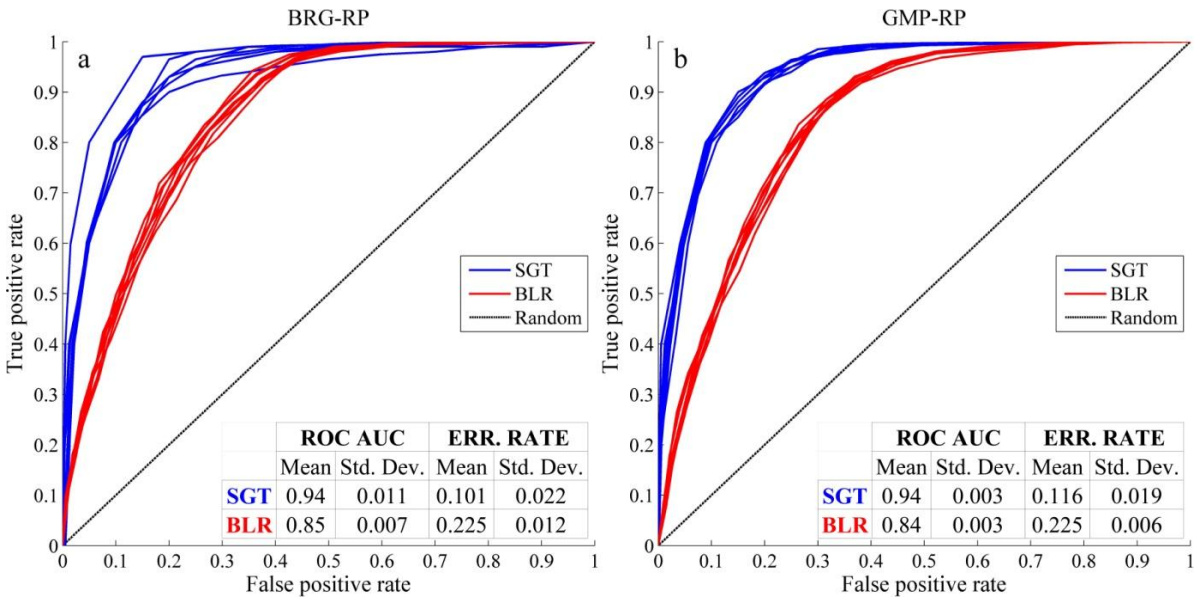

Figure 5.2.1 - Receiver Operating Curve (ROC) plots for Briga (BRG-RP: a) and Giampilieri (GMP-RP: b) random partition based models. Binary Logistic Regression (BLR) and Stochastic Gradient Treeboost models (SGT) are compared (red and blu curves, respectively).

At the same time, according to Hosmer and Lemeshow (2000) BLR models performed with lower but excellent AUCs (close to 0.85) and higher error rates (0.225). With regard to the stability of the prediction skill of the models through the eight replicates, a greater robustness of the model was clearly shown for BLR for the Giampilieri catchment, while no significant difference was observed for the Briga catchment. For both the catchments, the better performance of SGT-models emerged in the sector corresponding to the greater probabilities on the extreme left side of the plot.

By looking at the susceptibility maps produced by the two different techniques (Fig. 5.2.2), expressing the mean probability values computed through the eight *RP*-replicates,

differences can be observed, generally corresponding to a smoother and less binarized classification of the probabilities for BLR.

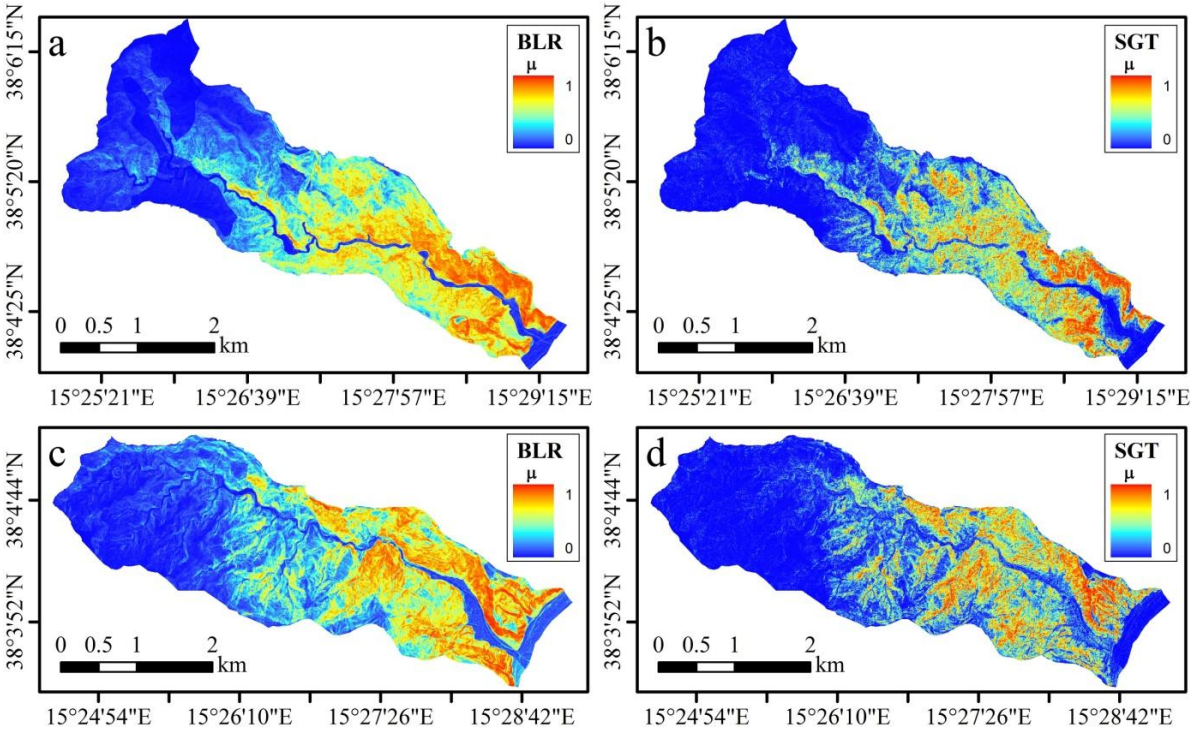

Figure 5.2.2 - Susceptibility maps of the Briga (BRG: a, b) and Giampilieri (GMP: c, d) catchments, obtained as mean probability on the eight replicates, as derived from Binary Logistic Regression (BLR: a, c) and Stochastic Gradient Treeboost (SGT: b, d) random partition based modelling (RP).

At a first glance, the location of the most susceptible areas (the red pixels) roughly coincides between the two algorithms, being concentrated in the south-eastern sectors of both the catchments. The only evident exception was in the south-easternmost edge of the Giampilieri catchment, whose susceptibility level is higher for BLR than for SGT.

The precision of the estimated susceptibilities of each mapped pixel was represented by error maps (Fig. 5.2.3), where the dispersion of the eight *RP* estimates of probability was expressed by the width of a 2σ interval. Comparing the four error maps clearly highlights the higher precision of BLR for the susceptible south-eastern sectors, in particular for the Briga catchment.

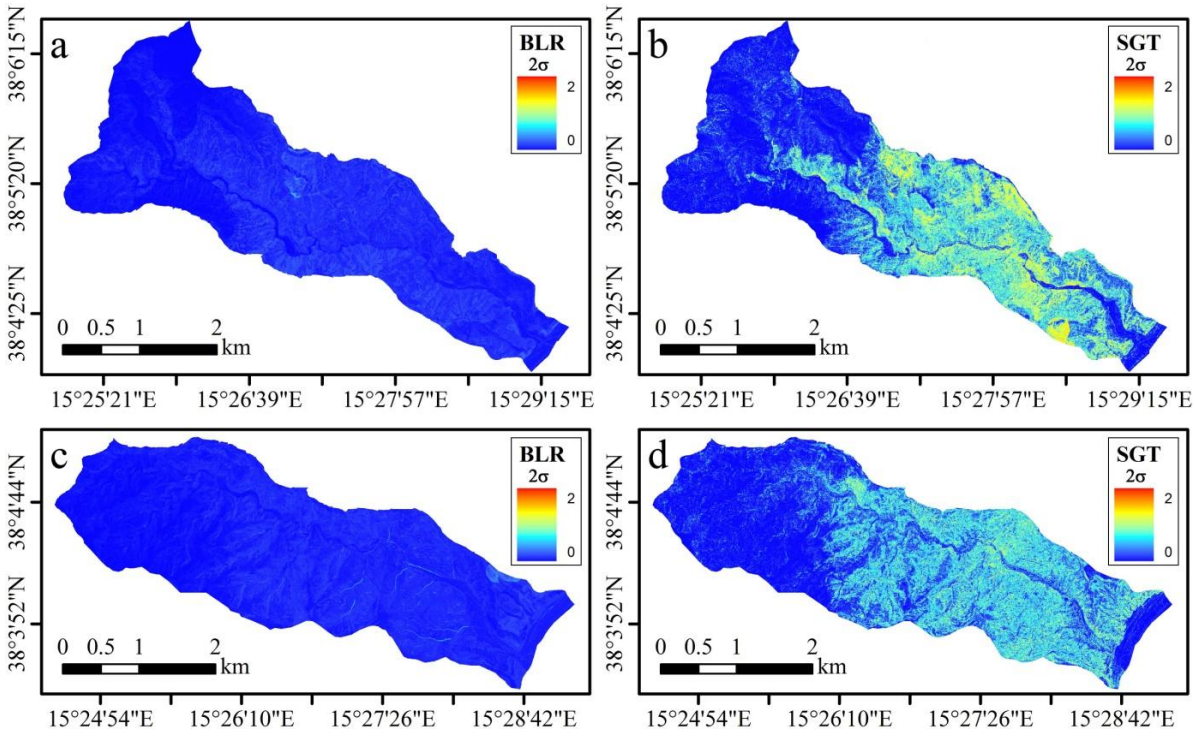

Figure 5.2.3 - Susceptibility error maps of the Briga (BRG: a, b) and Giampilieri (GMP: c, d) catchments, obtained as 2σ interval on the eight replicates, as derived from Binary Logistic Regression (BLR: a, c) and Stochastic Gradient Treeboost (SGT: b, d) random partition based modelling (RP).

By intersecting the 2.5×10^6 (BRG) + 2.6×10^6 (GMP) values of mean probability and the corresponding 2σ, error density plots have been obtained, depicting the relationships between susceptibility level and precision (Fig. 5.2.4). As expected the data shows a quadratic trend, but with a very different shape: BLR data are fit with one tenth lower negative x^2 and positive x coefficients (Figs. 5.2.4c, f), less steep left (low probability) and right (high probability) tails and much more limited spread along the 2σ axis for the intermediate mean probability values. Furthermore, the density of the pixels for SGT is very asymmetrically distributed, with very dense clouds at the low mean probability tail and constant lower values over the 0.1-1 probability interval. A lower number of pixels clearly characterizes the 0.3-0.7 interval for SGT. The BLR plots clearly shows a much more linear distribution of pixels along the mean probability axis, with a marked symmetrical shape for GMP-*RP*.

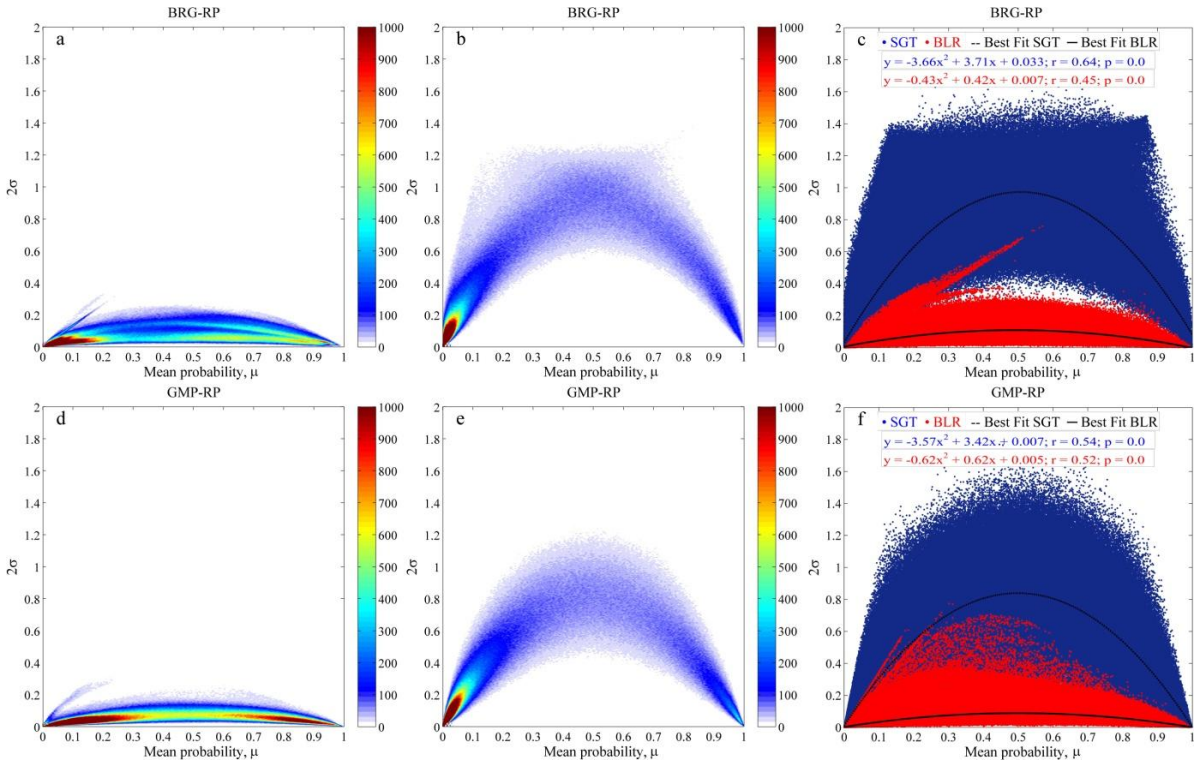

Figure 5.2.4 - Error density plots for the Briga (BRG: a, b, c) and Giampilieri (GMP: d, e, f) catchments, obtained as 2s interval on the eight replicates, as derived from Binary Logistic Regression (BLR: a, d) and Stochastic Gradient Treeboost (SGT: b, e) partition based modelling (RP). Densities are computed on a 0.005 side squared cell of a background mesh grid. In the right plots (c, f), single data are merged and quadratic fitting curves and equations are shown.

With regard to the rank or importance and the role (beta coefficients and response curves) of the predictors (Tab. 5.2.1 and Fig. 5.2.5), a general congruence between the two methods arose. The main factors, which were selected at least 7 out of 8 times by the BLR, were: HEIGHT, GEO_CARG, SLONH, USE, ASP, LAND1 and LAND2. At the same time, SGT predictor importance (PI) ranking includes the same set of variables as the most important. Consistency was found also between the sign of the beta coefficients and the slope of the response curves of the predictors.

Just small differences in the ranking among this set of factors was observed between the two catchments.

BRIGA (BRG)						GIAMPILIERI (GMP)					
Variables	FREQ.	MEAN		ST. DEV.		*Variables*	FREQ.	MEAN		ST. DEV.	
	v	Rank	β	Rank	β		v	Rank	β	Rank	β
HEIGHT	8	1	-0.0069	0	0.0002	HEIGHT	8	1	-0.0052	0	0.0002
GEO_CARG_bb	8	2	-3.306	0	0.2182	SLONH	8	2	0.0910	0	0.0108
SLONH	8	3	0.06072	0	0.0161	USE_3.2.2	8	3	0.9263	0	0.0450
USE_3.2.2	8	4	1.4542	0	0.7186	GEO_CARG_bb	8	4	-2.1438	0	0.1100
USE_3.1.2	8	6.75	-1.6375	1.7525	0.842	GEO_CARG_MLEa	8	5	-1.1187	0	0.0834
GEO_CARG_SPDb	8	8.625	1.2497	1.8468	0.1225	ASP_N	8	6	-1.0957	0	0.2314
LAND1_VSRV	8	10.875	-0.497	2.2321	0.0333	ASP_NE	8	7	-0.6370	0	0.1921
LAND2_MT	8	13.125	0.4042	3.1819	0.1409	LAND2_MT	8	12.2500	0.4607	2.8158	0.0988
SPISLO	8	14.25	0.4214	3.5355	0.0905	GEO_CARG_SPDb	8	13.2500	-1.9324	3.0119	0.2999
LAND1_USV	8	14.75	-0.4949	2.2519	0.0666	LAND2_VSRV	8	16.3750	-0.3538	3.5431	0.0579
LAND1_LRHBV	8	16.875	-0.4379	2.031	0.0847	LAND1_VSRV	7	8.4286	-0.2933	1.1339	0.0898
GEO_CARG_PCTc	8	20.625	-3.9035	3.7772	4.1314	USE_2.2.3	7	12.2857	-0.6058	2.1381	0.1178
ASP_SE	8	13.875	0.2049	4.764	0.4741	SLO	7	14.5714	-0.0288	2.6367	0.0063
ASP_S	5	6.6666	0.9409	2.1602	0.095	SPINH	6	19.2857	0.2078	2.2147	0.0411
ASP_SW	5	6	1.0037	1	0.0748	PRC5_CONV	6	13.6667	0.0348	3.2660	0.0053
ASP_W	5	11.8	0.6687	1.9235	0.0777	LAND1_UID	6	18.8333	0.2714	3.0605	0.0519
ASP_N	5	12	-0.9059	8.6891	0.507	CUR5_CONV	5	11.6	-0.0187	3.7148	0.0043
USE_2.2.6	5	17.4	1.1373	3.5071	0.6382	ASP_E	5	12.4	-0.4366	2.7019	0.0568
USE_2.2.3	5	20.2	0.4693	2.7749	0.8272	ASP_NW	5	15.2	-0.4257	2.6833	0.0779
SLO	5	20.6	-0.026	4.3359	0.0086	LAND2_BOS	5	18.2	-0.3632	4.1473	0.0713
LAND2_VSRV	5	17.8	-0.5392	1.4832	0.1837	FLANH	5	20	-0.0002	3.6742	0.0001
CUR5_CONC	4	18.25	0.0211	7.0415	0.005	LAND2_LRHBV	5	20.6	0.3992	1.6733	0.0548
LAND2_USV	4	18.25	-0.4227	6.994	0.1351	ASP_SE	4	18	-0.2550	3.5590	0.0342
USE_3.2.3	4	20	1.1591	2.5819	0.4849	ASP_S	4	13.6667	0.4785	6.6583	0.1710
GEO_CARG_PCTa	4	23.5	0.6958	1	0.0338	ASP_W	3	14.3333	0.5673	3.7859	0.1075
GEO_CARG_ASI	4	24.75	-13.2425	2.6299	0.3477	ASP_SW	3	14.6667	0.4235	5.5076	0.1147
ASP_NE	3	7.3333	-0.9253	2.0816	0.156	LAND1_BOS	3	19	0.9161	4.5826	0.1858
ASP_E	3	8	-0.7848	1.732	0.0389	GEO_CARG_FDNb	3	23	0.1817	2.6458	0.0191
PRC5_CONC	6	10.6666	-0.0432	2.1602	0.008	CUR5_CONC	2	9.5	0.0250	0.7071	0.0021
ASP_NW	3	14	-0.8283	1.732	0.1429	PLC5_CONV	2	10	-0.0355	2.8284	0.0088
LAND2_LRP	6	20.6666	0.7168	3.6697	0.1267	LAND1_LVP	3	17.6667	-0.9249	5.0332	0.1879
LAND2_FRTMT	3	21.3333	-0.3097	1.5275	0.0395	TWISLO	2	23	0.5578	0	0.0283
LAND2_UID	3	22	0.4602	2	0.0642	LAND1_USV	1	17	-0.2841	/	/
CUR5_CONV	2	17	-0.0209	9.8994	0.0053	FLA	1	20	-0.0001	/	/
PLC5_CONV	1	21	-0.0261	/	/	SPISLO	1	21	-0.1865	/	/
TWI	1	25	-0.1511	/	/						
GEO_CARG_FDNb	1	26	-0.2179	/	/						
LAND2_BOS	2	20	0.431	1.4142	0.0831						
LAND2_LVP	1	25	0.7962	/	/						

Table 5.2.2 - Selected predictors for the RP-models.

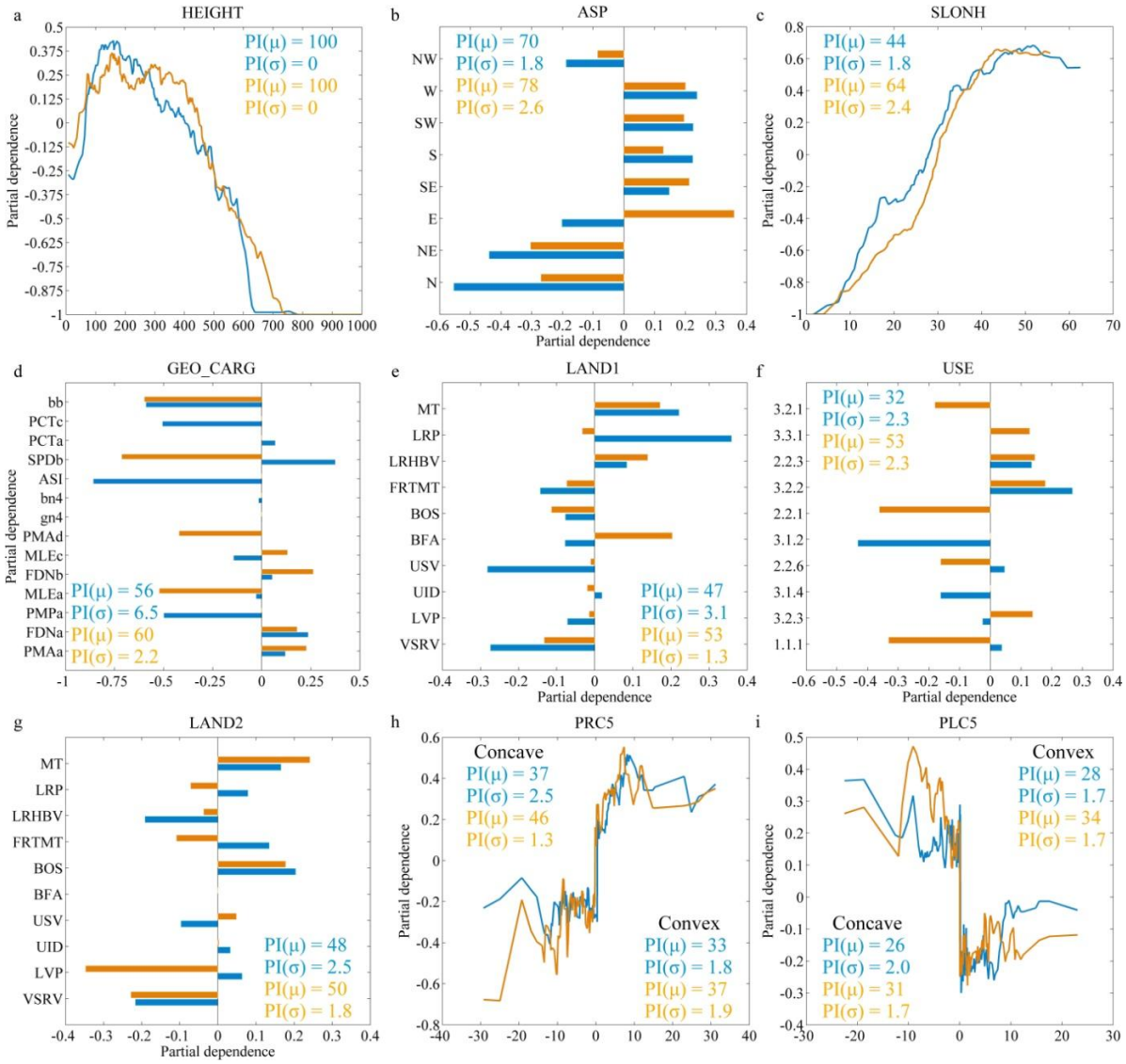

Figure 5.2.5 - Response curves and predictor importances of the independent variables, from Stochastic Gradient Treeboost modelling.

5.2.6 *Results for the SP-models*

Intersecting the eight datasets prepared for the Briga and the Giampilieri catchments for *RP*-modelling with the eight datasets, 64 space partition-based models were validated. Their inner structure (i.e. factors and coefficients) is the same as the corresponding BRG-*RP* models, whilst their performance is evaluated in matching positives and negatives in the Giampilieri catchment.

The comparison of the prediction skill of the sixty-four BLR and SGT *SP*-models (Fig. 5.2.6) demonstrated an equivalent performance for the two methods (ROC_AUC = 0.83 and 0.84 for BLR and SGT, respectively). However, the BLR curves are less steep in the first sector, but perform better in the middle to lower probability scale. Moreover, with the exception of one replicate over sixty-four, all the BLR ROC curves are almost coincident, attesting for a higher stability of the spatial partition- based regression through the replicates.

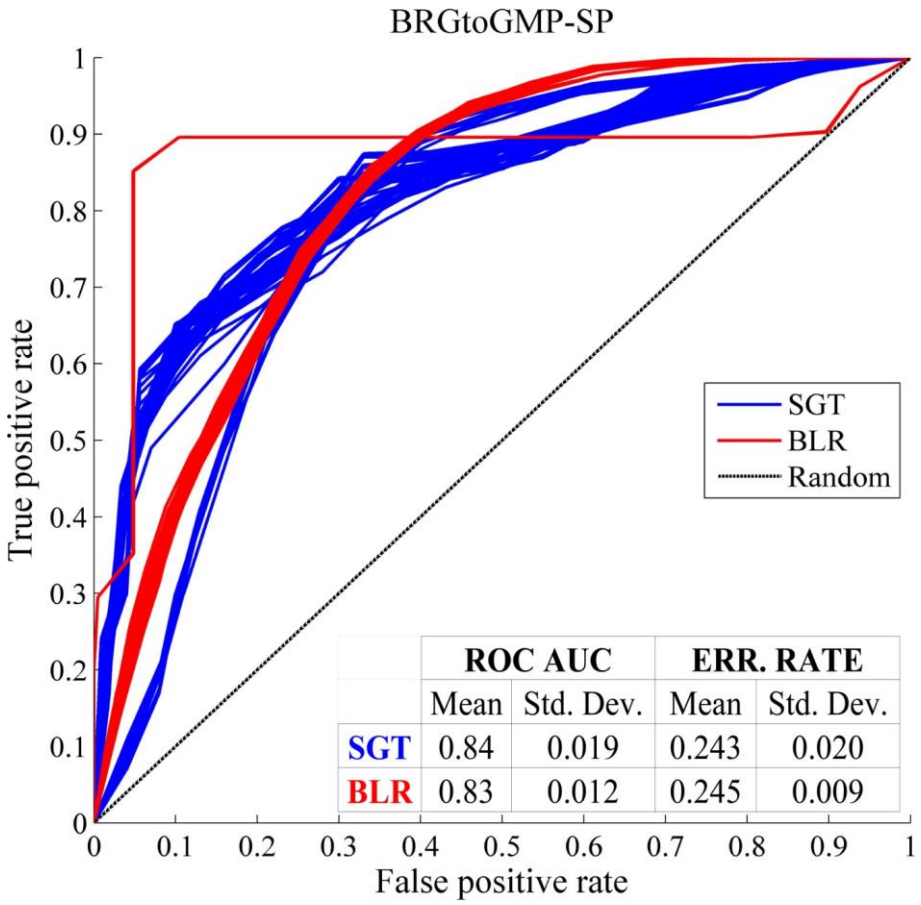

Figure 5.2.6 - Receiver Operating Curve (ROC) plots for the Briga to Giampilieri spatial partition based model (BRGtoGMP-SP). Binary Logistic Regression (BLR) and Stochastic Gradient Treeboost models (SGT) are compared (red and blu curves, respectively).

The analysis of the *SP* susceptibility maps (Figs. 5.2.7a, b) confirmed the differences that were highlighted from the GMP-*RP* models (Fig. 5.2.2), with a smoother distribution for BLR and a higher susceptibility in the south-easternmost edge of the catchment.

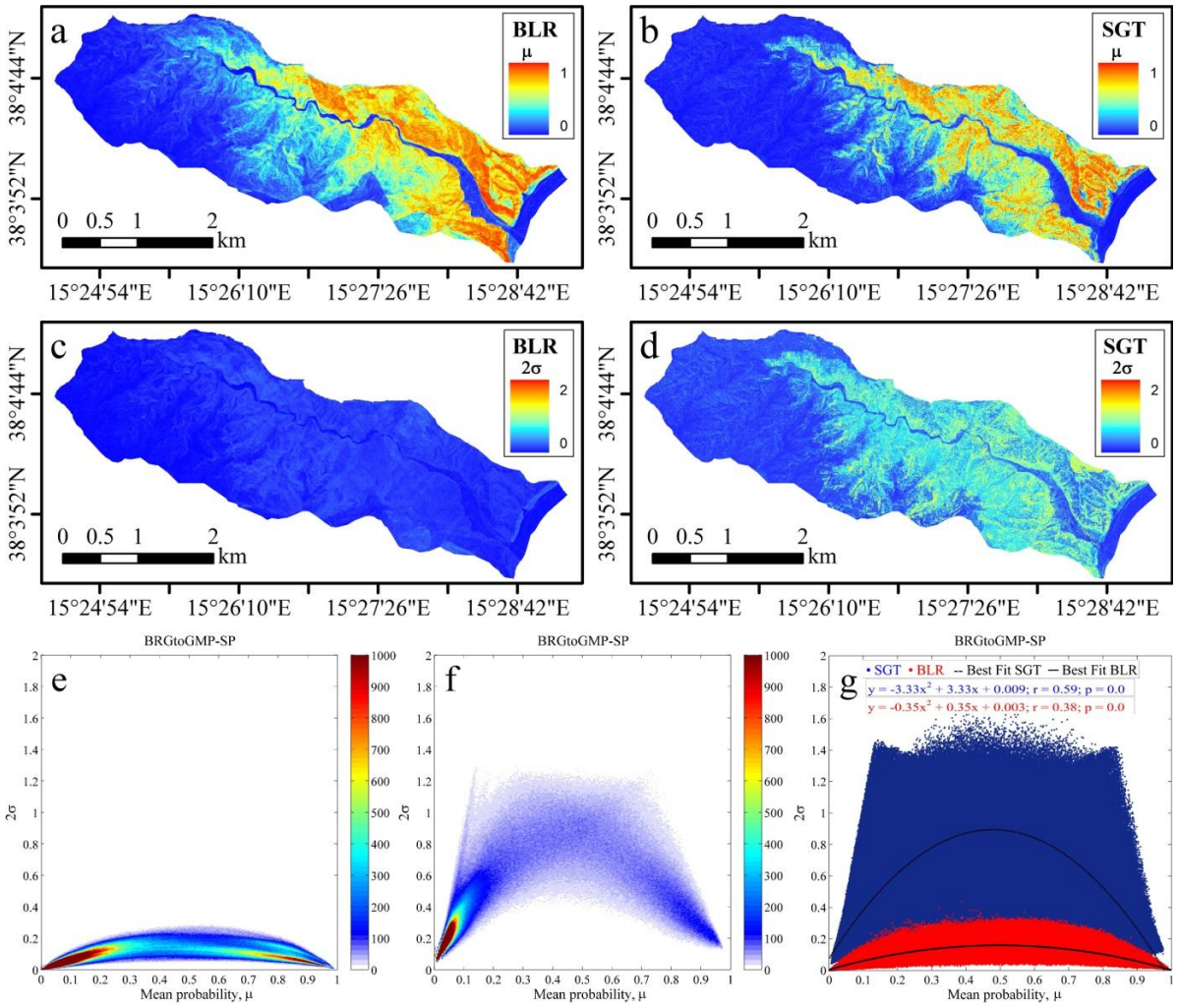

Figure 5.2.7 - Results for the Briga to Giampilieri space partition-based model (BRGtoGMP-SP). Susceptibility, error maps and plots, estimated through the sixty-four intersected replicates, from Binary Logistic Regression (BLR: a, c and e, respectively), and Stochastic Gradient Treeboost (SGT: b, d and f, respectively), SP-modelling. Densities on the error plots are computed on 0.005 side squared cell of a background mesh grid. In the low-right corner (g), single data are merged and quadratic fitting curves and equations are shown.

Again, the error maps (Figs. 5.2.7c, d) and the error density plots confirmed the higher precision of BLR, shown by more linear and symmetrical distribution of pixels along the mean probability axis, with a maximum 2σ slightly above 0.2 at 0.5 against a five times higher value for SGT (Figs. 5.2.7e, f). That was also confirmed by the coefficients of the quadratic fitting equation, which are five times higher for SGT (Fig. 5.2.7g).

5.2.7 *Discussion*

On the basis of the results we obtained in this research, the comparison between binary logistic regression and stochastic gradient treeboost indicated a higher prediction skill but lower precision for the latter, together with a lower robustness for random partition based models. The two statistical modelling methods do not greatly differ in the selection (rank or predictor importance) and the parameterization (coefficients or response curves) of the independent variables or predictors. At the same time, when analysing the predictive performances for spatial partition-based modelling, the advantage of SGT in terms of prediction skill vanishes, while its lower robustness and precision still hold.

In spite of the very high prediction skill while working on a single dataset or replicate, SGT showed a lower reliability with respect to BLR when moving through the data domain, regressing replicates which are randomly extracted from the whole dataset. Even when comparing random partition generated replicates, which share the positives, the dispersions of the estimated probabilities was higher than those produced from BLR (Fig. 5.2.3). This loss in precision is associated with error plots that clearly show a strong binarization of the estimated probabilities (very high or very low values are largely dominant) and a too high quadratic component, denoting a very low precision for the intermediate probability range (Fig. 5.2.4). These limits in generalizing the regressed model to match unknown cases, also reflect on the prediction skill, when trying to perform a spatial partition based validation. In this case, we observed for SGT a prediction skill almost equivalent to BLR together with a lower precision. Again, it seems that SGT models depend too strictly on the training dataset and that, in case of spatial partition modelling, led to a lower precision and no prediction skill advantage.

It is worth noting that we selected the SGT algorithm because it should minimize overfitting effects, which typically affect CART techniques (Brenning, 2005; Ciampi, 1991, Liu et al., 2011).

To further explore the difference between the two modelling techniques in terms of prediction costs, we prepared the maps of residuals for the three types of models (BRG-*RP*, GMP-*RP*, BRGtoGMP-*SP*), which were intersected with the LIP distribution (Fig. 5.2.8).

These maps were obtained by subtracting the BLR from the SGT probability values. The summary plot (Fig. 5.2.8d) clearly shows that for the *RP*-models, the LIPs are much more concentrated in those pixels where SGT produces a higher value of probability. For the *SP*-models, this difference tends to reduce to about 10%. On the basis of this further processing, we verified that SGT is the best method in matching the known training positives for *RP*-models, whilst for *SP*-models, whose positives are obviously unknown, the two methods performed with similar results.

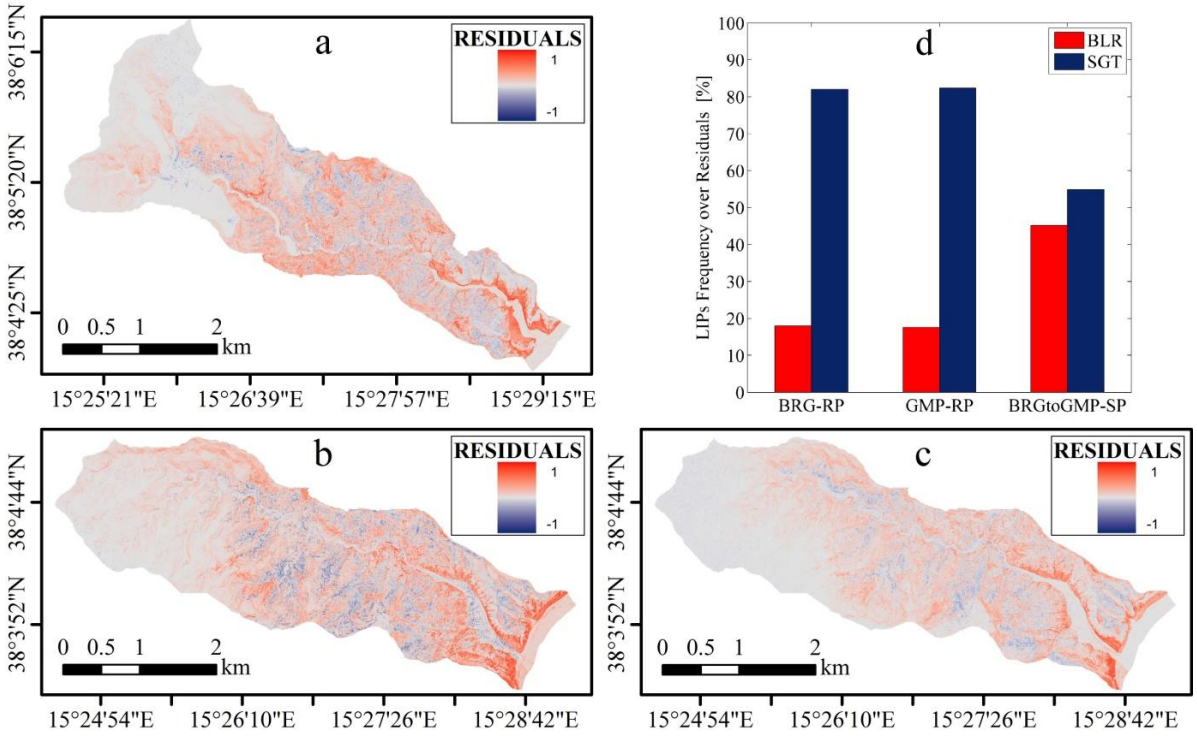

Figure 5.2.8 - Map of the residuals, obtained by subtracting BLR from SGT mean probabilities, for the Briga (BRG-RP: a) and Giampilieri (GMP-RP: b) random partition-based model and for the Briga to Giampilieri space partition-based model (BRGtoGMP-SP: c). The plot in (d) shows for the three models the distribution of the LIPs on negative (susc_BLR>susc_SGT), in red) and positive (susc_BLR<susc_SGT), in blu) residual pixels.

However, if we adopt the 0.5 probability threshold to binarize the pixels into predicted positives and negatives (Fig. 5.2.9), we observe that the lower error rates for SGT *RP*-models is mainly connected with a higher true negative rate than true positive rate (only 10% more). At the same time, for both the methods, the dispersion of the prediction results is larger for TN than for TP and more emphasized for the Briga models.

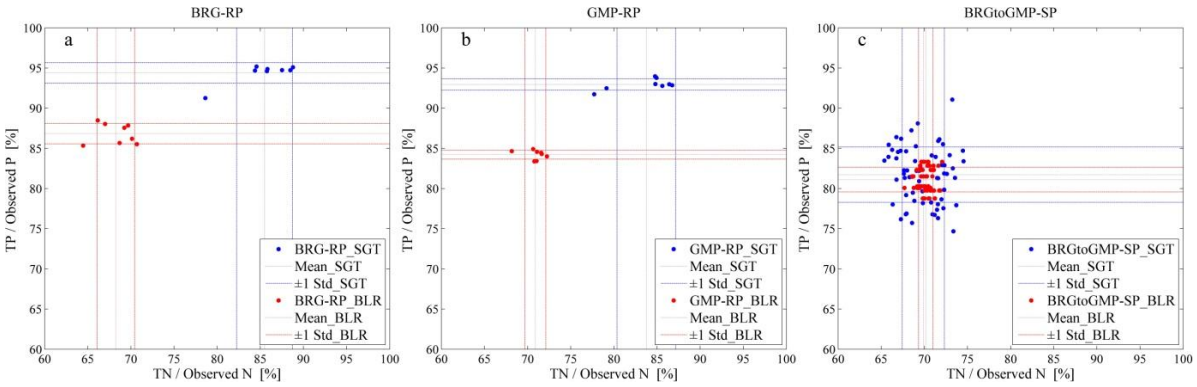

Figura 5.2.9 - Confusion plots for the Briga (a) and Giampilieri (b) eigth random partition-based models and for the Briga to Giampilieri sixty-four space partition-based models (c).

When analysing the spatial partition-based models (Fig. 5.2.9c), we verified a shift of the SGT toward the BLR performance, associated with a higher dispersion both in TP and TN. As expected, both the methods suffer from a lowering in TP and TN performances (shifting towards the origin of the confusion plot), but for BLR this is limited to few percentage units, against tens for SGT. At the same time, the dispersion for SGT is twice that of BLR.

The last insight in the comparison between BLR and SGT was based on the punctual relationship between the probabilities estimated from the two methods, rather than in the analysis of the prediction performances of the derived models. Figure 5.2.10 shows the density plot of the two mean probabilities over a squared meshgrid with 0.005 side length.

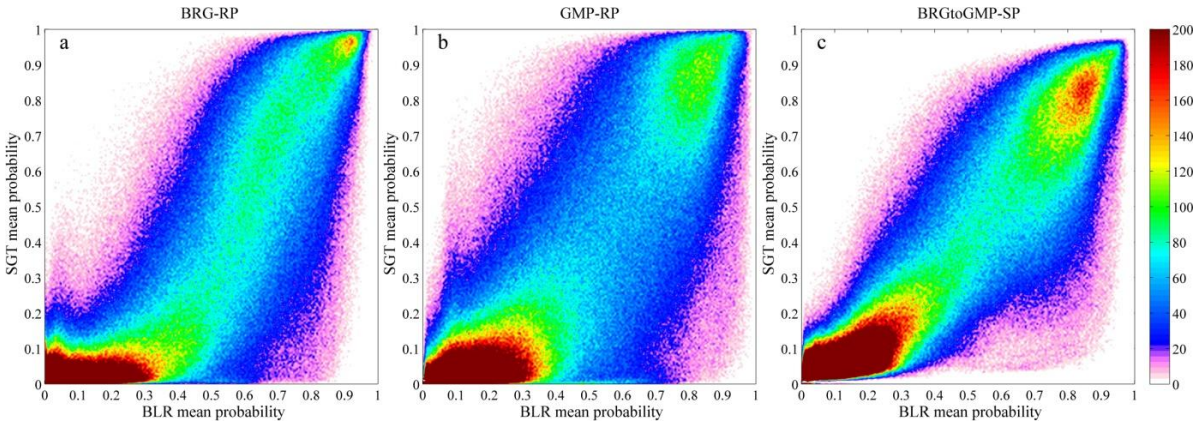

Figure 5.2.10 - Comparison density plots for susceptibilities derived from Binary Logistic Regression and Stochastic Gradient Treeboost, for the eight Briga (a) and eight Giampilieri (b) random partition-based models and for the sixty-four Briga to Giampilieri space partition-based models (c).

The general congruence between the two methods is responsible for the positive correlation that can be observed at a first glance. However, the plots also highlight the different behaviour of the two methods in classifying the cases, which is represented by a general sigmoidal shape of the distribution. This shape is a result of the greater linear classification of BLR, which allows the method to discriminate among the very low and very high probabilities. SGT depicts a very binarized world, with the higher concentrations outside the 0.1-0.75 probability interval. For the same reason, the central sector of the plots describes a very steep elongated point-cloud, again denoting the higher skill of BLR in discriminating intermediate probabilities.

However, it is worth noting that the aforementioned differences in the classifiers are slightly smoothed for *SP*-models (Fig. 5.2.10c) and almost absent for the more susceptible cluster of pixels in the upper right corner.

5.2.8 *Conclusions*

Comparing statistical modelling techniques has recently become more high profile among the scientific topics in the framework of landslide susceptibility studies. In fact, once the scientific community has almost unanimously shared a general approach to the issue through the model building and validation strategies, the topic of assessing advantages and draw-backs of the available statistical techniques has become more relevant.

In this paper we carried out a comparison between binary logistic regression and stochastic gradient treeboost including a complete validation of the model reliability and imposing a stress condition for the modelling techniques, which were compared under random-partition and spatial partition model building and validation strategies.

Generally, both the techniques guaranteed high predictive performances throughout the whole modelling process, with SGT predominantly demonstrating to be the more skilled method. However, a deeper insight into the reliability of the models allowed us to verify the higher precision of BLR, for all the modelling strategies and its equal prediction skill for spatial partition.

If we choose to assign the same weight to the prediction performance as well as its variance when evaluating the quality of a method, then the BLR performed the most reliable analysis.

The SGT results suggest that the attempt of the boosting approach to reduce the model bias exceedingly works, causing high variance between models instead of balancing them and imposing a low upper limit to the Real Error (Vapnik 1995). This is not surprising given that this is a common problem of tree-based learning algorithms. In addition, it is worth highlighting that combining a bias-reducing meta-algorithm such as the stochastic gradient boosting, and a tree-based learning algorithm such as CART, the prediction still suffered from high variance, even five times greater than the BLR. The limit may reside on the choice of a decision tree algorithm as the core weak learner in order to build predictive models. On the other hand, the Binary Logistic Regression, in spite of its relative simplicity, provided excellent prediction performances associated with low variances.

The stochastic structure of the models strongly controls their flexibility, so that a more performing but constrained method such as SGT, suffered from high sensitivity to any data modification. Conversely to the BLR, which produces only one regressed coefficient for each factor, the SGT gives a deeper insight on the relation between the model dependence and the whole scale or modalities of each predictor, providing continuous partial dependency values. However, the fragmented and discontinuous structure of SGT models itself seems to limit their reliability as well as their skill in producing generalizable results, suitable for spatial partition modelling.

The result of the present research could also be used in order to define optimal conditions for selecting between BLR and SGT algorithms in landslide susceptibility assessment studies. The SGT proved to be highly performing in case of *RP*-modelling; in general this could suggest the application of this method for small catchments or areas with a dense distribution of homogeneous predictors. On the other hand, the BLR proved in *SP*-modelling to be more adaptive or less sensitive to predictor changes. This condition could lead to application of BLR in contexts of bigger catchments, where changes in the predictor spatial distributions will have a stronger control on the final model.

5.3 MAXIMUM ENTROPY METHOD AND ASTER DATA FOR ASSESSING DEBRIS FLOW AND DEBRIS SLIDE SUSCEPTIBILITY FOR THE GIAMPILIERI CATCHMENT (NORTH-EASTERN SICILY, ITALY.

Lombardo, L., Bachofer, F., Cama, M., Maerker, M., Rotigliano, E., Earth Surface Processes and Landforma, submitted.

5.3.1 *Research objectives*

This study aims to compare the performances of Maximum Entropy method in assessing classified landslide susceptibilities within the Mediterranean region for multiple-occurrence regional landslide events by integrating different predictors, both DEM and remote sensing derived. The selected test site coincides with the catchment of the Giampilieri stream, located in the north-eastern sector of Sicily (southern Italy). Within this area a presence-only-based prediction approach was applied in order to model the debris flows and debris slides activation, generated during the disaster locally occurred on the first of October 2009. In this occasion, thousands of rapid shallow landslides triggered in the time lapse of few hours as a response to an extreme storm. The set of predictors used in this experiment comprises primary and secondary topographic attributes as well as vegetation and mineral indexes obtained by processing multispectral ASTER images. Both the selected data sources for predictors date prior to the disaster. A random time partition technique was adopted for validation, generating fifty models for each of the two considered movement typologies in order to assess accuracy, precision and reliability of the models. The debris slide and debris flow susceptibility models produced analogous almost excellent performances with the first type being the best fitted. The evaluation of the probability estimates around the mean value for each mapped pixel shows an inverted relationship, with the most robust models corresponding to the debris flows. The difference in behaviour could be interpreted in terms of statistical constraints due to the high number of cases to be fitted in the two landslide typologies. In terms of the role of each predictor within the modelling phase, debris flows appeared to be primary controlled by topographic attributes whilst the debris slide were better explained by remotely sensed derived indexes, particularly by the presence of previous wildfires across the slope. The overall excellent performances of the two models suggest promising perspective for the application of presence-only methods, which have limited application in the international literature, at the

same time suggesting new applications for integrated predictor sets. Whether remote sensing derived predictors would prove to produce systematically reliable results, exportation procedures from distant areas around the worlds could be performed enabling new frontiers for landslide susceptibility studies.

5.3.2 *Introduction*

Several among the most recent contributions in landslide susceptibility studies focussed on integrating remote sensing technology to improve the final prediction (Aman et al., 2014; Bai et al. 2013; Günther et al., 2014; Miller 2013; Mondini and Chang, 2014; Reichenbach et al., 2014; Youssef et al., 2014). The majority of the community introduces vegetation indexes among the predictors or uses the satellite imagery to derive digital elevation models (DEMs) and subsequently topographic attributes (Huang et al., 2007; Oh et al., 2012; Pradhan et al., 2010) to be used as causative factors. In this paper we propose to exploit the availability of Advanced Spaceborne Thermal Emission and Reflection Radiometer (ASTER) satellite images, in order to calculate spatially distributed vegetation and mineral indices to be included, together with the more common DEM-derived topographic covariates and CORINE land cover data among the set of predictors for landslide susceptibility purposes. The spectral characteristics of the ASTER sensor allow the calculation of a broad range of mineral indices (Rowan and Mars, 2003; Yamaguchi and Naito, 2003; Rowan et al., 2005; Mars and Rowan, 2010; Pour et al., 2011; Mulder et al., 2011). The spectral information was also used in different studies to decipher soil surfaces, as well as hydrological and erosional issues. Among the others, typical applications for ASTER data are: the detection of sandy soil surfaces (e.g., Breuning et al., 2008), the parametrisation of hydrological models (e.g., Ismail and Ravichandran, 2008) or land cover classification for erosion risk mapping (e.g., Yuksel et al., 2008). For the present case study, the authors hypothesized that the remotely derived information on the superficial soil composition can be approximated to the composition of the shallow moving masses displaced during the 2009 disaster, thus effectively contributing to the susceptibility models as proxy independent variables for local properties of the weathered layer.

Another important topic in landslide susceptibility researches is the method upon which the final models are built. Common practises involve the use of stochastic and/or data mining methods relying on presence-absence techniques (e.g., Eker et al., 2014; Ermini et al., 2005; Pourghasemi et al., 2013; Lombardo et al., 2014). In this research we decided to pursue a presence-only approach, which has been recently introduced within the landslide scientific community (Convertino et al., 2013; Davis et Sims, 2013; Park et al., 2014) by applying the Maximum Entropy (MAXENT) algorithm (Elith et al., 2011; Phillips et al., 2004 and 2006; Phillips and Miroslav, 2008). This code was developed by the Department of Computer Science of the Princeton University and has generally found its main application in ecological sciences for species habitat modelling (Brambilla et al., 2014; Isaac et al., 2013; Liu et al., 2013). However, recent applications in geomorphology (Felicisimo et al., 2013) proved the usefulness of this method even in landslide susceptibility comparative studies. The presence-only approach does not rely on the contribution of negative (no-landslide or absence) cases within the calibration and validation phases. This can be of great importance for landslide susceptibility assessment, as the use of methods which requires for balanced (landslide/no-landslide) datasets poses the need of regressing datasets which include, together with the unstable cases, an equal number of randomly selected stable cases; this could lead to problems when the extracted subsets are not representative of the whole mapped area. Solving this limit requires for heavy computational procedures which are typically based on multi-extraction routines (e.g., Costanzo et al. 2014; Lombardo et al., 2014). For this reason, we used the MAXENT algorithm to predict landslides in the study area of the Giampilieri catchment (north-eastern Sicily, Italy), which was the site of a multiple-occurrence regional landslide event (MORLE; Crozier, 2005) on the first of October 2009. In that occasion, hundreds of landslides, primarily consisting in debris flow/avalanche, activated as debris slide or debris flow from the head and intermediate sectors of the slopes, downhill propagating as channelled or unchannelled flows (debris flows or debris avalanches, according to Hungr, 2005).

In this work, an attempt to stochastically ascertain the differences in the triggering phase between the debris flows and debris slides by using MAXENT and an integrated set of predictors expressing geomorphometric features as well as vegetation and mineral indexes derived from satellite imagery was made. The validation of the models was performed on a 50-fold cross-validation procedure, allowing us to evaluate the reliability of the fitting, the

prediction skill, the coherence in the predictor selection, and the precision of the susceptibility estimates.

5.3.3 *Maximum Entropy*

In a famous contribution of Information Theory and Statistical Mechanics, Jaynes, E.T. (1957) defined the maximum entropy estimation as the least biased possible estimate on a given information. In other words, when applying predictive algorithms, the best model should coincide with the one that has Maximum Entropy. The complexity of this method hindered its real applications until the advent of computers enough powerful to handle complex problems. This method was then introduced for the first time by Berger et al. (1996) and Della Pietra et al. (1997). Several developments have subsequently been proposed to this algorithm and its potential application in different areas of science. Phillips et al. (2004, 2006) presented an integrated approach (MAXENT) of maximum entropy and GIS technologies for species distribution modelling where the application of this algorithm maximises the entropy in a geographic space.

In the present contribution we exploit the MAXENT approach in modelling species distributions to model the point occurrences of classified landslides, with a similar assumption to that described in Convertino et al. (2013). In fact, Maximum entropy is a presence-only method that uses only positive cases to derive functional relationships between the dependent and independent variables to depict the spatial prediction. Elith et al. (2011) illustrate the MAXENT model architecture as needing the conditional density of the covariates at the presence sites, $f1(z)$, the unconditional density of covariates across the study area, $f(z)$, and the proportion of occupied sites in the landscape, $\Pr(y = 1)$, in order to depict the probability of presence conditioned on environment, $\Pr(y = 1|z)$. The papers of Phillips et al. (2006) and Elith et al. (2011) jointly explain two concepts. The first one states that maximising the entropy of the probability, given the species is present, that it is found at pixel x is equivalent to minimizing the relative entropy of $f1(z)$ relative to $f(z)$. The second key concept uses the findings of Della Pietra et al. (1997) resulting in an equivalence between the minimization of the relative entropy and a Gibbs distribution:

$f1(z) = f(z)e\eta(z)$, given $\eta(z) = \alpha + \beta * h(z)$;

where h(z) is the vector of covariates, β is the vector of coefficients and α is a normalizing constant ensuring that $f1(z)$ integrates to 1. In order to find the solution Maxent firstly converts all the covariates scaling their domain between 0 and 1, then calculating λ_j, an error bound for each covariate. This error bound is used to regularise (Tibshirani, 1996) the model when Maxent maximise the relative entropy subject to it:

$$\max_{\alpha,\beta} \frac{1}{m}\sum_{i=1}^{m} \ln(f(z_i)e^{\eta(z_i)}) - \sum_{j=1}^{n} \lambda_j|\beta_j|$$

Due to the impossibility of knowing exactly the proportion of occupied sites in the landscape or the prevalence over the space (Word et al., 2009), the algorithm performs some key steps to reach the best model. It initially calculates the raw output by estimating $f1(z)/f(z)$ and use this ratio to obtain insights on the relative suitability of one place compared to another. The next step is performed by calculating the logarithm of the raw output $\eta(z) = \log(f1(z)/f(z))$. By treating it as a logit score and calibrating the intercept, a parameter τ can be derived which expresses the probabilities of presence at sites with the natural conditions for the species. By knowing τ, the non identifiability of prevalence can be solved thus making possible to complete the following relationship: $Pr(y = 1|z) = f1(z)Pr(y = 1)/f(z)$.

The parameterisation for the 2 suites of fifty models has been setup with a training and test proportions of 75/25% for each of the hundred calculated models. Each replicate randomly selected 25% of test cases without replacement from the whole dataset leaving the remaining cases for the model evaluation. The initial prevalence or probability of presence at ordinary occurrence points was set to 0.5. Moreover, the maximum number of iteration before stopping the model building was set to 500; however a convergence threshold was applied to interrupt the training phase when the drop in log loss per iteration falls below a value of 0.00001.

5.3.4 *ASTER data and derived vegetation and mineral indexes.*

ASTER was launched together with NASA's TERRA spacecraft in December 1999 (Yamaguchi et al., 1998). The ASTER sensor includes three subsystems with 3 bands in the visible-near infrared (VNIR; 0.52 – 0.86 nm), six bands in the shortwave infrared (SWIR; 1.6 – 2.43 nm) and five bands in the thermal infrared (TIR; 8.125 – 11.65 nm) wavelength regions.

The ground resolution of the VNIR bands is 15 m, 30 m for SWIR and 90 m for TIR (Fujisada, 1995). The ASTER L1B scene was acquired at the 21th July 2007 (09:59 UTC), which was before the Giampilieri disaster occurred.

Several pre-processing steps were applied before further analyses were performed. The SWIR bands of the L1B data suffer from cross-detector leakage. Following Iwasaki et al. (2002), crosstalk correction was applied using software developed by the Earth Remote Sensing Data Applications Centre (ERSDAC, Japan). The ASTER scene was co-registered with sub-pixel accuracy to a Landsat 7 ETM+ (L1T) panchromatic scene with 15 m ground resolution (2000-09-22). Landsat datasets are provided with a sub-pixel spatial accuracy and are therefore a reliable spatial reference for ASTER products (Gao et al., 2009; Behling et al., 2014). A radiometric correction was conducted applying the radiative transfer code MODTRAN®5 (Berk et al., 2008) implemented in the ATCOR package (Richter and Schlaepfer, 2014).

After the pre-processing, several multispectral indices were derived from the ASTER VNIR/ SWIR bands. The proposed indices are mostly simple band ratios, which are sensitive to surfaces and their reflection and absorption properties for certain spectral wavelength. Distinct wavelengths emphasize the presence or absence of surface cover (Rowan & Mars, 2003; Mulder et al., 2011). This study doesn't aim at discriminating the different mineral compositions in the study area, but at detecting trends which help to explain the occurrence of landslides. From an extensive literature review a broad range of indices were collected and processed for the analysis (Tab. 5.3.1). In particular, we selected a group of sixteen indices, referring to different categories. The set of vegetation indices includes: i) Stress related Vegetation Index (STVI, Pour and Hashim 2011); ii) Medium Resolution Normalized Difference Vegetation Index (NDVI, Rouse et al. 1974); iii) Burn Index (Hudak et al. 2004). With regards to the Mineral indexes computed from the ASTER scene, several indices were obtained to approximate the local shallow soils. For this reason, the broad families of mineral covariates can be clustered into: i) silicates, ii) carbonate-mafic, iii) iron.

Index and literature reference	Formula	Variable
Alteration/Laterite (BIERWIRTH	(4/5)	Alter_I
Burn Index (HUDAK et al. 2004)	(3-	BURN_I
Calcite (POUR & HASHIM 2011)	(6/8)*(9/8	CALC_I
CCE (ROWAN & MARS 2003)	(7+9)/8	CCE_I
Clay 1 (ROWAN & MARS 2003)	(5+7)/6	Clay1_I

Clay 2 (BIERWITH 2002)	(5*7)/(6*6	Clay2_I
Dolomite (ROWAN & MARS 2003)	(6+8)/7	Dolomite_I
Kaolinitic (HEWSON et al. 2001)	(7/5)	Kaolinitic_
Kaolin Group (CUDAHY 2012)	(6/5)	Kaol_G
Kaolinite (POUR & HASHIM 2011)	(4/5)*(8/6	Kaol_I
MgOH Group (CUDAHY 2012)	(6+9)/(7+	MgOH_G
Muscovite (HEWSON et al. 2001)	(7/6)	Muscovite
NDVI (ROUSE et al. 1974)	(3-2)/3+2)	NDVI
OH 1 (POUR & HASHIM 2011)	(7/6)*(4/6	OH1_I
PHI (HEWSON et al. 2001)	(5/6)	PHI_I
STVI (POUR & HASHIM 2011)	(3/2)*(1/2	STVI

Table 5.3.1 - Spectral indices derived from ASTER VNIR and SWIR bands. Bold indices were selected for further processing taking aside those that were linearly linked or expected as being locally absent due to geological conditions.

5.3.5 *Topographic attributes and land cover*.

Both the two sources of data for topographic and land cover site characterization were taken from before event source layers: a high resolution model (2m cell) obtained by a LIDAR coverage dated at 2007 (Tab. 5.3.2 and 5.3.3) and the 2006 CORINE land cover (Tab. 3). The DEM-derived attributes were obtained by using SAGA GIS (Conrad, 2005) tools, obtaining thirteen covariates, namely: i) Aspect; ii) Slope steepness (Horn, 1981); iii) Relative Slope position (Kleber, 1997); iv) Plan Curvature; v) Profile Curvature; vi) Mass Balance Index (Hensel and Bork, 1988); vii) LS Factor; viii) Topographic Wetness Index (Beven and Kirkby, 1979); ix) Convergence Index (Köthe and Lehmeier, 1993); x) Landform Classification with 20-100m search radii; xi) Stream Power Index (Moore et al., 1991); xii) SPISLO (Lombardo et al., 2014); xiii) TWISLO (Lombardo et al., 2014).

Land use classes mapped through the CORINE 2006 map were also considered as a proxy variable expressing the anthropic control on the environment and specific vegetation cover.

Continuous predictors	
Attribute	**Variable**
Aspect	Aspect
Convergence Index	Conv_I
Slope-Length Factor	LS_Fact

Mass Balance Index	Mass_BI
Plan Curvature	Plan_C
Profile Curvature	Prof_C
Relative Slope	RS_Pos
Slope Steepness	Slope
Stream Power Index	SPI
SPISLO	SPISLO
Topographic	TWI
TWISLO	TWISLO

Table 5.3.2 - Continuous predictors.

Categorical predictors		
Attribute	**Code**	**Variable**
Landform Classification	1	V-shape river valleys
	2	Local valley in plains
	3	Upland incised drainages
	4	U-shape valleys
	5	Broad flat areas
	6	Broad open slopes
	7	Flat ridge tops mesa tops
	8	Flat ridge/hilltops within broad
	9	Local ridge in plains
	10	Mountain tops
Land Use	1	Continuous urban fabric
	2	Sparsely vegetated areas
	4	Mixed groves
	5	Coniferous
	7	Non-irrigated arable land
	9	Grassland
	10	Olive groves
	11	Erosion scars, badlands, rock
	12	Shrubland

Table 5.3.3 - Categorical predictors.

5.3.6 *Datasets.*

A susceptibility model has to product a probability estimation of new activation for each of the mapping units in which the mapped area is partitioned. The choice of the mapping unit is a key factor in landslide susceptibility studies (Carrara et al., 1995; Hansen, 1984; Luckman et

al., 1999; van Westen et al., 1993, 1997). According to the size of the highest resolution obtained for the recorded wavelengths in ASTER data and to the spatial resolution in the parameter domain selected, in the present contribution we selected a raster based model, with 15m square grid cell. As a result, the geographic space coinciding with the catchment of Giampilieri was partitioned into 47084, 15m-side, squared cells each of which was assigned the values of the whole set or predictors.

To set the status (stable/unstable) of the outcome for each cell, we extracted from each landslide polygon a landslide identification point (LIP), corresponding to the highest 2m pixel along the crown. We then classified as unstable all those cells hosting a LIP, under the hypothesis that, for so shallow and narrow failure surfaces, a 15m area could be enough large to "reflect" in the predictors domain those before-event conditions which lead to the 2009 activations. The 1121 extracted LIPs were further subdivided into debris flow (824) and debris slide (297) cases.

Figure 5.3.1 shows the normalised univariate distribution of the predictors for the two types of mass movements as well as the whole catchment of the Giampilieri stream. Differences for each independent variable can be ascertained among the distributions of debris flows (red line), debris slides (blue line) and the catchment itself (green line) supporting a clear non-random sampling between the general setting at the basin scale and at the two slope instability scales.

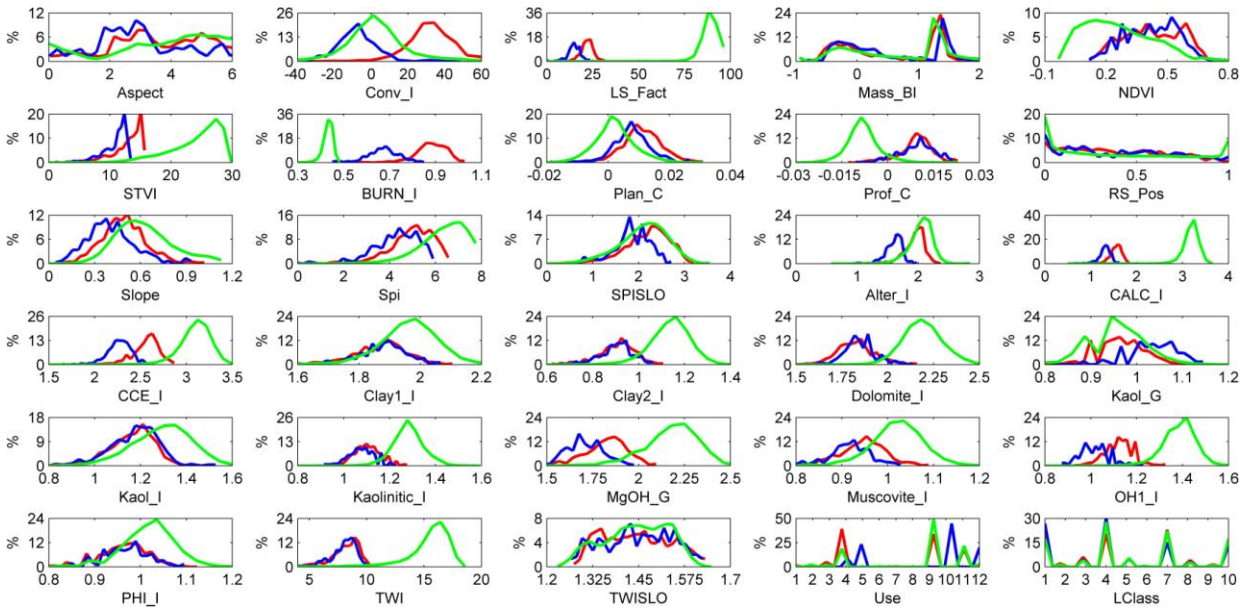

Figure 5.3.1 - Univariate normalized distribution of predictors among the two modelled landslide types and the whole catchment: in red, debris flows; in blue, debris slides, in green the, catchment of Giampilieri.

5.3.7 *Validation*

The validation of a predictive model for landslides has to provide a quantitative estimation of its goodness of fit, prediction skill, robustness and geomorphological adequacy. A largely adopted strategy for validating the predictive models by using a coeval landslide inventory is to randomly partitioning it into a training and a test subset, the first used for calibration, the second for validation. Once a model is obtained, we can cross its predicted probabilities with the presence/absence of training and test events, so to calculate metrics for fitting and prediction skill, respectively. In particular, the results of validation can be analysed in the space of Receiver Operating Characteristic (ROC) plots, reporting the varying threshold True Positive (TP) Vs. False Positive (FP) trade-off performance, which can be expressed by the Area Under Curve (AUC) metric. At the same time, for measuring both the precision and the accuracy of a model we need a replication of the assessment so that mean values and dispersion of the produced probability estimations can be analysed for significance.

As the predictive models are based on the regression of a set of covariates, an analysis of the role of each selected variable has to complete the validation procedure. Jack-knife methods can be used for estimating the contribution of each single variable in the whole performance of the models, for example by comparing the performance of single *i*-variable model, with that obtained by using all but the *i* variable itself. The loss in the ROC-AUCs resulting in a variable suppression indicates, together with the AUC of the single variable model, the importance that a variable assumes in the whole modelling procedure. The same can be estimated in terms of predictor importance, which are computed by MAXENT in regressing the model. If single variable effects are performed also on a multi-folds procedures, the reliability of the inner structure of the model can be also assessed.

Finally, the validation of a landslide susceptibility model cannot be said completed if no adequacy analysis has been performed so to explain in terms of geomorphological modeling the predicted phenomena. To describe the role that is assumed by the single predictors, the MAXENT algorithm produces as output the response curves, which depict how the values or classes of the predictors are correlated with the outcome.

In this research we implemented a random split of the regressed datasets using 75% and 25% for calibration and validation, respectively. Besides, the splitting procedure was performed

50 times, so that the precision and accuracy was estimated both for evaluating the performance metrics and predictor importance. Besides, exploiting the fifty replicates, we could compute mean values and standard deviations for probabilities and errors, which were reported in the susceptibility and error maps, as well as variable-response plots, in which position and dispersion of the model dependence have been plotted in the domain of each predictor.

5.3.8 *Results*

Figure 5.3.2 shows the results of the validation of the obtained debris slide and debris flow susceptibility models. The goodness of fit of the two suites of fifty models proved to be outstanding (Hosmer and Lemeshow, 2000) on average for the debris slide (0.91), whilst being slightly lower for the debris flow (0.85). With regard to the prediction skill, the performances converged to an almost excellent fitting with average test AUC values of 0.79.

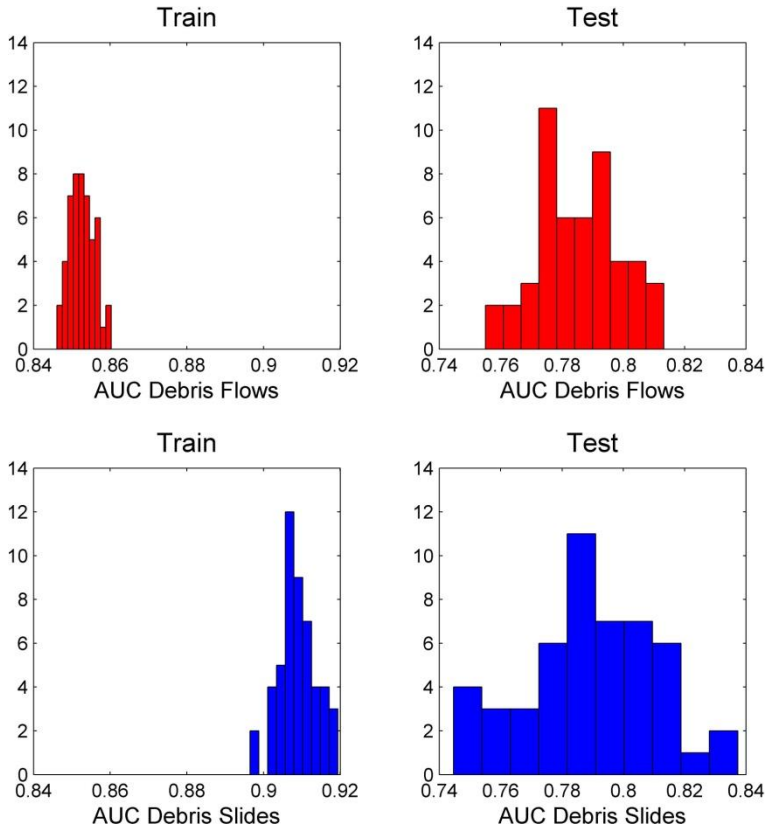

Figure 5.3.2 - Univariate AUC distribution between the two landslide classes and between the training and test phases.

Analysing the shape of the corresponding ROC-curves (Fig. 5.3.3), the shift between training and test phases becomes evident highlighting a strong stability among replicates in the first phase and a greater variability in the second one, particularly for debris slides.

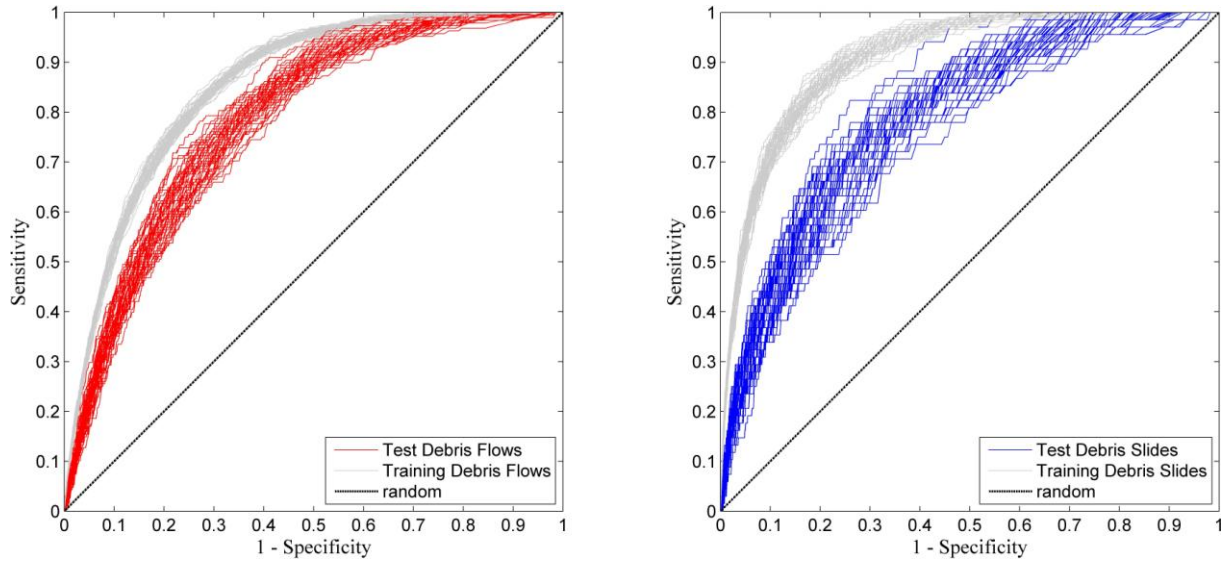

Figure 5.3.3 - ROC curves calculated for debris flows and debris slides during the training and test phases.

Nevertheless, the standard deviation for test AUC reached 0.013 for debris flow and 0.021 for debris slide, attesting for stable prediction throughout the modelling procedure for both the classes.

The two susceptibility maps show (Fig. 5.3.4) a common non-susceptible region located approximately at the catchment ridge, whilst the central and the lower sectors depict different occurrence probabilities between the two landslide typologies. Some differences between the debris flow and debris slide susceptibility maps are in fact evident at a first glance, with the latter being characterised by high probability values only on the northern flank of the catchment. The debris flow susceptibility maps shows a similar pattern; however, some highly susceptible areas were produced also for the southern sector.

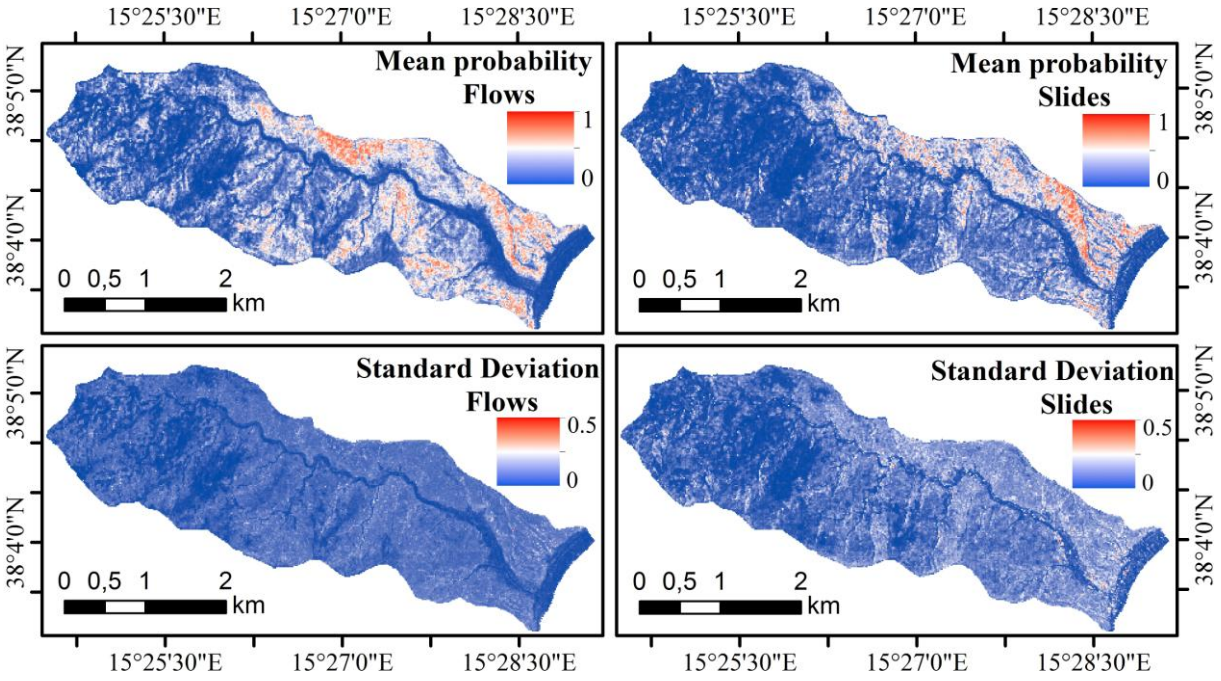

Figure 5.3.4 - Landslide average susceptibility maps associated with the corresponding dispersion.

By intersecting the mean probabilities with the corresponding dispersion, measured by a two interval, the model error for each cell in the catchment was estimated. The Figure 5.3.5 shows that the greatest robustness was obtained for the stable conditions (low susceptibility) with a strong density of point on the left tail of the plots. The central sector (intermediate susceptibility) was characterised by the strongest variations with the debris slide class being on average twice as unstable as the debris flow one. The right side of the error plots indicate that the models are stable also in predicting highly susceptible cells, with almost no cases with probability higher than 0.9, for the two typologies.

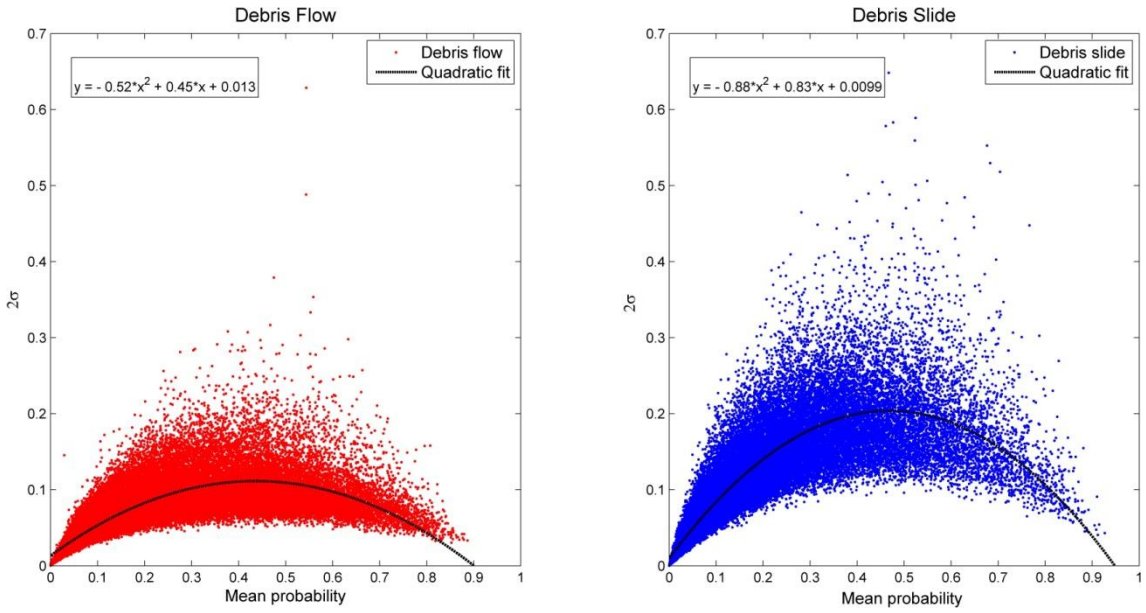

Figure 5.3.5 - Error plot for the two landslide classes, average probability plotted against the corresponding standard deviation measured by a two-times interval.

With regards to the role of the primary covariates within the modelling phase, clear differences arose between classes when analysing the jackknife tests performed between the two types of mass movements.

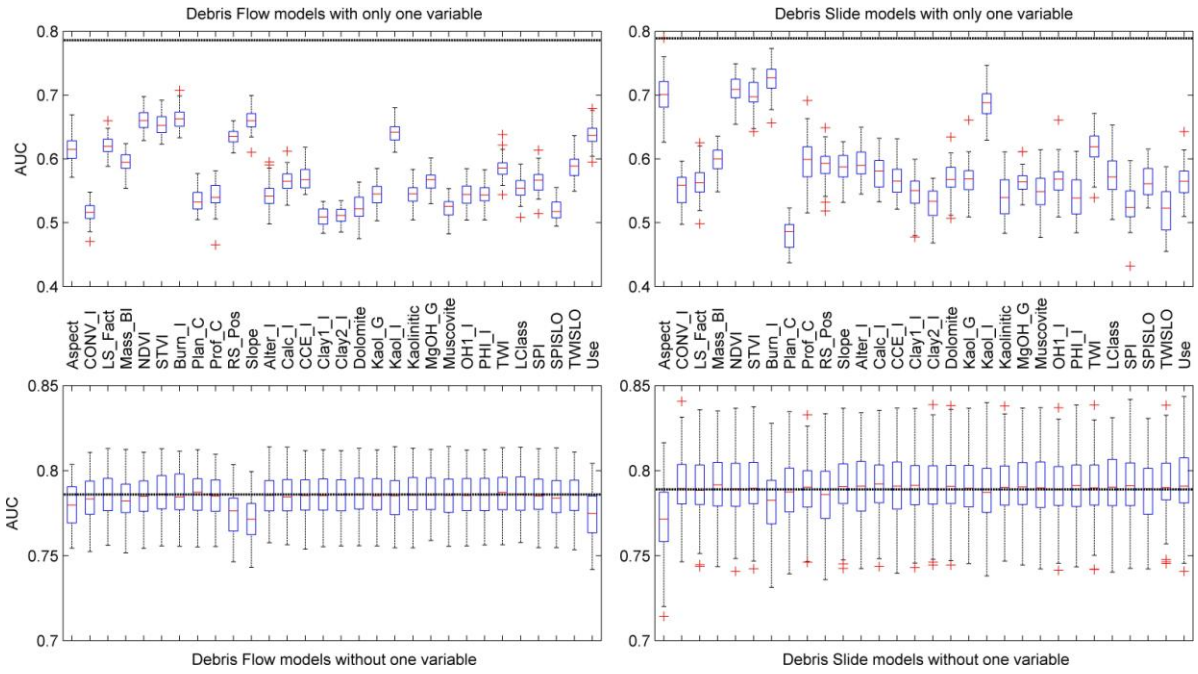

Figure 5.3.6 - Jackkife test for the two landslide types.

The debris flow class showed a greater control (Fig. 5.3.6) from topographic attributes with Slope, Steepness and Relative Slope Position being constantly the most important covariates together with the Burn index.

Conversely, the debris slide models were primarily controlled (Fig. 5.3.6) by Burn and Normalised Difference Vegetation indexes together with Slope Aspect.

The Predictor Importance is a fundamental information to establish those covariates dominating the final probabilities computed by each models; however, it should be coupled with response curves to complete the analyses on the covariates (Marker et al., 2011). It should be noted that response curves are created during the training phase and their interpretation allows inferring useful relationships between single independent variables and the modelled landslides, without directly influencing the final probability outcome. In particular, the response curves generated by the two modelled landslide typologies (5.3.7) generally showed similar trends suggesting a common trigger and consequent failure dynamics.

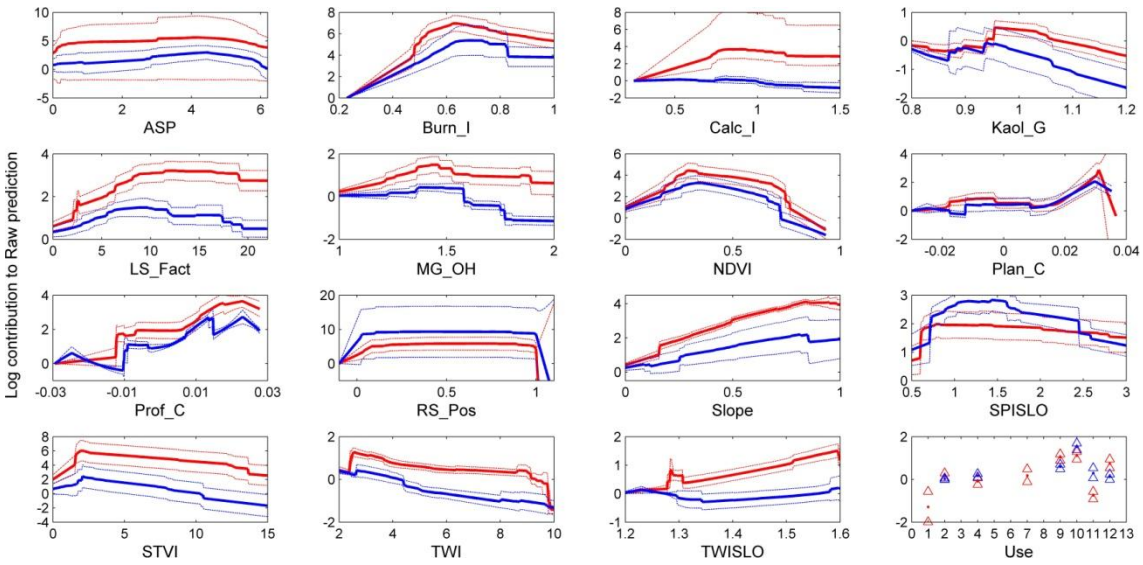

Figure 5.3.7 - Debris slide and debris flow response curves, blue and red, respectively.

Among those covariates that played a fundamental role in the final models, the interpretation of the response curves suggests that the slope has a positive influence for both the landslide typologies, being greater for the debris flows. With regard to the NDVI both landslide typologies were positively affected until a value of approximately 0.4; within this window the NDVI expresses low vegetation density whilst from this threshold onward the trend becomes

negative according to an increase in local greenness. The Burn index expresses presence of fire from a minimum value of zero coinciding with natural condition up to its maximum value, which represents presence of ashes. The Burn index response curve shows a positive correlation with both landslide initiation types until the range between 0.5 and 0.7, where the maximum influence is reached and burned condition are present. From 0.7 onward the relationship decreases; however it should be noticed that few locations were marked with such high values as shown in figure 5.3.1.

The response curves of the relative slope position show an increasing trend from the minimum of zero, coinciding with the river network, to the maximum value of 1, corresponding to the water divides where the contribution to the prediction reaches the asymptotes. The response curve related to the Kaolin Group shows a narrow positive correlation between 0.9 and 1 whilst the remaining domain is anticorrelated to the landslide occurrence. In particular the positive relationship range is wider for debris flow then debris slide, for which is almost constantly negative. A similar trend is shown in the TWI response curve, with debris slides trigger having a negative correlation to the Topographic Wetness Index except in the interval between 2 and 4, whilst debris flows are almost constantly positively correlated to the TWI across its entire domain. The Corine 2006 land use shows a broad agreement between the two landslide typologies, with Use9 (Grassland), Use10 (Olive groves), and Use12 (Shrubland) contributing to landslide prone conditions. Use11 (Erosion scars, badlands, rock outcrops) performs differently between the two landslide types, having a positive effect on debris flows and a negative one on debris slides. The response curve of the latter class indicates that Use1 and Use7 corresponding to continuous urban fabric and non-irrigated arable land respectively have a negative correlation to the actual trigger of debris slides.

5.3.9 *Discussion and conclusions*

Simultaneous widespread landslide activations pose a serious threat to human lives and infrastructures. Urban planners need to integrate reliable landslide susceptibility maps to their schemes in order to plan the best response to potential disasters. Classified landslide susceptibilities represent the best solution when anticipating different geomorphological

responses and consequently different potential mass movements behaviours across the slopes. An important subject strongly affecting the final production of landslide susceptibility maps is represented by the acquisition of the data upon which susceptibility models are built through different available techniques. In this contribution we selected a presence-only method to depict the landslide proneness by integrating two primary sources of predictors, namely DEM- and remote sensing- derived. The first source of data is currently the most used for landslide spatial prediction studies; however high resolution digital elevation models are not always available. To cope with this limitation we tested the contribution of ASTER-derived vegetation and mineral indexes in order to support the actual landslide susceptibility modelling procedure. Within the international community the use of vegetation indexes is commonly bounded to the Normalised Difference Vegetation Index. We decided to also consider the STVI (Stress Related Vegetation Index) and the Burn Index to express altered and burned vegetation respectively due to a series of forest fires spread during the summer 2007 (http://www.comune.messina.it/il-comune/ufficio-urbanistica/catasto-incendi/catasto-incendi-eventi-2007). Unfortunately fires occur systematically each summer in the area, triggered for natural and human causes, for this reason the Burn Index, being derived from the ASTER scene acquired on the 21th July 2007 was able to capture the fires burned up throughout June and July. In fact, recent studies (Cannon et al., 2008; Cannon and DeGraffe, 2009; Jackson and Roering, 2009; Martin, 2007; Ren et al., 2011) have confirmed the important role of burned vegetation to new landslide activations by mechanism of piping effect (Leslie et al., 2014) where roots and rootlets were present in the soil column as well as the shallow planar water-repellence effect (DeBano, 2000, 2003; MacDonald and Huffman, 2004; McNabb et al., 1989; Robichaud, 2000, 2013). The combined piping and impermeabilisation phenomena can affect the activation of debris flow and debris slide differently influencing the two mass movements.

Vegetation information was coupled with another set of mineral indexes derived from ASTER scenes. Each of the mineral layer was used as a proxy variable for the mechanical properties of the outcropping regolithic mantle.

Response curves were used in conjunction with the corresponding predictor importances to singularly establish how each primary predictors were linked to the actual landslide occurrences and the strength with which it contributed to the final models. As a consequence differences were ascertained between debris flows and debris slides with a primary control of topographic attributes corresponding for the former whilst the latter appeared to be more

controlled by the remote sensing covariates. In particular, for the debris slide, with the exception of the Slope Aspect, vegetation and mineral indexes acted as the major activation contributors. For the latter type, the most relevant predictor proved to be the Slope Aspect actually; this covariate is usually assumed as a proxy for strata attitude, which for the specific mass movement could have played an important role in the failure mechanism approximating shallow sliding layers. Debris slides appeared to have been primarily controlled also by the presence of burned vegetation through the fifty replicated. This result, coupled with the topographic aspect effect can be interpreted through the shallow presence of planar water repellent layers that could have led to an initial planar movement subsequently evolved into debris avalanches or flows as a function of the geomorphic control. The Burn Index appeared to strongly affect also the debris flow class but with a lesser extent. For this type of mass movement, differently from debris slides, the important role of burned vegetation can be interpreted as due to the piping effect combined with other topographic conditions in order to give rise to landslide trigger. The most relevant mineral index was the Kaolin Group (Cudahy, 2012). This is an important information considering that most of local lithotypes include metamorphosed clays and also that from geomorphological surveys part of the failure mechanism started where schistosity was present. Ultimately, it is worth noting that despite presence-only methods do not capitalise on the absence information, in the present work the Maximum Entropy approach produced almost excellent predictions and effectively discriminated the two landslide triggering mechanisms.

5.4 COMPLEMENTARY RESEARCHES

The framework of the present thesis is included within a broader research group focussing on landslide susceptibility applications. Further analyses have been performed to those described above collaborating with other researchers of the University of Palermo, Department of Earth and Sea Sciences. Four complementary subjects have been deepened in the team with specific objectives related to pixel size role of grid-cell based susceptibility assessment, integration of source and propagation susceptibilities, role of negatives within the landslide susceptibility modelling, and geotechnical soil parameterisation to enhance landslide predictive modelling. Due to partial contributions to these topics, the present thesis will shortly describe some of their primary findings and results.

5.4.1 *Exploring relationships between pixel size and accuracy for debris flow susceptibility models: a test in the Giampilieri catchment (Sicily, Italy).*

This test primarily addresses the issue related to the resolution of the mapping unit and the corresponding ability to predict shallow landslide distributions. Only a limited number of scientific papers have been published on this subject (Fuchs et al., 2014; Legorreta Paulin et al., 2010; Penna et al., 2014) primary considering the role of the grid resolution within physically based susceptibility models. The present experiment aims to deepen the knowledge on the contribution of the pixel size of the adopted mapping units to the susceptibility models obtained through stochastic approach. The chosen test site was the Giampilieri catchment where the landslide scenario exhibited on the 1st of October 2009 has been reproduced by adopting different squared mapping units diversified as a function of their pixel size expression. In order to evaluate the quality of different cell-based susceptibility maps obtained by applying Binary Logistic Regression, a combined prediction skill and accuracy criterion has been used.

The parameter space and the geographic space have been resized to describe the spatial resolution of 2m, 8m, 16m and 32m cell sides. A multi-fold cross validation technique, based on the generation of eight replicates for each model suite has been adopted to validate and compare different model outcomes.

The results confirmed the high predictive performances of the suites 2m, 8m and 16m, both in terms of goodness of fit and prediction skill. Conversely the 32m suite, constantly produced the worst performance and robustness.

The predictor selection for all the four suites, frequently clustered around a specific set of covariates, namely: height, steepness, outcropping lithology, soil use, aspect and topographic curvatures.

Differently from what expected, the overall comparison proved that the best performances were achieved adopting a 16m mapping unit, this outcome was supported by the best prediction skill, with average AUC value of 0.836 and a limited instability in prediction throughout the replicates, with a standard deviation of 0.019.

This research demonstrates that there are no significant losses in the predictive performance by adopting a coarser pixel resolution of the mapping unit. The results confirm that, at least for shallow flow-like landslides, the high resolution of the mapping unit and hence of the original digital elevation model does not provide the best solution in assessing the landslide susceptibility of a given area. This can be interpreted as a closer dimension of the coarser pixel size to the real instability phenomena, whilst the highly resolved data could introduce noise to the modelling procedure rather than adding consistent information.

5.4.2 *Integration of source and propagation susceptibilities*

Debris flow are among the most hazardous phenomena in nature, for this reason the susceptibility assessment is of primary importance. Deterministic approaches seem to be the most suited for runout modelling. However, due to variability of the local controlling factors they are difficult to be applied at the regional scale. For this reason, in this research we used a simplified approach coupling a statistical method to define the source area and a flow direction algorithm to simulate the propagation phase. The propagation phase was evaluated using FLOW-R (Flow path assessment of gravitational hazards at a Regional scale), a tool developed in Matlab in which different flow direction algorithms are implemented.

The study area is Giampilieri catchment (Sicily-Italy) which was hit by an extreme rainfall event on the 1st October 2009 causing the trigger of thousands of debris flow and

approximately 1 million euros of damages and 37 fatalities. The available dataset for the area is an extensive debris flow inventory and a High resolution spatially distributed dataset.

The first purpose of this research was to simulate the 2009 event. The propagation was calculated using Holmgren's algorithm coupled with a friction law, starting from the triggering point of 2009 event. The best model parameters were defined by an iterative validation process through ROC-AUC test, using the mapped deposition areas as observed positive cases.

The second objective of this study was to calculate the debris flow susceptibility applying binary logistic regression (BLR) for the identification of the source areas the Holmgren algorithm for the propagation simulation. In particular, the model resulting by the application of BLR was validated using a cross folded validation procedure and the source areas were selected using a threshold value in susceptibility of 0,75. Subsequently, the propagation model (Holmgren algorithm + friction law), previously parametrized during the simulation of the 2009, was applied generating the final susceptibility map which shows the probability of triggering and propagation of debris flow for extreme events.

The results showed that it is possible to successfully simulate the 2009 event with using a simple flow direction algorithm. Moreover, coupling the two algorithms BLR and Holmgren algorithm it was possible to evaluate the susceptibility connected to extreme events for the Giampilieri area. The resulting map represents, by now, the first attempt in evaluating the susceptibility in terms of propagation and can be used to identify areas where further studies will be carried out.

5.4.3 *Chrono-validation Predicting storm triggered debris flow events: application to the 2009 Ionian-Peloritan disaster (Sicily, Italy).*

The development of susceptibility maps for landslides triggered by extreme meteorological events is of primary importance due to the population pressure in hazardous zones. The main assumption on which landslide susceptibility stochastic modelling lays is that the past is the key to the future. This means that a predictive model able to correctly classify a past known landslide scenario will be able to predict a future unknown one as well. However, storm triggered landslide events in the Mediterranean region typically result in a randomness both in time recurrence and magnitude. Therefore these extreme meteorological events could

pose some limits on the operative validity of such expectation. This is the case of the 2007/2009 couple of events, which recently hit north-eastern Sicily resulting in largely different disaster scenarios.

The study area considered in this study, is the the Itala torrent (Messina, southern Italy) which is located in the southern Peloritan Mountains in the epicenter of both 2007 and 2009 landslide events.

The purpose of this study is to investigate the ability of a susceptibly model to predict storm triggered debris flow when trained with previous landslide inventory. To assess the landslide susceptibility, stepwise binary logistic regression was applied to a set of predictors and a landslide inventory.

The landslides activated in the occasion of the two close heavy rainfall events have been mapped by integrating remote and field surveys and result in two landslide inventories including 73 landslides, activated in 2007, and 616 landslides triggered by the 2009 storm.

The set of predictors used as independent variables in landslide susceptibility assessment were derived from a 2m-cell digital elevation model and a 1:50,000 scale geologic map. The quality of the models have been evaluated using two types of validation procedures: self-validation, based on the random partition of each coeval subinventory, and chrono-validation, based on the temporal partition of the landslide inventory. It was therefore possible to analyze the performances both of 2007 in predicting the 2009 trained models (forward-chronovalidation) and of the 2009 in predicting the 2007 (backward chronovalidation).

The results showed that the susceptibility evaluated using the 2007 inventory is able to produce good results in predicting the 2009 event and vice versa. However, a loss of prediction skills between the chrono-validated and self-validated models is shown, especially in backward validation. Although this result apparently holds the main assumption' the past is the key of the future', the loss of performance highlights that the homogeneity of the trigger events should be previously verified in deep both in terms of spatial distribution and intensity.

6 OVERALL DISCUSSION AND CONCLUSIONS

The present thesis encompasses experiments designed to deal with methodological aspects of landslide susceptibility modelling. The driving purpose was to evaluate whether it is possible to export landslide prediction images from a source to a target area of interest using different algorithms and datasets. The first experiment demonstrated that the landslide scenario within the target catchment of Giampilieri was effectively reconstructed carrying out the learning phase within a different watershed. This outcome can be contextualised within the broader topic of climate changes. In fact, the constantly diversifying patterns of climatic discharges in terms of precipitation magnitude, spatial and temporal frequencies, pose serious issues for urban planners dealing with geomorphic risks. If predictive models are based upon past landslide activations due to average rainfall stresses the resulting susceptibility maps could strongly underestimate scenarios caused by storms or long-term precipitation extreme outliers. This is the case of the Mediterranean sector, specifically in Italy, where in recent years the community assisted to a sudden increase of calamitous occurrences triggered by unprecedented meteorological events. In this region, landslide inventories generated by extreme storms are scattered in time and space leaving gaps in areas that could be exposed to such disasters in the next future. Susceptibility exportation could be proposed as a supplementary if not a stand-alone procedure to limit the damage caused by underestimating the slope geomorphological responses to exceptional storms. Model can be trained in areas already struck by such events, thus incorporating their morphodynamic effects and then exported to target areas where urban plans need to integrate predictions from worst case landslide scenarios. The domain of validity of the exportation process is constrained by a similarity threshold between the two areas which yet needs to be further considered. In the present experiment the two test catchments were selected in close proximity; however, future tests will be aimed at establishing the exportation validity domain by evaluating the relationship between predictors similarity and prediction performances.

Recent applications in different areas of the geosciences have exploited satellite imagery to derive a wide range of vegetation and mineral indexes. Another important step toward the spatial exportation could involve the integration of remotely sensed covariates within the modelling phase thus effectively limiting the cost of informative layers and the geographic limit

of data availability. In addition, also the potential application of exportation procedures could benefit from remotely sensed data supporting landslide susceptibility assessments built between completely different areas exhibiting analogous mass movement and triggers. This topic has also been investigated within the present thesis, limiting the tests to establish the effectiveness of remote sensing predictors within classified susceptibility models.

Ultimately, according to the scientific literature, numerous methods can be used to achieve reliable landslide susceptibility assessments. Due to a recently-reached broad agreement among scientists regarding the model building and validation strategies, one of the common topics has become comparing the performances of different algorithms for landslide spatial prediction. In this thesis two methods have been tested to export susceptibility models both relying on presence-absence data. The results highlighted that one of the two codes could be better suited for model transfer between areas with limited spatial variability in the predictor domain ensuring high performances. The second algorithm is less powerful but less sensible to spatial variations at the same time, suggesting its use when exportation procedure would be applied between areas with limited similarity.

7 REFERENCES

Agnesi V., Rasa` R., Puglisi C., Gioe` C., Privitera B., Cappadonia C., Conoscenti C., Pino P., Rotigliano E., 2009. La franosita diffusa dell'1 Ottobre 2009 nel territorio ionico-peloritano della Provincia di Messina: stato delle indagini e prime considerazioni sulle dinamiche geomorfiche attivate. Geologi di Sicilia 4:23–30.

Ahrendt, A., Zuquette, L.V., 2003. Triggering factors of landslides in Campos do Jordão city, Brazil. Bulletin of Engineering Geology and the Environment 62 (3), pp. 231-244.

Akgün, A., Türk, N., 2011. Mapping erosion susceptibility by a multivariate statistical method: A case study from the Ayvalik region, NW Turkey. Computers & Geosciences 37, 1515-1524.

Aleotti, P. and Chowdhury, R., 1999. Landslide hazard assessment: summary review and new perspectives, Bulletin of Engineering Geology and the Environment, 58: 21-44.

Alexander, D.E., 2008. A brief survey of GIS in mass-movement studies, with reflections on theory and methods. Geomorphology 94 (3-4), pp. 261-267.

Althuwaynee, O.F., Pradhan, B., Park, H.-J., Lee, J.H., 2014. A novel ensemble bivariate statistical evidential belief function with knowledge-based analytical hierarchy process and multivariate statistical logistic regression for landslide susceptibility mapping. Catena 114, pp. 21-36.

Aman, S.N.A., Latif, Z.A.,Pradhan, B., 2014. Spatial probabilistic approach on landslide susceptibility assessment from high resolution sensors derived parameters. IOP Conference Series: Earth and Environmental Science 18 (1), 012057.

Ardizzone, F.; Basile, G.; Cardinali, M.; Casagli, N.; Del Conte, S.; Del Ventisette, C.; Fiorucci, F.; Gigli, G.; Garfagnoli, F.; Guzzetti, F., 2012. Landslide inventory map for the Briga and the Giampilieri catchments, NE Sicily, Italy. J. Doi:10.1080/17445647.2012.694271.

Aronica, G.T., Brigandí, G., Morey, N., 2012. Flash floods and debris flow in the city area of Messina, north-east part of Sicily, Italy in October 2009: The case of the Giampilieri catchment. Natural Hazards and Earth System Science 12 (5), pp. 1295-1309.

Atkinson, P.M., Massari, R., 1998. Generalised linear modelling of susceptibility to landsliding in the central Apennines, Italy. Computers & Geosciences, 24 (4), 373-385. Doi: 10.1016/S0098-3004(97)00117-9.

Baeza, C., Lantada, N., Moya, J., 2010. Influence of sample and terrain unit on landslide susceptibility assessment at La Pobla de Lillet, Eastern Pyrenees, Spain. Environmental Earth Sciences 60 (1), pp. 155-167.

Bai, S.-B., Wang, J., Lü, G.-N., Zhou, P.-G., Hou, S.-S., Xu, S.-N., 2010. GIS-based logistic regression for landslide susceptibility mapping of the Zhongxian segment in the Three Gorges area, China. Geomorphology, 115(1–2), 23-31.
Doi: 10.1016/j.geomorph.2009.09.025.

Bai, S., Xu, Q., Wang, J., Zhou, P., 2014. Pre-conditioning factors and susceptibility assessments of Wenchuan earthquake landslide at the Zhouqu segment of Bailongjiang basin, China. Journal of the Geological Society of India 82 (5), pp. 575-582.

Bates, R.L. and J. Jackson, 1987. Glossary of Geology: Alexandria, Virginia. 1st Edn., American Geological Institute, New York, pp: 788.

Baum, R.L., Coe, J.A., Godt, J.W., Harp, E.L., Reid, M.E. Savage, W.Z., Schulz, W.H., Brien, D.L., Chleborad, A.F., McKenna, J.P., and Michael, J.A., 2005, Regional Landslide-Hazard Assessment for Seattle, Washington, USA: Landslides, v. 2, no. 4, p. 266-279, Doi: 10.1007/s10346-005-0023-y

Behling, R., Roessner, S., Segl, K., Kleinschmit, B. Kaufmann, H., 2014. Robust automated image co-registration of optical multi-sensor time series data: database generation for multi-temporal landslide detection. Remote sensing, 6, 2572-2600.

Berger, A.L. Della Pietra, V.J., Della Pietra, S.A., 1996. A maximum entropy approach to natural language processing, Computational Linguistics, v.22 n.1, p.39-71.

Berk, A., P.K. Acharya, L.S. Bernstein, G.P. Anderson, P. Lewis, J.H. Chetwynd, M.L. Hoke, 2008. Band Model Method for Modeling Atmospheric Propagation at Arbitrarily Fine Spectral Resolution, U.S. Patent #7433806.

Beven and Kirkby 1979. A physically based variable contributing area model of basin hydrology. Hydrological Sciences Bulletin, 24, pp. 43–69.

Beven, K.J., Wood, E.F., and Sivapalan, M., 1988. On hydrological heterogeneity - catchment morphology and catchment response, J. Hydrol., 100, 353–375.

Bierwirth, P., 2002: Evaluation of ASTER Satellite Data for Geological Applications. Consultancy Report to Geoscience Australia.

Bonardi G., Messina A., Perrone V., Russo M., Russo S. and Zuppetta A. (1980) La finestra tettonica di Cardeto (Reggio Calabria). Rend. Soc. Geol. It., 3: 3-4.

Bonardi, G., Cavazza, W., Perrone, V., Rossi, S., 2001. Calabria–Peloritani Terrane and Northern Ionian Sea, in: G.B. Vai, I.P. Martini (Eds.), Anatomy of an Orogen: the Apennines and Adjacent Mediterranean Basins, Kluwer Academic Publishers, Dordrecht / Boston / London, pp. 287–306.

Bonardi, G., De Capoa, P., Staso, A.D., Estévez, A., Martín-Martín, M., Martín-Rojas, I., Perrone, V., Tent-Manclús, J.E., 2003. Oligocene-to-early miocene depositional and structural evolution of the Calabria-Peloritani Arc southern terrane (Italy) and geodynamic correlations with the Spain betics and Morocco rif. Geodinamica Acta 16 (2-6), pp. 149-169.

Borgatti, L., Soldati, M., 2010. Landslides as a geomorphological proxy for climate change: A record from the Dolomites (northern Italy). Geomorphology, 120(1–2), 56-64. Doi: 10.1016/j.geomorph.2009.09.015.

Brabb EE (1984) Innovative approaches to landslide hazard mapping. Proc IV ISL, Toronto 1: 307 – 324.

Brabb, E.E., 1984. Innovative approaches to landslide hazard and risk mapping. Proc. of the IV International Symposium on Landslides, Toronto, 1, pp. 307–323.

Brambilla, M., Saporetti, F., 2014. Modelling distribution of habitats required for different uses by the same species: Implications for conservation at the regional scale. Biological Conservation 174, pp. 39-46.

Brenning, A., 2008. Statistical geocomputing combining R and SAGA: The example of landslide susceptibility analysis with generalized additive models. In: J. Böhner, T. Blaschke & L. Montanarella (eds.), SAGA – Seconds Out (= Hamburger Beiträge zur Physischen Geographie und Landschaftsökologie, vol. 19), p. 23-32.

Breunig, F.M., Galvão, L.S., Formaggio, A.R., 2008. Detection of sandy soil surfaces using aster-derived reflectance, emissivity and elevation data: potential for the identification of land degradation. - International journal of remote sensing 29 (6): 1833-1840.

Burrough, P.A. and Mcdonell, R.A., 1998. Principles of Geographical Information Systems. Oxford University Press, New York, p. 190.

Burrough, P.A., van Gaans, P.F.M., MacMillan, R.A., 2000. High-resolution landform classification using fuzzy k-means. Fuzzy Sets and Systems 113, 37-52.

Caine N (1980) The rainfall intensity-duration control of shallow landslides and debris flows. Geogr Ann A 62: 23–27.

Calvo, L., Haddad, B., Pastor, M.,Palacios, D., 2014. Runout and deposit morphology of Bingham fluid as a function of initial volume: implication for debris flow modelling. Natural Hazards, in press.

Campbell R.H., 1975. Soil slips, debris flows, and rainstorms in the Santa Monica Mountains and vicinity, southern California. In: US Geological Survey Professional Paper 851. Washington DC: U.S. Government Printing Office, 51 pp.

Can, T., Nefeslioglu, H.A., Gokceoglu, C., Sonmez, H., Duman, T.Y., 2005. Susceptibility assessments of shallow earthflows triggered by heavy rainfall at three catchments by logistic regression analyses. Geomorphology, 72 (1–4),250-271. Doi: 10.1016/j.geomorph.2005.05.011.

Cannon SH, Ellen S.D., 1985. Rainfall conditions for abundant debris avalanches, San Francisco Bay region, California. Calif Geol 38: 267–272.

Cannon, S.H., Gartner, J.E., Wilson, R.C., Bowers, J.C., Laber, J.L. 2008. Storm rainfall conditions for floods and debris flows from recently burned areas in southwestern Colorado and southern California. Geomorphology 96 (3-4), pp. 250-269.

Cannon, S.H., DeGraff, J., 2009. The increasing wildfire and post-fire debris-flow threat in western USA, and implications for consequences of climate change. Landslides - Disaster Risk Reduction pp. 177-190.

Carrara, A., Catalano, E., Sorriso Valvo, M., Reali, C., Merenda, L., Rizzo, V., 1977. Landslide morphometry and typology in two zones, Calabria, Italy. Bulletin of the International Association of Engineering Geology 16, 8-13.

Carrara, A., 1988. Drainage and divide networks derived from high–fidelity digital terrain models. In: Chung, C.-J. F., et al. (eds.) Quantitative analysis of mineral and energy resources. NATO–ASI Series, D. Reidel Publishing Co., Dordrecht, 581-597.

Carrara, A., Cardinali, M., Detti, R., Guzzetti, F., Pasqui, V., Reichenbach, P., 1991. GIS techniques and statistical models in evaluating landslide hazard. Earth Surface Processes and Landforms 16, 427-445.

Carrara, A., Cardinali, M., Guzzetti, F. and Reichenbach, P., 1995. GIS technology in mapping landslide hazard. In: Carrara, A. and Guzzetti, F. (eds.) Geographycal Information Systems in Assessing Natural Hazards. Kluwer Academic Publisher, Dordrecht, The Netherlands, 135-175.

Carrara, A., Guzzetti, F., Cardinali, M. and Reichenbach, P. (1999) Use of GIS Technology in the Prediction and Monitoring of Landslide Hazard. Natural Hazards, 20:2-3 117-135.

Carrara, A., and Pike, R.J., 2008. GIS technology and models for assessing landslide hazard and risk. Geomorphology, 94, 257-260.

Casagli, N., Catani, F., Puglisi, C., Delmonaco, G., Ermini, L., Margottini, C., 2004. An inventory-based approach to landslide susceptibility assessment and its application to the Virginio River Basin, Italy. Environmental and Engineering Geoscience, 10 (3), pp. 203-216.

Catalano, S., De Guidi, G., 2003. Late Quaternary uplift of northeastern Sicily: Relation with the active normal faulting deformation. Journal of Geodynamics 36 (4), pp. 445-467.

Casalbore, D., Chiocci, F.L.,Mugnozza, G.S., Tommasi, P.,Sposato, A., 2011. Flash-flood hyperpycnal flows generating shallow-water landslides at Fiumara mouths in Western Messina Strait (Italy). Marine Geophysical Research 32 (1), pp. 257-271.

Catalano, S., De Guidi, G., Monaco, C., Tortorici, G., Tortorici, L., 2003. Long-term behaviour of the late Quaternary normal faults in the Straits of Messina area (Calabrian arc): Structural and morphological constraints. Quaternary International 101-102 (1), pp. 81-91.

Chen, H.X., Zhang, L.M., Zhang, S., 2014. Evolution of debris flow properties and physical interactions in debris-flow mixtures in the Wenchuan earthquake zone. Engineering Geology, in press.

Cheng, Y., Huo, A., Zhang, J., Lu, Y., 2014. Early warning of meteorological geohazard in the Loess Plateau: a study in Huangling County of Shaanxi Province in China. Environmental Earth Sciences, in press.

Chiou, I.-J., Chen, C.-H., Liu, W.-L.,Huang, S.-M., Chang, Y.-M., 2014. Methodology of disaster risk assessment for debris flows in a river basin. Stochastic Environmental Research and Risk Assessment, in press.

Clerici, A., Perego, S., Tellini, C.,Vescovi, P., 2002. A procedure for landslide susceptibility zonation by the conditional analysis method. Geomorphology 48 (4), pp. 349-364.

Clerici, A., Perego, S., Tellini, C.,Vescovi, P., 2006. A GIS-based automated procedure for landslide susceptibility mapping by the Conditional Analysis method: The Baganza valley case study (Italian Northern Apennines). Environmental Geology 50 (7), pp. 941-961.

Conforti, M., Robustelli, G., Muto, F.,Critelli, S., 2012. Application and validation of bivariate GIS-based landslide susceptibility assessment for the Vitravo river catchment (Calabria, south Italy). Natural Hazards, 61 (1), pp. 127-141.

Conforti, M., Pascale, S., Robustelli, G., Sdao, F., 2014. Evaluation of prediction capability of the artificial neural networks for mapping landslide susceptibility in the Turbolo River catchment (northern Calabria, Italy). Catena 113, pp. 236-250.

Conoscenti, C., Maggio, C.,Rotigliano, E., 2008. GIS analysis to assess landslide susceptibility in a fluvial basin of NW Sicily (Italy). Geomorphology 94 (3-4), pp. 325-339.

Conrad, O., 2006. SAGA – Program Structure and Current State of Implementation. in: Böhner, J., McCloy, K.R. & Strobl, J. [Eds.]: SAGA – Analysis and Modelling Applications. Göttinger Geographische Abhandlungen, 115: 39-52.

Convertino, M., Troccoli, A., Catani, F., 2014. Detecting fingerprints of landslide drivers: A MaxEnt model. Journal of Geophysical Research: Earth Surface 118 (3), pp. 1367-1386.

Costanzo, D., Rotigliano, E., Irigaray, C., Jiménez-Perálvarez, J.D., Chacón, J., 2012a. Factors selection in landslide susceptibility modelling on large scale following the gis matrix method: Application to the river Beiro basin (Spain). Natural Hazards and Earth System Science 12 (2), pp. 327-340.

Costanzo, D., Chacón, J.,Conoscenti, C., Irigaray, C.,Rotigliano, E., 2014. Forward logistic regression for earth-flow landslide susceptibility assessment in the Platani river basin (southern Sicily, Italy). Landslides 11 (4), pp. 639-653.

Crozier MJ (1986) Landslides: causes, consequences and environment. London: Croom Helm, 252 pp.

Crozier, M.J., 2005. Multiple-occurrence regional landslide events in New Zealand: Hazard management issues. Landslides 2 (4), pp. 247-256. DOI: 10.1007/s10346-005-0019-7

Cruden DM. 1991. A simple definition of a landslide. Bulletin of the International Association of Engineering Geology 43, 27–29.

Cruden D.M., Varnes D.J., 1996. Landslide types and processes. In: Special report 247: landslides: investigation and mitigation. Transportation Research Board, Washington DC.

Cudahy, T., 2012. Satellite ASTER GeoscienceProduct. – Notes for Australia; CSIRO: http://c3dmm.csiro.au/WA_ASTER/WA%20ASTER%20Geoscience%20Product%20Notes%2015112011.pdf (16.6.2014).

Davis, J.D., Sims, S.M., 2013. Physical and maximum entropy models applied to inventories of hillslope sediment sources. Journal of Soils and Sediments 13 (10), pp. 1784-1801.

Debano, L.F., 2000. The role of fire and soil heating on water repellency in wildland environments: A review. Journal of Hydrology 231-232, pp. 195-206.

Debano, L.F., 2003. The role of fire and soil heating on water repellency. Soil Water Repellency: Occurrence, Consequences, and Amelioration pp. 193-202.

De Guidi G, Scudero S., 2013. Landslide susceptibility assessment in the Peloritani Mts. (Sicily, Italy) and clues for tectonic control of relief processes. Nat Hazards Earth Syst Sci 13:949–963. Doi:10.5194/nhess-13-949-2013

Della Pietra, S., Della Pietra, V., Lafferty, J., 1997. Inducing features of random fields. IEEE Transactions on Pattern Analysis and Machine Intelligence 19 (4), pp. 380-393.

Del Prete, M., Guadagno, F.M.,Hawkins, A.B., 1998. Preliminary report on the landslides of 5 May 1998, Campania, southern Italy. Bulletin of Engineering Geology and the Environment 57 (2), pp. 113-129.

Del Ventisette C, Garfagnoli F, Ciampalini A, Battistini A, Gigli G, Moretti S, Casagli N (2012) Anintegrated approach to the study of catastrophic debris-flows: geological hazard and human influence. Nat Hazards Earth Syst Sci 12:2907–2922. Doi:10.5194/nhess-12-2907-2012.

Deng, Y., 2007. New trends in digital terrain analysis : landform definition, representation, and classification. Progress in Physical Geography 31, 405-419.

Denizman, C., 2003. Morphometric and spatial distribution parameters of karstic depressions, lower Suwannee River Basin, Florida. J. Cave Karst Stud., 65: 29-35.

Dhakal A.S. and Sidle R.C., 2004. Distributed simulations of landslides for different rainfall conditions. Hydrological Processes Volume 18, Issue 4, pages 757–776, March 2004.

Dietrich, E.W., Reiss, R., Hsu, M-L. and Montgomery, D.R. (1995) A process–based model for colluvial soil depth and shallow landsliding using digital elevation data. Hydrological Process, 9: 383-400.

Dietrich, W.E., Bellugi, D., Real de Asua, R., 2001. Land Use and Watersheds: Human Influence on Hydrology and Geomorphology in Urban and Forest Areas, 2, pp. 195-227. Wigmosta M. S. and Burges, S. J., Am. Geoph. Union, Water Science and Application.

Dikau, R., Brunsden, D., Schrott, L. and Ibsen, M.-L., (eds.) 1996. Landslide recognition. Identification, movements and causes. John Wiley & Sons Ltd, Chichester, England, 251 p.

Di Stefano, E., Agate M., Incarbona, A., Russo, F., Sprovieri, R., Bonomo S., 2012. Late Quaternary high uplift rates in northeastern Sicily: evidence from calcareous nannofossils and benthic and planktonic foraminifera. Facies 58:1–15.

Dunn, M. and R. Hickey, 1998, The Effect of Slope Algorithms on Slope Estimates within a GIS. Cartography, v. 27, no. 1, pp. 9 – 15.

Eidsvig, U.M.K., Papathoma-Köhle, M., Du, J., Glade, T., Vangelsten, B.V., 2014. Quantification of model uncertainty in debris flow vulnerability assessment. Engineering Geology 181, pp. 15-26.

Eker, A.M., Dikmen, M., Cambazoğlu, S., Düzgün, Ş.H.B., Akgün, H., 2014. Evaluation and comparison of landslide susceptibility mapping methods: a case study for the Ulus district, Bartın, northern Turkey. International Journal of Geographical Information Science, In press.

Elith, J., S. Phillips, T. Hastie, M. Dudík, Y. Chee, and C. Yates, 2011. A statistical explanation of MaxEnt for ecologists, Divers. Distrib., 17, 43–47, doi:10.1111/j.1472-4642.2010.00725.x.

Elkadiri, R., Sultan, M., Youssef, A.M., Elbayoumi, T., Chase, R., Bulkhi, A.B., Al-Katheeri, M.M., 2014. A Remote Sensing-Based Approach for Debris-Flow Susceptibility Assessment Using Artificial Neural Networks and Logistic Regression Modeling. IEEE Journal of Selected Topics in Applied Earth Observations and Remote Sensing, in press.

Ermini, L., Catani, F., Casagli, N., 2005. Artificial Neural Networks applied to landslide susceptibility assessment. Geomorphology 66 (1-4 SPEC. ISS.), pp. 327-343.

Fairfield, J. and P. Laymarie, 1991. Drainage networks from grid digital elevation models. Water Resour. Res., 27: 709-717.

Famiglietti, J.S. and Wood, E.F., 1991. Evapotranspiration and runoff from large land areas – land surface hydrology for atmospheric general-circulation models, Surv. Geophys., 12, 179–204.

Federici, P.R., Puccinelli, A.,Cantarelli, E., Casarosa, N., D'Amato Avanzi, G., Falaschi, F., Giannecchini, R., Pochini, A., Ribolini, A., Bottai, M., Salvati, N., Testi, C., 2007.

Multidisciplinary investigations in evaluating landslide susceptibility-An example in the Serchio River valley (Italy). Quaternary International 171-172 (SPEC. ISS.), pp. 52-63.

Felicísimo, Á.M., Cuartero, A.,Remondo, J., Quirós, E., 2013. Mapping landslide susceptibility with logistic regression, multiple adaptive regression splines, classification and regression trees, and maximum entropy methods: A comparative study. Landslides 10 (2), pp. 175-189.

Ferla, P., 1994. The augen-gneisses of the Peloritani Mountains (Sicily, Italy): compositional and genetic aspects of a pre-Hercynian granitoid event. Periodico di Mineralogia 63 (1-3), pp. 213-233.

Florinsky, I.V., 1998a. Accuracy of local topographic variables derived from digital elevation models. International Journal of Geographical Information Science 12 (1), 47–61.

Florinsky, I.V., 1998b. Combined analysis of digital terrain models and remotely sensed data in landscape investigations. Progress in Physical Geography 22 (1), 33-60.

Florinsky I.V., 2012. Digital Terrain Analysis In Soil Science And Geology. Elsevier / Academic Press, 2012 Amsterdam, 379 p.

Fuchs, M., Torizin, J., Kühn, F., 2014. The effect of DEM resolution on the computation of the factor of safety using an infinite slope model. Geomorphology 224, pp. 16-26.

Fujisada, H., 1995. Design and performance of ASTER instrument. proceedings of Spie, the International society for optical engineering, 2583, 16-25.

Gallant, J.C., Wilson, J.P., 2000. Primary topographic attributes. In: Wilson, J.P., Gallant, J.C. (Eds.), Terrain Analysis: Principles and Applications. Wiley, New York, pp. 51-85.

Gao, F., Masek, J. and Wolfe, R. E., 2009. Automated registration and orthorectification package for Landsat and Landsat-like data processing. Journal of applied remote sensing 3, 1 033515-033515-20.

Gartner, J.E., Cannon, S.H., Santi, P.M., 2014. Empirical models for predicting volumes of sediment deposited by debris flows and sediment-laden floods in the transverse ranges of southern California. Engineering Geology 176, pp. 45-56.

Giunta G, Somma R (1996) Nuove osservazioni sulla struttura dell‘Unita` di Alı`(Monti Peloritani, Sicilia). Boll Soc Geol Ital 115:489–500.

Glade, T. and Crozier, M., 2005. Landslide hazard and risk, edited by: Glade T., Anderson M. m and Crozier M., Wiley, Chichester.

Glade, T., Crozier, M.J., 2005b. A review of Scale Dependency in Landslide Hazard and Risk Analysis, in: Glade, T., Anderson, M., Crozier, M.J. (Eds.), Landslide hazard and risk. John Wiley and Sons, pp. 75-138.

Godt, J.W., Baum, R.L., Savage, W.Z., Salciarini, D., Schulz, W.H., Harp, E.L., 2008. Transient deterministic shallow landslide modeling: Requirements for susceptibility and hazard assessments in a GIS framework. Engineering Geology 102 (3-4), pp. 214-226.

Griffiths, J.S. (1999) Proving the occurrence and cause of a landslide in a legal context. Bulletin of Engineering Geology and the Environment, 58: 75-85.

Gruber, S., Peckham, S., 2009. Land-surface parameters and objects in hydrology. Developments in Soil Science 33 (C), pp. 171-194

Günther, A., Reichenbach, P., Malet, J-P., van Den Eeckhaut, M., Hervás, J., Dashwood, C., Guzzetti, F., 2013. Tier-based approaches for landslide susceptibility assessment in Europe. Landslides 10 (5), pp. 529-546.

Günther, A., Van Den Eeckhaut, M.,Malet, J.-P., Reichenbach, P., Hervás, J., 2014. Climate-physiographically differentiated Pan-European landslide susceptibility assessment using spatial multi-criteria evaluation and transnational landslide information. Geomorphology 224, pp. 69-85.

Guzzetti, F., Carrara, A., Cardinali, M. and Reichenbach, P. (1999) Landslide hazard evaluation: an aid to a sustainable development. Geomorphology, 31: 181-216.

Guzzetti, F., Reichenbach, P.,Cardinali, M., Galli, M., Ardizzone, F., 2005. Probabilistic landslide hazard assessment at the basin scale. Geomorphology 72 (1-4), pp. 272-299.

Guzzetti, F., 2006. Landslide Hazard and Risk Assessment. Ph.D. Thesis, University of Bonn, Germany.

Guzzetti, F., Reichenbach, P.,Ardizzone, F., Cardinali, M., Galli, M., 2006. Estimating the quality of landslide susceptibility models. Geomorphology, 81 (1-2), pp. 166-184.

Hansen, A. (1984a) Landslide hazard analysis. In: Brunsden, D. and Prior, D.B. (eds.) Slope instability, Wiley & Sons, New York, 523-602.

Hengl, T., Reuter, H.I. (Eds.), 2009. Geomorphometry: concepts, software, applications. Developments in Soil Science, 33. Elsevier, Amsterdam.

Hengxing L., Chenghu Z., Lee C.F., Sijing W., Faquan W., 2003. Rainfall-induced landslide stability analysis in response to transient pore pressure. Science in China Ser. E Technological Sciences 01/2003; 46:52-68.

Hensel, H., and Bork, H.R., 1988. EDV-gestützte Bilanzierung von Erosion und Akkumulation in kleinen Einzugsgebieten unter Verwendung der modifizierten Universal Soil Loss Equation. – Landschaftsökologisches Messen und Auswerten 2, 2/3: 107-136.

Hewson, R.D., Cudahy, T.J., Mizuhiko, S., Ueda, K. & Mauger, A.J., 2005. Seamless geological map generation using ASTER in the Broken HillCurnamona province of Australia. – RemoteSensing of Environment 99 (1 –2): 159 –172.

Hoek, E., Bray, J., 1997. Rock Slope Engineering. The Institution of Mining and Metallurgy, London, p. 402.

Hong, Y., Adler, R.F., Huffman, G.J., 2008. Satellite remote sensing for global landslide monitoring. Eos 88 (37), pp. 357-358.

Horn B.K.P.,1981. Hill shading and the reflectance map. Proceedings of the IEEE. 69 (1): 14-47.

Hosmer, D.W., and Lemeshow, S., 2000. Applied Logistic Regression. Wiley, New York.

Hudak, A.T., Robichaud, P., Evans, J.S., Clark, J., Lannom, K., Morgan, P., Stone, C., 2004. Field validation of Burned Area Reflectance Classifiation (BARC) products for post fie assessment. – University of Nebraska, Lincoln, NE, USA.

Hungr, O., Evans, S.G., Bovis, M.J.,Hutchinson, J.N., 2001. A review of the classification of landslides of the flow type. Environmental and Engineering Geoscience, 7 (3), pp. 221-238.

Hungr, O., Corominas, J., Eberhardt, E., 2005. Estimating landslide motion mechanisms, travel distance and velocity. In: Hungr, O., Fell, R., Couture, R., Eberhardt, E. (Eds.), Landslide Risk Management. Taylor and Francis, London, pp. 99–128.

Hungr, O., Leroueil, S., Picarelli, L., 2014. The Varnes classification of landslide types, an update. Landslides 11 (2), pp. 167-194.

Hutchinson, J.N., 1988. General report: morphological and geotechnical parameters of landslides in relation to geology and hydrogeology. Landslides. Proc. 5th symposium, Lausanne, 1988. Vol. 1 pp. 3-35.

Hutchinson, J.N. and Chandler, M.P., 1991. A preliminary landslide hazard zonation of the Undercliff of the Isle of Wight. Slope Stability Engineering, Thomas Telford, London, 197-205.

Hutchinson, J.N. (1995) Keynote paper: Landslide hazard assessment. In: Bell (ed.) Landslides, A.A. Balkema, Rotterdam, 1805-1841.

Iovine, G.G.R., Greco, R., Gariano, S.L., Pellegrino, A.D., Terranova, O.G., 2014. Shallow-landslide susceptibility in the Costa Viola mountain ridge (southern Calabria, Italy) with considerations on the role of causal factors. Natural Hazards 73 (1), pp. 111-136.

Isamil, J., Ravichandran, S., 2008. Rusle model application for soil erosion assessment using remote sensing and Gis. Water resources management, 22, 83-102.

Isaac, B., White, J., Ierodiaconou, D.,Cooke, R., 2013. Response of a cryptic apex predator to a complete urban to forest gradient. Wildlife Research 40 (5), pp. 427-436.

Ismail, J., Ravichandran, S., 2008. RUSLE2 model application for soil erosion assessment using remote sensing and GIS. Water Resources Management, 22 (1), pp. 83-102.

Iverson, R.M., Reid, M.E., LaHusen, R.G., 1997. Debris-flow mobilization from landslides. Annual Review of Earth and Planetary Sciences 25, pp. 85-138.

Iverson, R.M., 2000. Landslide triggering by rain infiltration. Water Resources Research 36 (7), pp. 1897-1910.

Iwasaki, A., Fujisada, H., Akao, H., Shindou, O., Akagi, S., 2002. Enhancement of spectral separation performance for ASTER/SWIR. – SPIE,Infrared Spaceborne Remote Sensing IX 4486:42 –50, San Diego, CA, USA.

Iwahashi, J., Pike, R.J., 2007. Automated classifications of topography from DEMs by an unsupervised nested-means algorithm and a three-part geometric signature. Geomorphology 86, 409-440.

Iwasaki, A., Fujisada, H., Akao, H., Shindou, O. Akagi, S., 2002. Enhancement of spectral separation performance for ASTER/Swir. Proceedings of Spie, the International society for optical engineering, 4486, 42-50.

Jackson, M., Roering, J.J., 2009. Post-fire geomorphic response in steep, forested landscapes: Oregon Coast Range, USA. Quaternary Science Reviews 28 (11-12), pp. 1131-1146.

James, N., Sitharam, T.G., 2014. Assessment of Seismically Induced Landslide Hazard for the State of Karnataka Using GIS Technique. Journal of the Indian Society of Remote Sensing, 42 (1), pp. 73-89.

Jaynes, E. T. , 1957. Information Theory and Statistical Mechanics. Physical Review. Series II 106 (4): 620–630.

Jia, N., Mitani, Y., Xie, M.,Djamaluddin, I., 2012. Shallow landslide hazard assessment using a three-dimensional deterministic model in a mountainous area. Computers and Geotechnics, 45, pp. 1-10.

Johnson, K.A., Sitar, N., 1990. Hydrologic conditions leading to debris-flow initiation. Canadian geotechnical journal 27 (6), pp. 789-801.

Keaton, J.R., Haneberg, W.C., 2013. Landslide hazard inventories and uncertainty associated with ground truth. Global View of Engineering Geology and the Environment - Proceedings of the International Symposium and 9th Asian Regional Conference of IAEG pp. 105-110.

Key, C.H.; Z. Zhu; D. Ohlen; S. Howard; R. McKinley; and N. Benson, 2002. The normalized burn ratio and relationships to burn severity: ecology, remote sensing and implementation. In J.D. Greer, ed. Rapid Delivery of Remote Sensing Products. Proceedings of the Ninth Forest Service Remote Sensing Applications Conference, San Diego, CA 8-12 April, 2002. American Society for Photogrammetry and Remote Sensing, Bethesda, MD.

Kleber, A., 1997. Cover-beds as soil parent materials in mid-latitude regions. Catena 30: 197-213.

Kostić, S., Vasović, N., Franović, I., Jevremović, D., Mitrinovic, D., Todorović, K., 2014. Dynamics of landslide model with time delay and periodic parameter perturbations. Communications in Nonlinear Science and Numerical Simulation, 19 (9), pp. 3346-3361.

Köthe, R., and Lehmeier, F., 1993. SARA - Ein Programmsystem zur Automatischen Relief-Analyse. - Standort - Z. f. Angewandte Geographie, 4/93: 11-21; Köln.

Larsen, M.C., Wieczorek, G.F., 2006. Geomorphic effects of large debris flows and flash floods, northern Venezuela, 1999. Zeitschrift fur Geomorphologie, Supplementband 145, pp. 147-175.

Lee, S., Ryu, J.-H., Won, J.-S., Park, H.-J., 2004. Determination and application of the weights for landslide susceptibility mapping using an artificial neural network. Engineering Geology, 71 (3-4), pp. 289-302.

Legg, N.T., Meigs, A.J., Grant, G.E.,Kennard, P., 2014. Debris flow initiation in proglacial gullies on Mount Rainier, Washington. Geomorphology 226, pp. 24-260.

Legorreta Paulin, G., Bursik, M., Lugo-Hubp, J., Zamorano Orozco, J.J. 2010. Effect of pixel size on cartographic representation of shallow and deep-seated landslide, and its collateral effects on the forecasting of landslides by SINMAP and Multiple Logistic Regression landslide models. Physics and Chemistry of the Earth 35 (3-5), pp. 137-148.

Leynaud, D., Sultan, N., 2010. 3-D slope stability analysis: A probability approach applied to the nice slope (SE France). Marine Geology 269 (3-4), pp. 89-106.

Leslie, I.N., Heinse, R., Smith, A.M.S., McDaniel P.A., 2014. Root Decay and Fire Affect Soil Pipe Formation and Morphology in Forested Hillslopes with Restrictive Horizons. Soil Science Society of America Journal Vol. 78 No. 4, p. 1448-1457.

Lombardo, L., Cama, M., Maerker, M.,Rotigliano, E., 2014. A test of transferability for landslides susceptibility models under extreme climatic events: Application to the Messina 2009 disaster. Natural Hazards 74 (3), pp. 1951-1989.

Luckman, P.G., Gibson, R.D. and Derose, R.C., 1999. Landslide erosion risk to New Zealand pastoral steeplands productivity. Land Degradation & Development, 10:1 49-65.

MacDonald, L.H., Huffman, E.L., 2004. Post-fire soil water repellency: Persistence and soil moisture thresholds. Soil Science Society of America Journal 68 (5), pp. 1729-1734.

Malet, J.-P., van Asch, Th.W.J., van Beek, R., Maquaire, O. 2005. Forecasting the behaviour of complex landslides with a spatially distributed hydrological model. Natural Hazards and Earth System Science 5 (1), pp. 71-85.

Mancini, F., Ceppi, C., Ritrovato, G., 2010. GIS and statistical analysis for landslide susceptibility mapping in the Daunia area, Italy. Natural Hazards and Earth System Science, 10 (9), pp. 1851-1864.

Märker, M., Pelacani, S., Schröder, B., 2011. A functional entity approach to predict soil erosion processes in a small Plio-Pleistocene Mediterranean catchment in Northern Chianti, Italy. Geomorphology 125 (4), pp. 530-540.

Mars, J.C., and Rowan, L.C., 2010: Spectral assessment of new ASTER Swir surface reflectance data products for spectroscopic mapping of rocks and minerals. - Remote sensing of environment 114 (9): 2011-2025.

Mast, C.M., Arduino, P., Miller, G.R.,Mackenzie-Helnwein, P., 2014. Avalanche and landslide simulation using the material point method: flow dynamics and force interaction with structures. Computational Geosciences, in press.

Martin, Y.E., 2007. Wildfire disturbance and shallow landsliding in coastal British Columbia over millennial time scales: A numerical modelling study. Catena 69 (3), pp. 206-219.

Matsushi, Y., Hattanji, T., Matsukura, Y., 2006. Mechanisms of shallow landslides on soil-mantled hillslopes with permeable and impermeable bedrocks in the Boso Peninsula, Japan. Geomorphology 76 (1-2), pp. 92-108.

McNabb, D.H., Gaweda, F., Froehlich, H.A., 1989. Infiltration, water repellency, and soil moisture content after broadcast burning a forest site in southwest Oregon. Journal of Soil & Water Conservation 44 (1), pp. 87-90.

Mergili M, Fellin W, Moreiras St M, Stotter J (2012) Simulation of debris flow in the Central Andes based on Open Source GIS: possibilities, limitations, and parameter sensitivity. Nat Hazards 61:1051–1081. Doi:10.1007/s11069-011-9965-7.

Messina, A., Russo, S., Stagno, F., 1996. The crystalline basements of the Calabria–Peloritani Arc, IGC Project 276 Newsletter 6 (special issue), Messina, pp. 91–144.

Messina A, Somma R, Careri G, Carbone G, Macaione E (2004) Peloritani continental crust composition (southern Italy): geological and petrochemical evidences. Boll Soc Geol Ital 123:405–444.

Meyer, N.K., Schwanghart, W., Korup, O., Romstad, B., Etzelmüller, B., 2014. Estimating the topographic predictability of debris flows. Geomorphology 207, pp. 114-125.

Mihai, B., Dobre, R., Švulescu, I., 2014. La cartographic geómorphologique pour l'amélioration de l'infrastructure des grandes lignes de chemin de fer. Uné etude de cas en Roumanie [Geomorphotechnical map for railway mainline infrastructure improvement. A case study from Romania]. Geomorphologie: Relief, Processus, Environnement, (1), pp. 79-90.

Miller, A.J., 2013. Assessing landslide susceptibility by incorporating the surface cover index as a measurement of vegetative cover. Land Degradation and Development 24 (3), pp. 205-227.

Mondal, S., Maiti, R., 2012. Landslide Susceptibility Analysis of Shiv-Khola Watershed, Darjiling: A Remote Sensing & GIS Based Analytical Hierarchy Process (AHP). Journal of the Indian Society of Remote Sensing 40 (3), pp. 483-496.

Mondini, A.C., Chang, K.-T., 2014. Combining spectral and geoenvironmental information for probabilistic event landslide mapping. Geomorphology 213, pp. 183-189.

Moore, I. D., R. B. Grayson, and A. R. Ladson. 1991. Digital Terrain Modelling: A Review of Hydrological, Geomorphological and Biological Applications. Hydrological Processes, 5(1):3-30.

Montgomery, D.R., Dietrich, W.E., 1994. A physically based model for the topographic control on shallow landsliding. Water Resources Research 30 (4), pp. 1153-1171.

Moriguchi, S., Borja, R.I., Yashima, A.,Sawada, K., 2009. Estimating the impact force generated by granular flow on a rigid obstruction. Acta Geotechnica 4 (1), pp. 57-71.

Mulder, V.L., De Bruin, S., Schaepman, M.E. Mayr, T.R., 2011. The use of remote sensing in soil and terrain mapping — A review. - Geoderma 162 (1–2): 1-19.

Muntohar AS, Liao HJ (2010) Rainfall infiltration: infinite slope model for landslides triggering by rainstorm. Nat Hazards 54:967–984. Doi:10.1007/s11069-010-9518-5.

Nagarajan, R., Mukherjee, A., Roy, A. and Khire, M.V., 1998. temporal remote sensing data and GIS application in landslide hazard zonation of part of western Ghat, India. International Journal of Remote Sensing 19, pp. 573–585.

Nefeslioglu, H.A., Gokceoglu, C.,Sonmez, H., 2008. An assessment on the use of logistic regression and artificial neural networks with different sampling strategies for the preparation of landslide susceptibility maps. Engineering Geology 97 (3-4), pp. 171-191.

Nemcok, A., Pasek, J., Rybar, J., 1972. Classification of landslides and other mass movements. Rock Mech Felsmech Mec Roches 4 (2), pp. 71-78.

Ni, H., Zheng, W., Song, Z., Xu, W., 2014. Catastrophic debris flows triggered by a 4 July 2013 rainfall in Shimian, SW China: formation mechanism, disaster characteristics and the lessons learned. Landslides, in press.

Nikolopoulos, E.I., Crema, S., Marchi, L., Marra, F., Guzzetti, F., Borga, M. 2014. Impact of uncertainty in rainfall estimation on the identification of rainfall thresholds for debris flow occurrence. Geomorphology 221, pp. 286-297.

Oh, H.-J., Park, N.-W., Lee, S.-S., Lee, S., 2012. Extraction of landslide-related factors from ASTER imagery and its application to landslide susceptibility mapping. International Journal of Remote Sensing 33 (10), 545084, pp. 3211-3231.

Ohlmacher G.C., 2007. Plan curvature and landslide probability in regions dominated by earth flows and earth slides. Eng Geol 91(2–4)117–134. Doi:10.1016/j.enggeo.2007.01.005

Pachauri, A.K., Pant, M., 1992. Landslide hazard mapping based on geological attributes. Engineering Geology 32 (1-2), pp. 81-100.

Parise, M., Jibson, R.W., 2000. A seismic landslide susceptibility rating of geologic units based on analysis of characterstics of landslides triggered by the 17 January, 1994 Northridge, California earthquake. Engineering Geology 58 (3-4), pp. 251-270.

Park, N.-W., 2014. Using maximum entropy modeling for landslide susceptibility mapping with multiple geoenvironmental data sets. Environmental Earth Sciences, article in press.

Pastor, M., Haddad, B., Sorbino, G.,Cuomo, S., Drempetic, V., 2009. A depth-integrated, coupled SPH model for flow-like landslides and related phenomena. International Journal for Numerical and Analytical Methods in Geomechanics, 33 (2), pp. 143-172.

Pavlova, I., Jomelli, V., Brunstein, D., Grancher, D., Martin, E., Déqué, M., 2014. Debris flow activity related to recent climate conditions in the French Alps: A regional investigation. Geomorphology 219, pp. 248-259.

Penna, D., Borga, M., Aronica, G.T.,Brigandì, G., Tarolli, P., 2014. The influence of grid resolution on the prediction of natural and road-related shallow landslides. Hydrology and Earth System Sciences 18 (6), pp. 2127-2139.

Petley DN (1999) Failure envelopes of mudrocks at high effective stresses. In: Aplin AC, Fleet AJ, Macquaker JHS (eds) Physical properties of mud and mudstones, Geol Soc Lond Spec Publ 158.

Petley, D., 2012. Global patterns of loss of life from landslides. Geology 40 (10), pp. 927-930.

Petschko, H., Brenning, A., Bell, R.,Goetz, J., Glade, T., 2014. Assessing the quality of landslide susceptibility maps - Case study Lower Austria. Natural Hazards and Earth System Sciences 14 (1), pp. 95-118.

Phillips, S.J., Dudık, M., Schapire, R.E., 2004. A maximum entropy approach to species distribution modeling. In: Proceedings of the 21st International Conference on Machine Learning, ACM Press, New York, pp. 655–662.

Phillips, S., R. Anderson, and R. Schapire (2006), Maximum entropy modeling of species geographic distributions, Ecol. Model., 190(3-4), 231–259. Doi:10.1016/j.ecolmodel.-2005.03.026.

Phillips, S. J., and Miroslav, D., 2008. Modeling of species distributions with MaxEnt: New extensions and a comprehensive evaluation, Ecography, 31 (2), 161–175. Doi:10.1111/j.0906-7590.2008.5203.x.\

Pike, R.J. (1988) The geometric signature: quantifying landslide-terrain types from digital elevation models. Mathematical Geology, 20:5 491-511.

Platt, J.P., Compagnoni, R., 1990. Alpine ductile deformation and metamorphism in a Calabrian basement nappe (Aspromonte, south Italy). Eclogae Geologicae Helvetiae 83 (1), pp. 41-58.

Poiraud, A., 2014. Landslide susceptibility-certainty mapping by a multi-method approach: A case study in the Tertiary basin of Puy-en-Velay (Massif central, France). Geomorphology 216, pp. 208-224.

Pour, A.B., Hashim, M., Marghany, M., 2011. Using spectral mapping techniques on short wave infrared bands of aster remote sensing data for alteration mineral mapping in se Iran. - International journal of the physical sciences 6(4) 917-929.

Pourghasemi, H.R., Moradi, H.R.,Fatemi Aghda, S.M., 2013. Landslide susceptibility mapping by binary logistic regression, analytical hierarchy process, and statistical index models and assessment of their performances. Natural Hazards 69 (1), pp. 749-779.

Pradhan, B., Oh, H.-J., Buchroithner, M., 2010. Weights-of-evidence model applied to landslide susceptibility mapping in a tropical hilly area. Geomatics, Natural Hazards and Risk 1 (3), pp. 199-223.

Pradhan, A.M.S. and Kim, Y.-T., 2014. Relative effect method of landslide susceptibility zonation in weathered granite soil: A case study in Deokjeok-ri Creek, South Korea. Natural Hazards 72 (2), pp. 1189-1217.

Quan Luna, B., Blahut, J., Camera, C., van Westen, C., Apuani, T., Jetten, V., Sterlacchini, S., 2014. Physically based dynamic run-out modelling for quantitative debris flow risk assessment: A case study in Tresenda, northern Italy. Environmental Earth Sciences, 72 (3), pp. 645-661.

Raia, S., Alvioli, M., Rossi, M., Baum, R.L., Godt, J.W., Guzzetti, F., 2014. Improving predictive power of physically based rainfall-induced shallow landslide models: A probabilistic approach. Geoscientific Model Development, 7 (2), pp. 495-514.

Reichenbach, P., Busca, C., Mondini, A.C., Rossi, M., 2014. The Influence of Land Use Change on Landslide Susceptibility Zonation: The Briga Catchment Test Site (Messina, Italy). Environmental Management, in press.

Ren, D., Fu, R., Leslie, L.M.,Dickinson, R.E., 2011. Modeling the mudslide aftermath of the 2007 Southern California Wildfires. Natural Hazards 57 (2), pp. 327-343.

Rib, H.T. and Liang, T., 1978. Recognition and identification. In: Schuster, R.L. and Krizek, R.J. (eds.) Landslide Analysis and Control, National Academy of Sciences, Transportation Research Board Special Report 176, Washington, 34-80.

Richter, R. and Schläpfer, D., 2014. Atmospheric / topographic correction for satellite imagery (Atcor-2/3 user guide, version 8.3.1). - Dlr, Wessling, Germany.

Robichaud, P.R., Hungerford, R.D., 2000. Water repellency by laboratory burning of four northern Rocky Mountain forest soils. Journal of Hydrology 231-232, pp. 207-219.

Robichaud, P.R., Lewis, S.A.,Wagenbrenner, J.W., Ashmun, L.E.,Brown, R.E., 2013. Post-fire mulching for runoff and erosion mitigation. Part I: Effectiveness at reducing hillslope erosion rates. Catena 105, pp. 75-92.

Rodríguez J.L.G. and Suárez M.C.G., 2010. Comparison of mathematical algorithms for determining the slope angle in GIS environment. Aqua-LAC - Vol. 2 - Nº 2 - Sep. 2010. pp.78-82.

Rossi, M., Guzzetti, F.,Reichenbach, P., Mondini, A.C., Peruccacci, S., 2010. Optimal landslide susceptibility zonation based on multiple forecasts. Geomorphology 114 (3), pp. 129-142.

Rotigliano, E., Agnesi, V.,Cappadonia, C., Conoscenti, C., 2011. DocumentThe role of the diagnostic areas in the assessment of landslide susceptibility models: A test in the sicilian chain. Natural Hazards 58 (3), pp. 981-999.

Rotigliano, E., Cappadonia, C.,Conoscenti, C., Costanzo, D., Agnesi, V., 2012. Slope units-based flow susceptibility model: Using validation tests to select controlling factors. Natural Hazards, 61 (1), pp. 143-153.

Rouse J.W., Haas R.H., Schell J.A., Deering D.W., 1974. Monitoring vegetation systems in the Great Plains with ERTS. In: Fraden S.C., Marcanti E.P. and Becker M.A. (eds.), Third ERTS-1 Symposium, 10-14 Dec. 1973, NASA SP-351, Washington D.C. NASA, pp 309-317.

Rowan, L.C., and Mars, J.C., 2003. Lithologic mapping in the Mountain Pass, California area using Advanced Spaceborne Thermal Emission and Reflection Radiometer (ASTER) data. - Remote Sensing of Environment, 84 (3): 350-366.

Rowan, L. C., Mars, J.C., and Simpson, C.J., 2005. Lithologic mapping of the mordor, nt, australia ultramafic complex by using the Advanced Spaceborne Thermal Emission and Reflection radiometer (ASTER). - Remote sensing of environment 99 (1-2): 105-126.

Ruff, M., Czurda, K., 2008. Landslide susceptibility analysis with a heuristic approach in the Eastern Alps (Vorarlberg, Austria). Geomorphology, 94 (3-4), pp. 314-324.

Saha, A.K., Gupta, R.P., Sarkar, I.,Arora, M.K., Csaplovics, E., 2005. An approach for GIS-based statistical landslide susceptibility zonation-with a case study in the Himalayas. Landslides, 2 (1), pp. 61-69.

Sarkar, S., Kanungo, D.P., 2004. An integrated approach for landslide susceptibility mapping using remote sensing and GIS. Photogrammetric Engineering and Remote Sensing 70 (5), pp. 617-625.

Sassa K., Canuti P., 2008. Landslides - Disaster Risk Reduction. Springer Science & Business Media, Dec 8, 2008.

Schuster, R.L., Highland, L.M., 2007. The third hans cloos lecture. Urban landslides: Socioeconomic impacts and overview of mitigative strategies. Bulletin of Engineering Geology and the Environment 66 (1), pp. 1-27.

Šilhán, K., Pánek, T., Hradecký, J.,Stoffel, M., 2014. Tree-age control on reconstructed debris-flow frequencies: Examples from a regional dendrogeomorphic reconstruction in the Crimean Mountains. Earth Surface Processes and Landforms, in press.

Sivapalan, M. and Wood, E.F., 1987. A multidimensional model of non-stationary space-time rainfall at the catchment scale, Water Resour. Res., 23, 1289–1299.

Sivapalan, M., Wood, E. F., and Beven, K. J., 1990. On hydrologic similarity. 3. A dimensionless flood frequency model using a generalized geomorphologic unit hydrograph and partial area runoff generation, Water Resour. Res., 26, 43–58.

Skidmore, A.K., 1989. A comparison of techniques for calculation gradient and aspect from a gridded digital elevation model. International Journal of Geographical Information Sciences 4 (1), 33–49.

Soeters R, van Westen C.J., 1996. Slope instability recognition, analysis and zonation. In: Turner AK, Schuster RL (eds) Landslides, investigation and mitigation. Transportation Research Board, National Research Council, special report 247, National Academy Press, Washington, pp 129–177.

Somma R., 2006. The south-western side of the Calabrian Arc (Peloritani Mountains): geological, structural and AMS evidence for passive clockwise rotations. J Geodyn 41(4):422–439. doi:10.1016/j.jog.2005.11.00

Somma R., Messina A., Mazzoli S., 2005. Syn-orogenic extension in the Peloritani Alpine Thrust Belt (NE Sicily, Italy): evidence from the Alı`Unit. Compte Rendus Ge`oscience Paris 337:861–871.

Sorriso-Valvo, M., Terranova, O., 2006. The Calabrian fiumara streams. Zeitschrift fur Geomorphologie, Supplementband (143), pp. 109-125.

Stoffel, M., Mendlik, T., Schneuwly-Bollschweiler, M., Gobiet, A., 2014. Possible impacts of climate change on debris-flow activity in the Swiss Alps. Climatic Change 122 (1-2), pp. 141-155.

Stockwell, D.R.B., and Noble, I.R., 1992. Induction of sets of rules from animal distribution data: a robust and informative method of data analysis. Mathematics and Computers in Simulation, 33, 385–390.

Stockwell, D., and Peters, D., 1999. The GARP modelling system: problems and solutions to automated spatial prediction. International Journal of Geographical Information Science, 13, 143–158.

Sujatha, E.R., Rajamanickam, V., 2011. Landslide susceptibility mapping of Tevankarai Ar sub-watershed, Kodaikkanal Taluk, India, using weighted similar choice fuzzy model. Natural Hazards 59 (1), pp. 401-425.

Süzen, M.L., Doyuran, V., 2004a. Data driven bivariate landslide susceptibility assessment using geographical information systems: A method and application to Asarsuyu catchment, Turkey. Engineering Geology 71 (3-4), pp. 303-321

Süzen, M.L., Doyuran, V., 2004b. A comparison of the GIS based landslide susceptibility assessment methods: Multivariate versus bivariate. Environmental Geology 45 (5), pp. 665-679.

Tagil S. and Jenness J., 2008. GIS-Based Automated Landform Classification and Topographic, Landcover and Geologic Attributes of Landforms Around the Yazoren Polje, Turkey. Journal of Applied Sciences, 8: 910-921.

Tibshirani, R. (1996). Regression shrinkage and selection via the lasso. Journal of the Royal Statistical Society, Series B 58,267–288.

Tortorici, L., Monaco, C., Tansi, C.,Cocina, O., 1995. Recent and active tectonics in the Calabrian arc (Southern Italy). Tectonophysics 243 (1-2), pp. 37-55.

Travelletti, J., Malet, J.-P., 2012. Characterization of the 3D geometry of flow-like landslides: A methodology based on the integration of heterogeneous multi-source data. Engineering Geology,128, pp. 30-48.

Tucker, C. and P. Sellers, Satellite remote sensing of primary production. International Journal of Remote Sensing, 1986, 7(11): p. 1395-1416.

Turkington, T., Ettema, J., Van Westen, C.J., Breinl, K., 2014. Empirical atmospheric thresholds for debris flows and flash floods in the southern French Alps. Natural Hazards and Earth System Sciences 14 (6), pp. 1517-1530.

Turner, A.K. and Schuster, R.L., (eds.) 1996. Landslides: Investigation and Mitigation. Washington, D.C., National Research Council, Transportation Research Board Special Report 247, 673 p.

Van Asch, Th.W.J., Buma, J., Van Beek, L.P.H. 1999. A view on some hydrological triggering systems in landslides. Geomorphology 30 (1-2), pp. 25-32. DOI: 10.1016/S0169-555X(99)00042-2.

Van Den Eeckhaut, M., Poesen, J.,Verstraeten, G., Vanacker, V., Moeyersons, J., Nyssen, J., van Beek, L.P.H., 2005. The effectiveness of hillshade maps and expert knowledge in mapping old deep-seated landslides. Geomorphology 67 (3-4), pp. 351-363.

Van Den Eeckhaut, M., Reichenbach, P., Guzzetti, F., Rossi, M., Poesen, J., 2009. Combined landslide inventory and susceptibility assessment based on different mapping units: An example from the Flemish Ardennes, Belgium. Natural Hazards and Earth System Science 9 (2), pp. 507-521.

van Westen, van Duren, I., Kruse, H.M.G. and Terlien, M.T.J., 1993. GISSIZ: training package for geographic information systems in slope instability zonation. ITC Publication number 15, 2 volumes, ITC, Enschede, The Netherlands.

van Westen, C.J., Rengers, N., Terlien, M.T.J.and Soeters, R., 1997. Prediction of the occurrence of slope instability phenomenalthrough GIS-based hazard zonation. Geologische Rundschau, 86: 404-414.

van Westen CJ (2000) The modelling of landslide hazards using GIS. Surv Geophys 21:241–255. Doi:10.1023/A:1006794127521.

van Westen CJ, van Asch TWJ, Soeters R., 2006. Landslide hazard and risk zonation—why is it still so difficult? Bull Eng Geol Env 65:167–184. Doi:10.1007/s10064-005-0023-0.

van Westen, C.J., Castellanos, E.,Kuriakose, S.L., 2008. Spatial data for landslide susceptibility, hazard, and vulnerability assessment: An overview. Engineering Geology 102 (3-4), pp. 112-131.

Varnes DJ. 1978. Slope movement types and process. In: R.L. Schuster and R.J. Krizek (Editors), Landslides: Analysis and Control-Transportation Research Board, Special Report. National Research Council, Washington D.C., pp. 11–33.

Varnes, D.J. and IAEG Commission on Landslides and other Mass-Movements (1984) Landslide hazard zonation: a review of principles and practice. The UNESCO Press, Paris, 63 p.

Vitale, S., Ciarcia, S., 2013. Tectono-stratigraphic and kinematic evolution of the southern Apennines/Calabria-Peloritani Terrane system (Italy). Tectonophysics 583, pp. 164-182.

Vorpahl, P., Elsenbeer, H., Märker, M., Schröder, B., 2012. How can statistical models help to determine driving factors of landslides?. Ecological Modelling 239, pp. 27-39.

Yamaguchi, Y. and Naito, C., 2003: spectral indices for lithologic discrimination and mapping by using the aster Swir bands. - international journal of remote sensing 24 (22): 4311-4323.

Yilmaz, I., 2010. Comparison of landslide susceptibility mapping methodologies for Koyulhisar, Turkey: Conditional probability, logistic regression, artificial neural networks, and support vector machine. Environmental Earth Sciences, 61 (4), pp. 821-836.

Youssef, A.M., Al-Kathery, M.,Pradhan, B., 2014. Landslide susceptibility mapping at Al-Hasher area, Jizan (Saudi Arabia) using GIS-based frequency ratio and index of entropy models. Geosciences Journal, article in press.

Yuksel, A., Gundogan, R., Akay, A., 2008. Using the remote sensing and Gis technology for erosion risk mapping of Kartalkaya dam watershed in Kahramanmaras, Turkey. Sensors, 8, 4851-4865.

Wang, L., Sawada, K., Moriguchi, S., 2012. GIS-based landslide susceptibility mapping using logistical regression method with LiDAR data in nature slopes. Disaster Advances 5 (4), pp. 258-263.

Ward, G., Hastie, T., Barry,S., Elith,J. & Leathwick,J.R.(2009) Presence-only data and the EM algorithm. Biometrics, 65, 554–563.

Wieczorek GF (1996) Landslide triggering mechanisms. In: Landslides: Investigation and Mitigation (Turner AK, Schuster RL, eds). Washington DC: Transportation Research Board, National Research Council, Special Report, 76–90.

Wilson RC (1989) Rainstorms, pore pressures, and debris flows: a theoretical framework. In: Landslides in a semi-arid environment (Morton DM, Sadler PM, eds). California: Publications of the Inland Geological Society, 2: 101–117.

Wilson, J.P., Gallant, J.C., 1996. EROS: A grid-based program for estimating spatially-distributed erosion indices. Computers and Geosciences 22 (7), pp. 707-712.

Wilson, J.P., Gallant, J.C (Eds.), 2000. Terrain Analysis—Principles and Applications, Wiley, New York.

WP/WLI (International Geotechnical Societies' UNESCO Working Party on World Landslide Inventory), 1991. A suggested method for reporting a landslide summary. Bulletin International Association for Engineering Geology, 43: 101-110.

Wu, X., Ren, F., Niu, R., Peng, L., 2013. Landslide spatial prediction based on slope units and support vector machines. Wuhan Daxue Xuebao (Xinxi Kexue Ban)/Geomatics and Information Science of Wuhan University 38 (12), pp. 1499-1503.

Yamaguchi, Y., Kahle, A.B., Tsu, H., Kawakami, T., Pniel, M. 1998. Overview of Advanced Spaceborne Thermal Emission and Reflection radiometer (ASTER). Geoscience and remote sensing, Ieee transactions on, 36, 1062-1071.

Yoshida, H., 2014. Hummock alignment in Japanese volcanic debris avalanches controlled by pre-avalanche slope of depositional area. Geomorphology, 223, pp. 67-80.

Youssef, A.M., Pradhan, B., Jebur, M.N., El-Harbi, H.M., 2014. Landslide susceptibility mapping using ensemble bivariate and multivariate statistical models in Fayfa area, Saudi Arabia. Environmental Earth Sciences, in press.

Yuksel, A., Gundogan, R., Akay, A., 2008. Using the remote sensing and Gis technology for erosion risk mapping of Kartalkaya dam watershed in Kahramanmaras, Turkey. Sensors, 8, 4851-4865.

Zevenbergen, L.W. and Thorne, C.R., 1987. Quantitative analysis of land surface topography. Earth Surface Processes and Landforms.